RELIABILITY-BASED PROGRESSIVE COLLAPSE AND REDUNDANCY ANALYSIS OF BRIDGE SYSTEMS

By

FENG MIAO

A dissertation submitted to the Graduate Faculty in Engineering in partial fulfillment of the requirements for the degree of Doctor of Philosophy,
The City University of New York
2014

This manuscript has been read and accepted for the Graduate Faculty in Engineering in Satisfaction of the dissertation requirement for the degree of Doctor of Philosophy

Date	Professor Michel Ghosn Chair of the Examining Committee
Date	Professor Ardie Walser Executive Officer

Professor Anil K. Agrawal

Professor Feng-Bao Lin

Professor Huabei Liu

Dr. Jian Wang

Supervisory Committee

THE CITY UNIVERSITY OF NEW YORK

Abstract

RELIABILITY-BASED PROGRESSIVE COLLAPSE AND REDUNDANCY ANALYSIS OF BRIDGE SYSTEMS

by

Feng Miao

Advisor: Professor Michel Ghosn

Highway bridges like most structural systems are usually designed on a member by member basis and little consideration is provided to the effect of a local failure on system safety. There are concerns that some systems optimized to meet code-specified member design criteria may not provide sufficient levels of structural redundancy to withstand a possible local failure. In fact, a local failure of one structural element may result in the failure of another element creating a chain reaction that might progress throughout the whole structure or a major portion of it leading to a catastrophic collapse. Several recent catastrophic structural collapses have alerted the structural engineering community to the importance of designing structures with sufficient levels of structural redundancy and robustness to make them capable of withstanding local failures and retaining some level of limited functionality. This has led several agencies to develop criteria for evaluating the robustness of structural systems. However, in a departure from LRFD-based code developments, these recently proposed criteria, which are based on deterministic concepts, do not properly account for the random material properties, the variations in the strengths of the members, or the uncertainties associated with modeling the response of structural systems. Furthermore, it is not clear if the existing criteria which were developed for office buildings are applicable to highway bridges subjected to highly stochastic live loads or whether these criteria will lead to

similar safety levels for different types of structures.

The object of this Dissertation is to propose a methodology to evaluate the redundancy of highway bridge systems and verify their ability to withstand progressive collapse should a local failure take place. In keeping with current code development approaches, the proposed methodology must be calibrated to provide an acceptable and consistent level of reliability for different types of structures accounting for the uncertainties in estimating the bridge behavior and material properties.

A first step for achieving the objectives of this study is to define non-subjective reliability-based criteria for evaluating the performance of originally intact bridge systems, those that have been subjected to local damage, and assessing the ability of the system to survive the sudden occurrence of local damage. The development of such reliability-based criteria requires the availability of probabilistic analysis algorithms capable of handling complex structural systems with low probability of failure. The review of existing structural system reliability methods shows that a Markov-Chain simulation known as the Subset Simulation method offers many advantages over other available methods for evaluating the reliability of complex structural systems with high numbers of failure modes and low probabilities of failure. To further improve the existing subset simulation algorithm, a hybrid Markov chain Monte Carlo method referred to as “RASS” is proposed. The proposed improvements include: a) a more efficient advanced Markov Chain sample generation algorithm; b) a Delayed Rejection process that allows partial local adaptation of the generated candidate samples at each time step of the Markov chain; c) an Adaptive Algorithm that uses the history of the chain to update the variances of the intermediate proposal probability distribution function; d) a Regeneration process to help in reducing the

correlation between the generated samples; and e) a componentwise generation of samples is used to reduce the computational effort associated with multivariate input.

This study demonstrates that the proposed simulation approach is robust to dimension size and is efficient in computing small probabilities of failure for complex structural systems. In addition, this approach can be used to obtain approximate expressions for the limit state equations for the pertinent failure modes.

The applicability of the proposed reliability algorithm in analyzing the system performance of bridge structures and evaluating their levels of redundancy as well as their ability to resist dynamic progressive collapse is demonstrated through several examples for typical I-girder bridges, steel box-girder bridges, and truss systems.

Since involved reliability analyses are beyond the day-to-day practice of bridge engineers, this study proposes an approach to develop a deterministic progressive collapse analysis method for bridges. Following current practice in the development of structural design codes, the deterministic analysis and associated criteria are calibrated to provide adequate and consistent levels of structural reliability for different bridge topologies. The validity of the proposed approach for calibrating progressive collapse analysis criteria is illustrated using two different bridge configurations subjected to different local damage scenarios.

DEDICATION

To my family

ACKNOWLEDGEMENTS

I would like to express my sincere gratitude and appreciation to my advisor, Professor Michel Ghosn for his continuous academic support, mentorship and moral support since the beginning of my graduate studies in the Department of Civil Engineering of CUNY/Graduate Center in the Fall of 2006.

My sincere appreciation also goes to the faculty members of the Department of Civil Engineering at the City College of New York for their help and encouragement during the past years; in particular, I would like to thank Professor Mumtaz Kassir, Professor Anil K. Agrawal, Professor Feng-Bao Lin, and Professor Huabei Liu. I also like to sincerely acknowledge the support of Dr. Jian Wang and Dr. S.K.AU for clarifying some of the intricacies of the Genetic Algorithm and classic Subset Simulation method, respectively.

I would also like to thank my fellow graduate students at the City College of New York for their help and assistance. I couldn't have finished writing my dissertation without their help.

Finally, I would like to give my thanks to my parents, my aunt, my husband and my son. None of this would have been possible without their love and patience. They have been a constant source of love, support and strength all these years.

TABLE OF CONTENTS

LIST OF FIGURES

LIST OF TABLES

CHAPTER ONE: INTRODUCTION

1.1 Problem Statement

Structural systems and in particular bridge systems are generally designed on a member by member basis and little consideration is provided to the effects of a local failure on system safety. A local failure of a ductile member may be associated with the plastification of the overloaded member which could allow the system to continue to carry additional load after the component reaches its strength limit by redistributing the additional load to members that have not reached their limiting capacities. The ability of a structural system to continue to carry load after a member reaches its limiting capacity is referred to as structural redundancy. Occasionally, the failure of one element may result in the failure of another element causing the failure to progress throughout a major part or even the whole structure. Such a system would be classified as nonredundant.

Alternatively, a brittle local failure may cause a structural component to shed its load to the adjoining members and the rest of the structure creating a cascading failure. In some cases, the recent literature has referred to such a phenomenon as progressive collapse. Progressive collapse occurs if a local structural damage causes a chain reaction of structural element failures. According to ASCE 7-10 (ASCE 2010), Progressive Collapse is defined as the spread of an initial local failure from element to element resulting, eventually, in the collapse of an entire structure or a disproportionately large part of it. A structure's insensitivity to a local failure has been defined as structural robustness in the recent literature. Historically, the ability of a structure to avoid progressive collapse used to also be defined as structural redundancy.

A structurally robust system is associated with two main characteristics: 1) The ability of the

system to withstand a sudden localized failure which may be associated with a sudden release of the strain energy embedded in the failing members, and 2) the ability of the damaged system to sustain some minimum level of loads after it survives the initial damaging event.

Depending on their topological configurations, their member ductility and the presence of alternate paths that help redistribute the loads around the region where the initial local failure occurred, different structural systems exhibit different degrees of redundancy and robustness. In past practice, the contributions of a system's redundancy and robustness to structural safety have been generally neglected when designing new structures or during the safety evaluation of existing structures. The goal of the designer has traditionally consisted of optimizing the design so that each member in the system is capable of carrying the code specified forces by interacting with the other members of the intact structural system configuration. However, several catastrophic bridge failures, most notably the Mianus River Bridge on I-95 in 1983, and more recently the collapse of the I-35W Mississippi River bridge in Minnesota in 2007 (Figure 1.1) and other well publicized events such as the collapse of Jiujiang bridge hit by a boat in China in 2007 (Figure 1.2), the collapse of the I-40 Bridge in Oklahoma in 2002 (Figure 1.3) or the collapse of Highway 19 Overpass in Laval Quebec in 2006 (Figure 1.4) and the collapse of a box girder Koror-Babeldaob Bridge in 1996 in Palau (Figure 1.5), have alerted the bridge engineering community to the importance of ensuring structural survivability after an initial local failure and the need to develop methods for assessing the redundancy and robustness of bridge systems.

Figure 1.1 Two different views of the I-35W Mississippi River bridge in Minnesota in 2007

Figure 1.2 Collapse of Jiujiang bridge in June 2007 in China

Figure 1.3 Collapse of I-40 Bridge in Oklahoma in 2002

Figure 1.4 Collapse of Highway 19 Overpass, Laval Quebec (2006)

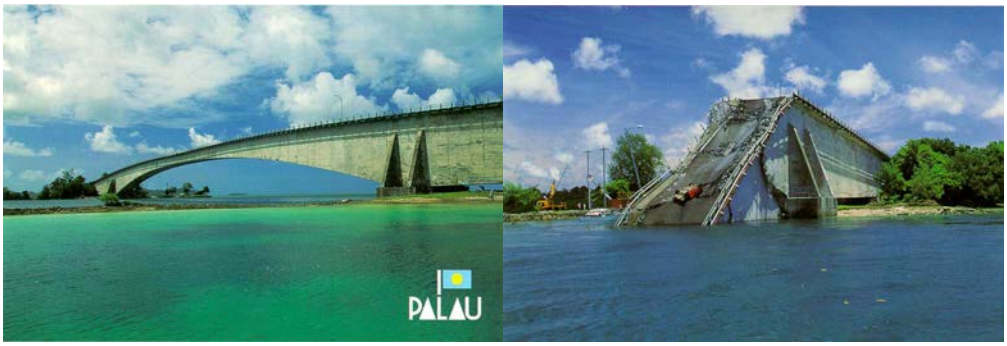

Figure 1.5 Collapse of the Koror-Babeldaob Bridge in 1996

The issue of structural collapse is of course not unique to bridges. Several similar high profile collapses of buildings, have led recent research projects to focus on analyzing the progressive collapse mechanisms of existing buildings and on developing guidelines for designing buildings with high levels of redundancy and robustness [Marjanishvili, 2004; Bazant et al., 2007; Ellingwood, 2006; Chen et al.,1996]. Although existing criteria to reduce the risk of progressive collapse have been developed for buildings using traditional deterministic methods by Marjanishvili (2004), the high levels of uncertainties associated with estimating the member strengths of new and deteriorated existing structures as well as the uncertainty in determining the location and intensity of the applied loads justify the use of probabilistic analysis methods Ellingwood (2011). The variability in member strength deterioration with time and space as well as the variations in the location of the applied loads, could even change the modes of failure as has been shown in recent research by (Biondini 2009) and as tragically learned from the collapse of the I-35 Minnesota Bridge which has survived an under-designed gusset plate for 40 years until the loading patterns on the deck were changed during deck rehabilitation. These observations highlight the importance of performing probabilistic analyses of structural system redundancy and robustness.

Although an outline has been proposed by Ellingwood (2006) describing how to account for member and load uncertainties when developing progressive collapse guidelines, as of this date, no specific probability-based methods for analyzing the progressive collapse of structural systems or for proposing robustness criteria have been established for buildings or bridges. Although establishing such probability-based criteria are necessary in order to remain consistent with current structural design codes and specifications, Starossek (2009) attributes the lack of

implementation of probabilistic methods to the unavailability of advanced techniques with the capability of performing progressive collapse analyses on realistic models of structural systems. Such criticism may not be entirely justified, as methods with various levels of accuracy have been developed for the probabilistic analysis of structural systems under various hazards especially earthquakes and wave loading (Chen and Zhang 1996; Karadeniz 2006; Korkmaz and Johnson 2007; Moarefzadeha and Melchers 2006; Paliou et al. 1990; Pan 2006; Wirsching 1984) and the probabilistic analysis of nuclear power plants (Valbuena and Modarres 2009; Ellingwood and Mori 1997; Reed and Gurbuz 1993).

Furthermore, Ghosn et al (1994) and Ghosn and Moses (1998), Liu, Ghosn et al (2001) as well as Wisniewski, Casas and Ghosn (2009) have used the Response Surface Method (RSM) and simplified probabilistic models to evaluate the redundancy of bridge superstructure and substructure systems and establish criteria for accounting for bridge redundancy during the design and safety evaluation of highway and railway bridge systems. To this date, the only known studies that provided non-subjective and quantifiable definitions of bridge redundancy along with specific criteria for assessing bridge redundancy are those of NCHRP Reports 406 and 458. The two NCHRP reports developed a framework for quantifying system redundancy and developed an approach for including system redundancy during the structural design and safety assessment of highway bridge superstructures and substructures. The approach consists of penalizing non-redundant designs by requiring that members of bridges with non-redundant configurations be designed with higher safety factors as compared to bridges with redundant configurations. Following modern reliability-based code calibration procedures, the proposed criteria in the NCHRP can be implemented using traditional deterministic analysis methods but are calibrated so

that the structures produce consistent levels of system reliability.

However, the criteria proposed by Ghosn & Moses (1998) were based on current practice in the safety evaluation of bridge structures established using simplified reliability analyses models that considered pre-identified single modes of failure. The simplified reliability methods were used in the recent past due to the difficulties encountered in using advanced reliability methods to analyze realistic models of structural systems. During the last three decades, the theory of structural system reliability has seen great advances and there currently exist several approaches for analyzing the reliability of complex structures. The most common methods include FORM, the Response Surface Method as well as basic simulation methods such as the Monte Carlo Simulation and its variants including the Latin Hypercube method. However, when the dimension and the complexity of the problem increases, these existing methods are known to be inefficient in evaluating small probabilities of failure (Melchers 1999).

Recent research in structural reliability methods have led to the development of advanced Markov-Chain based simulations techniques, such as the Subset Simulation method, which have been shown to be able to handle reliability problems with large numbers of random variables and low probabilities of failure. (Au and Beck, 2001). The applicability of the Markov-Chain simulations for the analysis of complex structural systems and for evaluating the redundancy and robustness of bridge systems have yet to be fully explored. The application of such an advanced reliability analysis tool is paramount for helping establish reliability-based criteria that can be used by the bridge engineering community to evaluate the redundancy and robustness of bridge systems in order to help avoid the recurrence of collapses similar to those described in this Chapter.

1.2 Dissertation Objectives and Research Approach

The objective of this Dissertation is to develop an advanced methodology to evaluate the reliability of bridge systems and perform a probabilistic analysis of bridge redundancy and robustness as well as the probability of progressive collapse should one member be suddenly damaged due to the occurrence of an external hazard. The implementation of such reliability analyses requires the availability of probabilistic analysis algorithms capable of handling complex structural systems with low probability of failure. Building on the success of the Subset Simulation method and to overcome some of its limitations, this study will propose a new Markov-chain based advanced simulation technique that will provide improvements on the stability and efficiency of the existing Subset Simulation algorithm.

Although the availability of advanced reliability algorithms will help expert engineers evaluate the redundancy and robustness of bridge systems directly, such involved reliability analyses are beyond the day-to-day practice of bridge engineers. Therefore, another objective of this Thesis is to develop a methodology that allows a bridge engineer to verify the ability of a bridge system to avoid progressive collapse using traditional deterministic methods. Traditionally, structural engineers checked the progressive collapse of buildings using the nonlinear methodology and criteria provided in the GSA and DOD guidelines for office buildings. Given the differences in the loads and configurations of bridge systems as compared to those of office buildings, the existing guidelines for buildings may not necessarily be applicable for the evaluation of the progressive collapse of bridges. Therefore, a new set of criteria must be developed for bridges. Following current practice in the development of structural design codes, criteria for analyzing the progressive collapse of bridges should be calibrated to provide adequate and consistent levels of reliability. The validity of the process that will be developed in this study

will be illustrated for different bridge configurations and for different damage scenarios.

1.3 Report Outline

The six chapters of this Dissertation describe the work done to achieve the objectives of this research study. Each of these chapters deals with separate but inherently integrated tasks. The outline of this dissertation is as follows:

Chapter 1, which is this chapter, presented the problem statement, the research objectives and the proposed research approach.

Chapter 2 presents a detailed review of the current state of the art on the analysis of the redundancy progressive collapse and the reliability assessment of structural systems in general and bridge systems in particular.

Chapter 3 describes a proposed probabilistic Simulation method referred to as RASS that can be used to efficiently analyze the reliability of structural systems. Several illustrative examples are presented to verify the advantages of this proposed method including its accuracy, efficiency and its ability to handle structural systems with complex failure regions, large numbers of random variables, and small probabilities of failure.

In Chapter 4, the proposed simulation procedure is applied to evaluate the redundancy and robustness of a truss bridge and a prestressed I-girder bridge. The statistical models used to perform the reliability analysis of truss bridge systems were developed in this study to account for bar failures in tension or compression. Also, probabilistic tri-linear shear stress-deformation and bilinear force-displacement models are developed to represent the behavior of the bolts and gusset

plates at the truss connections. The models for I-girder bridges are obtained based on the work done in previous studies.

In Chapter 5, the proposed simulation approach is applied to evaluate the redundancy and robustness of steel box-girder bridges. An approach is presented to analyze the behavior of damaged steel box girder bridges using a grillage analysis. The results of the analysis are compared to experimental results of a fractured box girder bridge available in the literature.

In Chapter 6, a probability-based procedure is described to perform a probabilistic analysis of progressive collapse should one member be suddenly damaged due to the occurrence of an external hazard. In order to avoid the need to perform a probabilistic progressive collapse analysis, the results of the reliability analysis are used to calibrate a deterministic analysis methodology and criteria to allow a bridge engineer to verify the ability of a bridge system using traditional analysis methods.

Chapter 7 summarizes the accomplishments of this Dissertation and offers guidelines for future research work on this subject.

CHAPTER TWO: REVIEW OF TECHNICAL LITERATURE

2.1 Introduction

This chapter presents a review of the literature on topics related to structural redundancy, robustness, progressive collapse and reliability assessment methods for structural systems and their application to bridges. Section 2.2 presents the definitions and describes existing methods for analyzing redundancy, robustness and progressive collapse of bridge structural systems. In particular, reliability-based approaches are emphasized. Section 2.3 describes existing structural system reliability assessment methods.

2.2 Progressive Collapse and Structural Redundancy and Robustness

2.2.1 Structural Redundancy and Robustness

Redundancy is defined as the provision of additional capacity to reduce the impact of component failures on system safety. For bridges, the availability of additional capacity allows some structural components to fail without bridge collapse. The additional strength of the system is often referred to as reserve strength.

Thus, a redundant structure may be defined as a structure which has additional structural capacity and reserve strength allowing it to carry a higher load than anticipated when considering the capacity of individual members.

Robustness is defined as the capability of a system to perform without failure under unexpected conditions or in an altered state. For structural systems, this definition is consistent with that advanced by Karamchandani, and Cornell (1989) who suggested that structural robustness would represent the ability of a structure to continue to carry some load after the

removal of a structural component. An alternate definition, states that structural robustness represents the capability of a structural system to survive extraordinary circumstances, beyond the scope of conventional design criteria (Björnsson 2010). Thus, in recent work structural robustness is associated with the capacity of a system to withstand the sudden removal of a member from the system accounting for the associated sudden release of the strain energy that was orginally in the member before it failed. This latter definition of robustness is consistent with recent effort to design structural systems that are capable of surviving the sudden removal of one element which is verified through the progressive collapse analysis of the systems.

The definitions for redundancy and robustness provided above are all related to system effects and the ability of the system to continue to carry load after the capacity of individual members are exceeded or after the removal of individual members from the system. In the past, "redundancy" has been adopted as an umbrella term to describe the capacity of a system to withstand all types of local failure. For example, traditionally, bridge engineers recognized three types of redundancy:

- Internal redundancy, where the failure of one element will not result in the failure of other elements of the same member.
- Structural redundancy, which is the result of continuity within a load path.
- Load path redundancy which is related to the number of supporting elements.

According to these definitions bridge engineers would consider two-girder bridges to be load path nonredundant. On the other hand, continuous spans would be considered structurally redundant. These traditional definitions are blanket definitions that do not necessarily take into consideration the ability of the system to redistribute the load to the alternate paths if they exist or

the ductility of the members in the system.

In this dissertation, in order to distinguish between the different types of redundancies that various researchers have been recently investigating the following terminology is used:

1. Redundancy is related to the ability of an originally intact system to resist collapse if the system is subjected to overloading.
2. Robustness is related to the ability of a damaged system which had been subjected to a local failure to continue to function albeit at a reduced system capacity level.
3. Resistance to progressive collapse describes the ability of a structural to survive a sudden local failure and the associated dynamic release of the embedded strain energy.

All the above definitions whether traditional or more recent are descriptive in nature and are not associated with quantifiable measures. Specifically, the traditional bridge engineering definitions do not differentiate between brittle and ductile behavior, do not explain how to account for the uncertainties in estimating member or system capacity, do not specify the type of loading, and do not account for member correlation. This has led many bridge engineers to observe that "the industry lacks a clear, objective, and quantifiable definition of redundancy, and there is no rational minimum benchmark that can be quantified in the design standards" leaving it up to "the bridge owner to select the design criteria of redundancy retrofits such as fracture environment, postfracture capacity, and postfracture performance" Crampton et al (2007).

In a first attempt at providing a method to incorporate redundancy criteria in the bridge design specifications, the AASHTO LRFD (2007) proposed the adoption of load modifiers in the design check equations to account for redundancy during the design of new bridges based on the recommendation of Frangopol and Nakib (1991). Specifically, the AASHTO LRFD recommends

using different load modifiers depending on the levels of bridge redundancy and ductility with values of 0.95, 1.0 or 1.05 for each of the redundancy and ductility properties. An additional factor is related to the importance of the structure in terms of defense/security consideration. However, the specs do not explain how to identify which bridges have low and high redundancy or how to define low and high ductility. As explained in the LRFD Commentary, the recommended values have been subjectively assigned pending additional research.

One the other hand, the LRFR option of the AASHTO MBE (2008) assigns a system factor to be applied on the resistance side of the rating equation with values ranging between 0.85 and 1.0 for bridge configurations that have been demonstrated to have low levels of redundancy. A Table provides some guidelines as to how to assign the appropriate system factor based on bridge geometries and configurations. Some state load rating manuals such as the Florida DOT (2012) have also developed their own sets of system factors. But, these were primarily based on very limited analyses and heavily relied on "engineering judgment".

The AASHTO MBE, also permits the implementation of a detailed analysis approach recommended in NCHRP 406 by Ghosn and Moses (1998) that allows system factors ranging between 0.80 and 1.20 depending on the results of a rigorous nonlinear analysis. Some States have successfully implemented the proposed methodology to justify saving bridges that would have been classified as nonredundant under the traditional definitions (Hubbard et al, 2004).

The importance of having redundancy evaluation methods codified in the manner proposed in NCHRP 406 has been endorsed in NCHRP Synthesis Report 354 by Dexter et al. (2005) who state that "the capacity of damaged superstructures, with Fracture Critical Members removed from the analysis, may be predicted with refined three-dimensional analysis. However, there is a strong

need to clarify the assumptions, load cases and factors, and dynamic effects in these analyses".

Current design specifications are calibrated to provide uniform levels of member safety expressed in terms of the reliability index β. As indicated by Mertz (2008), the application of the AASHTO LRFD load modifiers or the AASHTO LRFR system factors would mean that the structural members, which were originally calibrated to produce a member reliability index β=3.5, will be associated with higher or lower member reliability levels depending on the level of redundancy and ductility. This would be similar to current recommendations in ASCE 7-10 which propose different member reliabilities for different types of members based on the consequence of failure. For example, ASCE 7-10 recommends that a lower reliability level be used for ductile members in bending as compared to connections under shear. Thus, in order to remain consistent with the LRFD philosophy, the calibration of the system factors or load modifiers must be based on reliability methods. However, unlike the approach adopted during the calibration of the AASHTO LRFD that used member reliability as the basis for the calibration of the member resistance factors, the calibration of the redundancy criteria must be based on the reliability of the structural system rather than the individual members. System reliability methods will serve to account for the uncertainties associated with estimating a system's capacity, redundancy, and its robustness.

Although earlier work on structural redundancy was based on developing deterministic analysis methods, several studies have proposed reliability-based approaches to evaluate the probability of system collapse and evaluating system redundancy (Biondini et al. 2008; Chen and Zhang 1996; Frangopol and Nakib 1991; Frangopol and Curley 1987; Hendawi and Frangopol 1994; Paliou et al. 1990, Ellingwood 2006, Ellingwood 2009, Garrick et al. 2004, Ghosn and

Moses 1998, and Stewart and Netherton 2006, Yan and Chang 2010).

Ellingwood (2006 and 2009) suggested that the probability of structural collapse, P(C), due to different damage scenarios, L, caused by multiple hazards, E, be expressed as:

$$P(C) = \sum_E \sum_L P(C|LE)P(L|E)P(E) \tag{2.1}$$

Where $P(E)$ is the probability of occurrence of hazard E; $P(L|E)$ is probability of local failure, L, given the occurrence of E, and $P(C|LE)$ is the probability of structural collapse given the occurrence of a damage scenario L resulting from hazard, E. The probability of collapse will be obtained by summing over all possible hazards and all possible load failure scenarios. The conditional probability of collapse term $P(C|LE)$ is related to the analysis of the response of the bridge to a given damage scenario independently of what hazards have led to the damage. Equation (2.1) assumes independence between the conditional probabilities of failure $P(C|LE)$ calculated for different local failures. This assumption is not strictly speaking correct since we are dealing with the same structure even if it is subjected to different local damage scenarios following the occurrence of multiple hazards and collapse may be due to different failure modes.

The probability of structural collapse must be limited to an acceptable level of risk expressed in terms of a target probability level $P_{threshold}$ which can be determined based on a cost-benefit analysis or based on previous experience with successful designs. This can be represented as

$$P(C) \leq P_{threshold} \tag{2.2}$$

In some cases, the data may be insufficient to define $P(E)$. In such cases, Equation (2.1) can be replaced by

$$P(C|E) = \sum_E \sum_L P(C|L)P(L|E) \tag{2.3}$$

Although Ellingwood (2006, 2009) did not recommend values for $P_{threshold}$, he recommended that it be determined based on a cost-benefit analysis or a more comprehensive risk analysis. This has been hard to implement because of the difficulty of associating structural collapse with a cost to human lives and societal impact.

To this date, the only known studies that provided non-subjective and quantifiable definitions of bridge redundancy along with specific criteria for assessing bridge redundancy are those of Ghosn & Moses (1998) in NCHRP 406 which based their criteria on the performance of typical bridge configurations that have shown in the past adequate levels of redundancy.

2.2.2 Measures of Bridge Redundancy

In NCHRP 406 study, Ghosn & Moses (1998) used the reliability index $\beta_{member}=3.5$ as the basic member safety criterion as established during the calibration of the AASHTO LRFD specifications (AASHTO 2002; Nowak 1999). According to the NCHRP study , redundancy is defined in terms of the difference between the reliability index of the bridge system and the reliability index of the weakest components. The approach includes checking the redundancy of intact bridges under the effect of overloads as well as evaluating the risks to damaged bridges that have been subjected to local failures but have survived these failures. In that sense, checking the redundancy of damaged bridges would be equivalent to checking their structural robustness using the definitions advanced in this Dissertation.

According to NCHRP 406, four limit states are defined to ensure adequate bridge redundancy and system safety as well as functionality. These four limit states include: a) Member failure; b) Ultimate limit state; c) Functionality limit state; and d) Damaged condition limit state.

Figure 2.1 gives a conceptual representation of the behavior of a structure and the different levels that should be considered when evaluating member safety, system safety and system redundancy. For example, the solid line labeled “Intact system” may represent the applied load versus maximum vertical displacement of a ductile multi-girder bridge superstructure or the lateral load versus lateral displacement of a bridge bent or combined superstructure-substructure system. In this case, the load is incremented to study the behavior of an “intact system” that was not previously subjected to any damaging load or event.

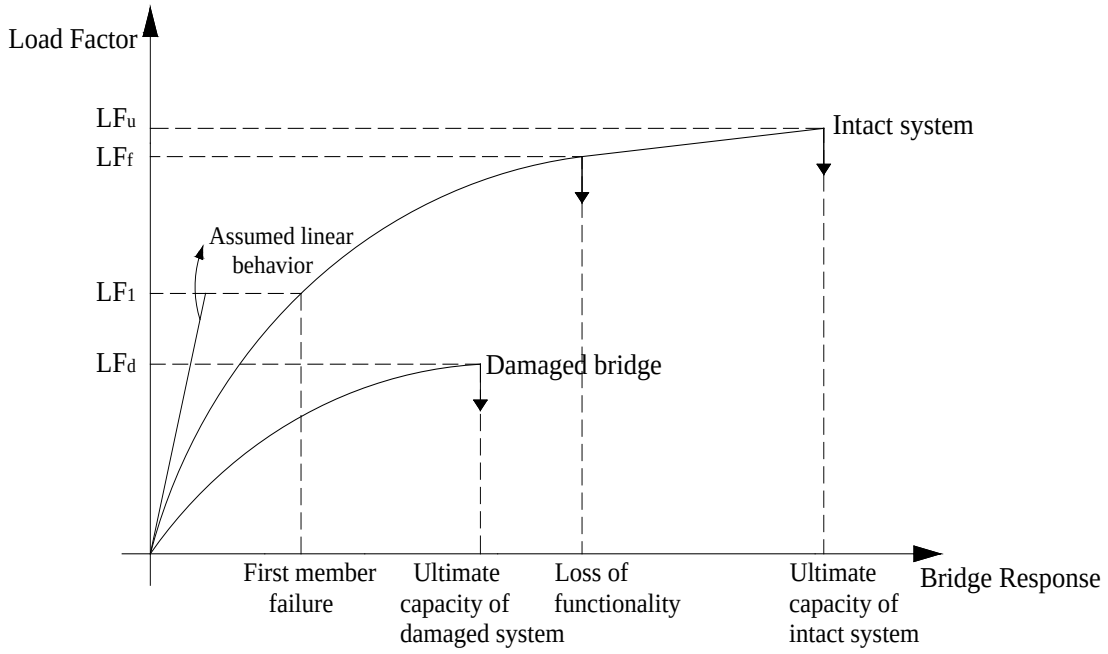

Figure 2.1 Representation of typical behavior of bridge systems

As an example, for the analysis of superstructures under vertical loads, assuming that the vertical live load applied has the configuration of the AASHTO HS-20 vehicle. The bridge is first loaded by the dead load and then the HS-20 load is applied. Usually, due to the presence of safety factors, no failure occurs after the application of the dead load plus the HS-20 load. The first structural member will fail when the HS-20 truck weight is multiplied by a factor LF1. LF1 would then be related to member safety. Note that if the bridge is under-designed or has major deficiencies, it is possible to have LF1 less than 1.0. Generally, the ultimate capacity of the whole bridge is not reached until the HS-20 truck weight is multiplied by a factor LFu. LFu would give an evaluation of system safety. Large vertical deformations rendering the bridge unfit for use are reached when the HS-20 truck weight is multiplied by a factor LFf. LFf gives a measure of system functionality. A bridge that has been loaded up to this point is said to have lost its functionality.

If the bridge has sustained major damage due to the brittle failure of one or more of its members, its behavior is represented by the curve labeled “damaged system”. A damaged bridge may be a bridge that has lost one of its members due to a collision by a truck or due to major degradation of the member capacity due to corrosion. Other damage scenarios may include the failure of a member due to a fatigue fracture or if some extreme event led to shearing off of the member. In this case, the ultimate capacity of the damaged bridge is reached when the weight of the HS-20 truck is multiplied by a factor LFd. LFd would give a measure of the remaining safety of a damaged system. As noted earlier, the ability of a damaged system to continue to carry load has been defined by some researchers as structural robustness. According to that definition, LFd would provide a measure of bridge robustness.

The comparisons between the load multipliers LFu, LFf, LFd and LF1would provide

non-subjective and quantifiable measures of system redundancy. Thus, NCHRP 406 defines three deterministic measures of the system's capacity as compared to the most critical member's capacity:

$$R_u = \frac{LF_U}{LF_1}, \quad R_f = \frac{LF_f}{LF_1}, \quad R_d = \frac{LF_d}{LF_1} \tag{2.4}$$

Where Ru =system reserve rati**o** for the ultimate limit state, Rf=system reserve ratio for the functionality limit state, Rd= system reserve ratio for the damage condition.

The load multipliers, LF_i, provide deterministic estimates of critical limit states that describe the safety of a structural system. These load multipliers are usually obtained by performing an incremental nonlinear Finite Element Analysis of the structure. Because of the presence of large uncertainties in estimating the parameters that control member properties, the bridge response, and the applied loads, the safety of the bridge members or system may be represented by the probability of failure, P_f, or the reliability index, β.

Both P_f and β can be evaluated for each of the four critical limit states identified in Figure 2.1. Assuming that the structural system or member capacity beyond the ability to carry the dead load expressed in terms of R', as well as the applied load, P, follow lognormal probability distributions, the relationship between the reliability index and the load multipliers, LF, for a bridge superstructure subjected to HS-20 truck loading can be approximated by:

$$\beta = \frac{\ln\left(\frac{\overline{R'}}{\overline{P}}\right)}{\sqrt{V_{R'}^2 + V_P^2}} = \frac{\ln\left(\frac{\overline{LF} \times HS20}{\overline{LL} \times HS20}\right)}{\sqrt{V_{LF}^2 + V_{LL}^2}} = \frac{\ln\left(\frac{\overline{LF}}{\overline{LL}}\right)}{\sqrt{V_{LF}^2 + V_{LL}^2}} \tag{2.5}$$

where LF is the load multiplier obtained from the incremental analysis, $LL \times HS20$ is the

expected maximum live load that will be applied on the superstructure within the appropriate return period. *HS20* is the load effect of the nominal HS-20 design truck. V_{LF} is the coefficient of variation of the bridge resistance defined as the standard deviation divided by the mean value. V_{LL} is the coefficient of variation of the applied live load. Both the resistance and the applied live load are expressed as a function of the HS-20 truck load effect which can then be factored out.

Equation (2.5) lumps all the random variables that control the load carrying capacity of a bridge structure into the load multipliers, LF. Advanced methods for evaluating the system reliability are available and have been implemented as described by Ghosn, Moses and Frangopol (2010) and other studies on structural reliability (Melchers, 1999).

Equation (2.5) or similar models for other probability distributions can be used to determine the reliability index, β, for any member or system limit state. The reliability indices corresponding to the load multipliers LF_1, LF_f, LF_u or LF_d of Figure 2.1 may be expressed respectively as β_{member}, $\beta_{functionality}$, $\beta_{ultimate}$, and $\beta_{damaged}$. The relationship between these four reliability indices can be investigated by studying the differences between them represented by $\Delta\beta_u$, $\Delta\beta_f$, $\Delta\beta_d$ which are respectively the relative reliability indices for the system's ultimate, functionality and damaged limit states and are defined as:

$$\Delta\beta_u = \beta_{ultimate} - \beta_{member}$$

$$\Delta\beta_f = \beta_{functionality} - \beta_{member} \qquad (2.6)$$

$$\Delta\beta_d = \beta_{damaged} - \beta_{member}$$

As an example, using the simplified lognormal reliability model for a superstructure under the effect of vertical live loading and assuming that the coefficients of variation of LF_u, LF_f, LF_d

and LF_1 are all equal to the same value, V_{LF}, the probabilistic and deterministic measures are found to be directly related to each other as shown in the following:

$$\Delta\beta_u = \beta_{ultimate} - \beta_{member} = \frac{\ln\left(\frac{\overline{LF_u}}{\overline{LL_{75}}}\right) - \ln\left(\frac{\overline{LF_1}}{\overline{LL_{75}}}\right)}{\sqrt{V_{LF}^2 + V_{LL}^2}} = \frac{\ln\left(\frac{\overline{LF_u}}{\overline{LF_1}}\right)}{\sqrt{V_{LF}^2 + V_{LL}^2}} = \frac{\ln(R_u)}{\sqrt{V_{LF}^2 + V_{LL}^2}}$$

$$\Delta\beta_f = \beta_{functiolity} - \beta_{member} = \frac{\ln\left(\frac{\overline{LF_f}}{\overline{LL_{75}}}\right) - \ln\left(\frac{\overline{LF_1}}{\overline{LL_{75}}}\right)}{\sqrt{V_{LF}^2 + V_{LL}^2}} = \frac{\ln\left(\frac{\overline{LF_f}}{\overline{LF_1}}\right)}{\sqrt{V_{LF}^2 + V_{LL}^2}} = \frac{\ln(R_f)}{\sqrt{V_{LF}^2 + V_{LL}^2}} \quad (2.7)$$

$$\Delta\beta_d = \beta_{damaged} - \beta_{member} = \frac{\ln\left(\frac{\overline{LF_d}}{\overline{LL_2}}\right) - \ln\left(\frac{\overline{LF_1}}{\overline{LL_{75}}}\right)}{\sqrt{V_{LF}^2 + V_{LL}^2}} = \frac{\ln\left(\frac{\overline{LF_f}}{\overline{LF_1}}\frac{\overline{LL_{75}}}{\overline{LL_2}}\right)}{\sqrt{V_{LF}^2 + V_{LL}^2}} = \frac{\ln\left(R_d\frac{\overline{LL_{75}}}{\overline{LL_2}}\right)}{\sqrt{V_{LF}^2 + V_{LL}^2}}$$

Note that for damaged bridges under the effect of the live load LL, the calculation of the reliability index for the damaged system is executed using the 2-year maximum load represented by the load multiplier, LL_2, rather than the maximum load for the 75-year design life represented by the load multiplier, LL_{75}. This distinction is made in order to determine the expected load that would be applied on a damaged bridge which is expected to be lower than the maximum lifetime load. The use of the two-year load is based on the assumption that any major damage to a bridge should, in a worst case scenario, be detected during the mandatory biennial inspection cycle and thus no bridge is expected to remain damaged for more than two years.

Based on the analyses described above, NCHRP 406 observed that bridge superstructures are considered to be adequately redundant if their redundancy ratios defined in Equation (2.4) satisfy the following criteria:

$$\text{Ru} \geq 1.30, \quad \text{Rf} \geq 1.10 \text{ and } \quad \text{Rd} \geq 0.50 \quad (2.8)$$

The above deterministic criteria correspond to the following reliability criteria

$$\Delta\beta_u \geq 0.85,\ \Delta\beta_f \geq 0.25 \text{ and } \Delta\beta_d \geq -2.70 \quad (2.9)$$

According to these criteria, a bridge will have an adequate level of redundancy and robustness when the differences between the system reliability index and the member reliability index under four critical limit states (member capacity, ultimate system capacity, system functionality, damaged condition) are higher than a set of target values given in Equation (2.9). The target values were determined based on bridge configurations which are known to provide adequate levels of safety and redundancy.

Bridges that do not satisfy the set criteria will have to be strengthened to increase their system reliability levels or else the bridge topology may be changed to meet the proposed criteria. It is noted that increasing member strength will not lead to higher redundancy level but will ensure higher overall member and system safety.

Following the criteria set by Ghosn & Moses (1998), the evaluation of the redundancy of a bridge system requires the calculation of the reliability index under the previously listed four limit states if probability of failure P(F) can be accurately calculated. However, the criteria proposed by Ghosn & Moses (1998) were based on current practice in the safety evaluation of bridge structures established using simplified analyses models that considered pre-identified single modes of failure. The simplified methods were used in the recent past due to the difficulties encountered in using existing reliability methods to analyze realistic models of structural systems. In fact, the theory of structural system reliability has seen great advances in the past three decades and there currently exist several approaches for analyzing the reliability of structures. Section 2.3 will review the existing reliability methods.

2.2.3 Progressive Collapse

Progressive collapse occurs if a local structural damage causes a chain reaction of structural elements failures, disproportionate to the initial damage. According to ASCE 7-05 (ASCE 2005), **Progressive Collapse** is defined as the spread of an initial local failure from element to element resulting, eventually, in the collapse of an entire structure or a disproportionately large part of it.

The Ronan Point collapse in England in 1968, initiated the interest of building engineers in the subject of progressive collapse. In the U.S., the collapse of the Twin Towers of the World Trade Center in 2001 following that of the Alfred P. Murrah Federal Building in downtown Oklahoma City in 1995 as well as the I-35W Mississippi River bridge in Minnesota in 2007 reawakened the interest in the subject of progressive collapse of buildings and bridges. As a result, engineers started considering partial damage scenarios to study the consequences of a failure on a building's structural integrity. Guidelines and codes were issued to provide assistance to building engineers. Specifically, the Federal Emergency Management Agency provides general guidance for performing progressive collapse analysis (FEMA 1997). The Eurocode has also provided general comments about designing structures to prevent damage to an extent disproportionate to the original abnormal loading event (Eurocode8 1994). More recently, both the General Services Administration (GSA) (GSA 2000) and the Department Of Defense (DOD) (DOD 2002) have issued guidelines which provide general information about the approach and method for performing a progressive collapse analysis. In addition, non-mandatory commentary of the American ASCE 7-10/ANSI A58 standard recommends several general approaches to design against progressive collapse (ASCE 2010).

Criteria for the progressive collapse have been established by the U.S. General Service

Administration (GSA) for Federal office buildings. However, no criteria are currently available for important bridge structures. Furthermore, the existing criteria were not established based on reliability principles as has been the case with recent structural design and safety assessment specifications.

Progressive Collapse includes two types of loadings (Marjanishvili 2004): The primary load which causes a structural element to fail, and the secondary loads which are generated due to the structural motions caused by the sudden brittle failure of the element. External abnormal loads, such as blast pressures due to explosive attacks, could cause primary loads, while secondary loads result from the internal static and dynamic forces that are caused by sudden changes in the load path through the structure's geometry. Although estimation of the primary loads is important, most analyses of progressive collapse have focused on the effects of the secondary loads. Focusing on the secondary loads makes the progressive collapse analysis process independent of the hazards that cause the sudden loss of the identified damage initiating elements.

Analysis methods used to evaluate the possibility of progressive collapse vary widely, ranging from the simple two-dimensional linear elastic procedure to complex three-dimensional nonlinear time history analysis. There have been a number of research efforts worldwide to quantify the nature of abnormal loading, which include linear-elastic static (Grierson et al. 2005; Kima and Kimb 2009; Marjanishvili 2004) ; nonlinear static (Marjanishvili 2004); linear-static dynamic (Kima and Kimb 2009; Marjanishvili 2004; Powell 2009); and nonlinear dynamic (Kaewkulchai and Williamson 2004; Khandelwal et al. 2009; Kima and Kimb 2009; Marjanishvili 2004). The simplest analysis methodology is static linear elastic analysis and the most exhaustive procedure is nonlinear dynamic analysis, which yields more accurate results. (Marjanishvili and Agnew 2006; Powell 2005) have shown that linear static and dynamic analysis cost the least time,

about 3 minutes, which is compared with 10 minutes for nonlinear static analysis and 60 minutes for nonlinear dynamic analysis using a computer with 3 GHZ CPU. Yet, linear elastic methods are notriously inaccurate to describe the response of a damaged system. Instead, researchers have generally favored the use of nonlinear static models and accounted for the dynamic effects that result from the sudden release of energy using a very conservative dynamic amplification factor applied on the total loads. The validity of this conservative approach to bridge structures has not been verified and there is a need to develop a methodology and criteria to analyze the progressive collapse of bridge systems using modern code development techniques that take into consideration all the uncertainties to verify that the methodology will lead to the design of bridge structures that will provide adequate levels of reliability.

The objective of this study is to use advanced reliability methods for analyzing the progressive collapse of bridge structures with the final goal of using such results for developing consistent reliability-based progressive collapse criteria that can be used on a regular basis in bridge engineering practice.

2.3 Structural Reliability Methods

Based on the above discussion it is clear that the evaluation of system safety, structural redundancy, robustness and the analysis of progressive collapse must be performed using structural reliability methods that take into consideration the uncertainties in assessing the material properties, the applied loads and the behavior of the system under the effect of the applied loads. Over the last three decades, researchers in the field of structural reliability have proposed several methods to solve problems related to estimating the reliability of complex structural systems. These methods can be broadly divided into three categories: a) methods based on approximate

solutions of the probability integral including the First-Order Reliability Method (FORM) and Second-Order Reliability Method (SORM), and the Response Surface Method (RSM); b) basic simulation methods such as the crude Monte-Carlo simulation, Importance Sampling, Latin Hypercube and Directional Sampling; and c) Recently developed Markov chain-based advanced simulation methods such as Subset Simulation (SS) and its variants, and Line Sampling-Stepwise Algorithm (LSA). For comparison purposes, this section gives some simple examples to illustrate how to implement the most common of these reliability methods for evaluating the probability of failure of structures.

The basic structural reliability problem can be described by considering only one load effect S resisted by one resistance R. For convenience, but without loss of generality, the structural element or system will be considered to have failed if its resistance R is less than the load effect S acting on it. Probability of failure can be expressed as:

$$P_f = \Pr[R \le S] \tag{2.10}$$

If R and S follow independent normal distributions, then

$$P_f = \Phi\left(-\frac{\overline{R} - \overline{S}}{\sqrt{\sigma_R^2 + \sigma_S^2}} \right) \tag{2.11}$$

Where, Φ is the cumulative function of the standard normal distribution. $\overline{R}$, $\overline{S}$ are the mean of R and S. σ_R^2 , σ_S^2 are the standard deviations of R and S.

For many problems, it may not be possible to reduce the structural reliability problem to a simple R versus S formulation with R and S independent random variables. In general, R and S are functions of basic variables and factors, such as the intensity of the applied loads, the response of

the structure to this load, material strength, and densities and perhaps the dimensions of the structure and other material properties. In such cases, the failure probability can be generalized as:

$$P_f = \Pr\{G(\Theta) \le 0\} = \int_{G(\Theta)} f(\Theta) d\Theta = \int I_F(\Theta) f(\Theta) d\Theta \qquad (2.12)$$

Where the vector $\Theta = [\theta_1, ...\theta_n]$ represents an uncertain state of the system with joint probability function $f(\Theta)$. $G(\Theta)$ is the failure or limit-state function, defining a safe state when G>0 and a failure state when G<0. The hyper-surface separating the safe from the failure domain G=0 is called the limit-state. F is the failure region. I_F is an indicator function; where $I_F(\Theta) = 1$ if $\Theta \in F$ and $I_F(\Theta) = 0$ otherwise.

2.3.1 First Order and Second Order Reliability Methods

The First Order and Second Order Reliability Methods (FORM and SORM) approximate the limit-state function with, respectively, a first-order or an incomplete second order function. FORM maps the joint probability function $f(\Theta)$ into a standard normal space in which the failure function separates the overall space into a failure and a safe domain. The standard normal space consists of the space where each random variable is shifted by its mean value and normalized with respect to its standard deviation. FORM would then find the location of the closest point on the failure surface to the mean value (which is know at the origin) to define the "design point" or the most likely failure point. In this case, the reliability index β is defined as the minimum distance between the origin to the failure function. If the limit state function is linear then it can be proven that $\Phi(-\beta) = P_f$ and the reliability problem reduces to an optimization problem that will search for the minimum distance. When the random variables are not Normal, the failure surface can still be represented in the standardized normal space, by assuming that a probability preserving

transformation $\Theta = T(U)$ exists where U is an independent standard normal vector that transforms the probability integral into

$$P_f = P\{G(\Theta) \le 0\} = \int_{G(\Theta)} f(\Theta)d\Theta = \int I_F(\Theta) f(\Theta)d\Theta = \int I_F(U)\Psi(U)dU \qquad (2.13)$$

Where $\Psi(U)$ is the n-dimensional standard normal density with independent components. Although such transformation functions are usually difficult to determine, an approximate transformation $\Theta = T(U)$ has been proposed by Rosenblatt (Rosenblatt 1952). In this case, the minimum distance, β, will lead to an approximation of the probability of failure:

$$P_f \approx \Phi(-\beta) \qquad (2.14)$$

Where $\beta = |U^*|$ is the reliability index which gives the shortest distance between the failure point and the origin of the normalized space, and Φ is the cumulative probability function of the standard normal distribution and U^* is found from

$$U^* = \min|U| \text{ for } \{U : G(U) \le 0\} \qquad (2.15)$$

The main computational task in FORM is to find the location of the U^*-point by an iterative algorithm. The failure function is replaced by its tangent hyperplane at U^* to facilitate this iterative algorithm. This first order expansion led to designating this algorithm as the First Order Reliability Method (FORM).

Using the first order expansion, the limit state function is approximated by $G = g(X_1^*, X_2^*, ..., X_n^*) + \sum_{i=1}^{n}(X_i - X_i^*)(\frac{\partial g}{\partial X_i})_{X^*} = 0$ and the mean of G,

$\mu_G = \sum_{i=1}^{n} (\mu_{X_i} - X_i^*) \left(\frac{\partial g}{\partial X_i} \right)_{X^*}$. If the random variables are independent, the standard deviation of G is obtained as, $\sigma_G = \sqrt{\sum_{i=1}^{n} \left(\sigma_{X_i} \frac{\partial g}{\partial X_i} \right)_{X^*}^2}$. Because the design point whose coordinates X_i^* cannot be known a priori, it is hard to obtain the reliability index $\beta = \frac{\mu_G}{\sigma_G}$. If σ_G is linearized such that

$$\sigma_G = \sum_{i=1}^{n} \alpha_i \, \sigma_{X_i} \left(\frac{\partial g}{\partial X_i} \right)_{X^*} \quad \text{where} \quad \alpha_i = \frac{\left(\sigma_{X_i} \frac{\partial g}{\partial X_i} \right)_{X^*}}{\sqrt{\sum_{j=1}^{n} \left(\sigma_{X_j} \frac{\partial g}{\partial X_j} \right)_{X^*}^2}},$$

then, $\beta = \frac{\mu_G}{\sigma_G} = \frac{\sum_{i=1}^{n} (\mu_{X_i} - X_i^*) \left(\frac{\partial g}{\partial X_i} \right)_{X^*}}{\sum_{i=1}^{n} \left[\alpha_i \sigma_{X_i} \left(\frac{\partial g}{\partial X_i} \right)_{X^*} \right]}$

where the design points $X_i = \mu_{X_i} - \beta \alpha_i \sigma_{X_i}$ (2.16)

The FORM algorithm for determining the design point can be generalized as follows:

1. Assume a reliability index β.
2. Choose initial values for design points $X_i^* = \mu_{X_i}$ (i=1,2…n where n is the number of random variables).
3. Calculate α_i.
4. Obtain new design points from Equation (2.16).
5. Repeat 4-5 until the design points are stable.
6. Plug in the design points into limit state function $G = g(X_1, X_2, ..., X_n) = 0$

7. Check if G=0. If G is not sufficiently close to zero, then assume a new reliability index $\beta_{m+1} = \beta_m - G_m \times \frac{\Delta\beta}{\Delta G}$ and repeat 4-6 until G=0 is satisfied.

8. The probability of failure is approximated by $P_f \approx \Phi(-\beta)$

Example:

An example from Rajashekhar and Ellingwood (1993) is selected to illustrate how to use FORM to calculate the probability of structural failure. This example involves a cantilever beam with a rectangular cross s ection subjected to a uniform loading. The limit sate of serviceability assumes that the maximum deflection at the free end should not exceed $L/325$, and is given by:

$$g = -\frac{wbL^4}{8EI} + \frac{L}{325} \tag{2.17}$$

Where, w, b, L, E and I are the uniform load, width, span length, modulus of elasticity and moment of inertia of the cross section, respectively. E and L are deterministic with fixed to 2.6×10^4 Mpa and 6 m, respectively. w and the depth of the cross section are normally distributed random variables with mean values of 1000N/m^2 and 250mm and Coefficients of variation of 0.2 and 0.15, respectively. If we substitute for E and L in Equation (2.11), then the limit state function becomes

$$G(\Theta) = 18.46154 - 7.476923*10^{10} * \frac{\theta_1}{\theta_2^3} = 0 \tag{2.18}$$

Where, θ_1 is the uniform load in MPa and θ_2 is the depth of the rectangular cross section in mm.

A trial and error solution shows that the design point is (1114.9 N/m^2, 165.3mm) for the limit state function drawn as curve a in Figure 2.2. The shortest distance between a and the origin leads to a reliability index β =2.33 which gives $P_f = \Phi(-\beta) = 9.903 \times 10^{-3}$. Unfortunately, since Equation (2.18) is nonlinear, the failure probability for normal variables cannot be given exactly by $P_f = \Phi(-\beta)$. This is illustrated in Figure 2.3, where the design point for curve a is also the design point for the limit state functions described by curves b and c. In terms of first-order theory, each of these limit states has an identical value of β, and hence an identical nominal failure probability $P_f = \Phi(-\beta)$: yet it is quite clear from Figure 2.3 that the actual probability contents of the respective failure regions are not identical. The magnitude of the error depends on how different the curves are from a straight line.

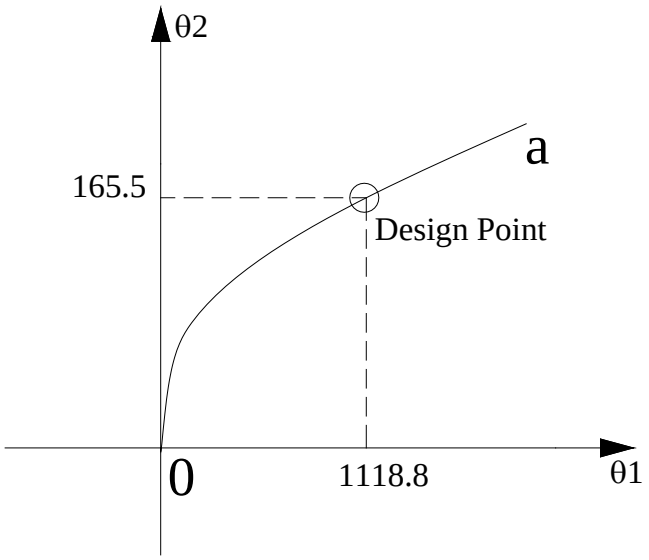

Figure 2.2 Limit State Function of Equation (2.12)

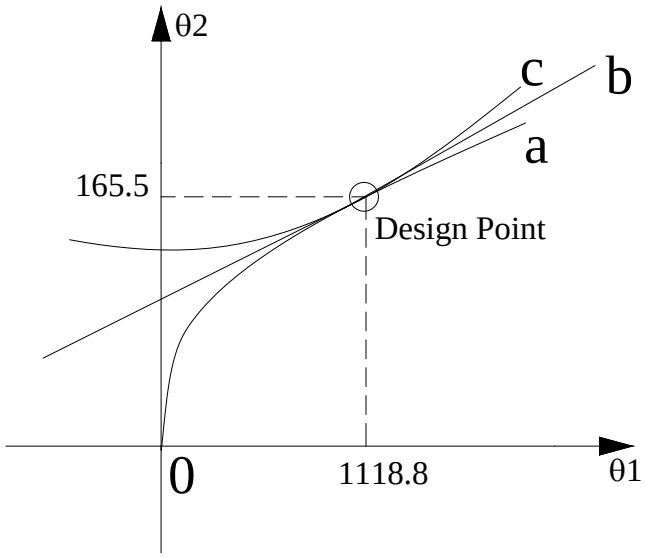

Figure 2.3 Inconsistency between β and P_f for different forms of limit state functions

The FORM algorithm is often very efficient and can converge to a reasonable avle of β after a few iterations. However, it requires the availability of an explicit formulation of the failure function. Also, this method is not robust when solving complex limit-state equations, such as a highly non-linear failure points or a combination of failure functions (Melchers 1999). SORM algorithms have also been used and lead to improved accuracy at the expense of higher levels of complexity of the algorithm. However, the need to have an explicit formulation of the limit state function and the difficulty of solving complex problems remain important hindrances for using SORM.

2.3.2 Response Surface Method (RSM)

In most practical problems, the limit state function can not be expressed in an explicit form. Rather it may be known implicitly through a numerical algorithm like a finite element analysis. The classic FORM and SORM algorithms cannot be implemented directly, as they require a closed

and preferably differentiable, form for the limit state function G. Therefore, the Response Surface Method (RSM) has been widely used for solving practical structural reliability problems. RSM provides a method to approximate the unknown limit state function by a polynomial function of order m (Rajashekhar and Ellingwood 1993). The basic procedure involves the identification of the unknown coefficients of an m^{th} order polynomial function $\tilde{G}$ that approximates the exact response limit state function around a design point candidate. The process needs to represent the structural response most accurately in the area around the design point, with lower accuracy acceptable elsewhere. If the approximating surface fits the point responses reasonably well, then a good estimate of the probability of failure can be obtained. The mathematical formulation of the procedure is presented as explained next.

Let the structural response be an implicit function $G(\Theta)$ with random variables Θ. Let $\bar{\theta}$ represent a set of points in Θ. The "response surface" approach is to seek a function $\bar{G}(\theta)$ which best fits the discrete set of values of $G(\bar{\theta})$. The unknown limit state function is often approximated by a polynomial function $\bar{G}(\theta)$ of order m. The order m of the polynomial selected for fitting to the discrete point outcomes will affect both the number of such evaluations required and the number of derivatives which need to be estimated. It is true up to a certain degree that a higher polynomial improves the accuracy of the approximation at the expense of additional computation (Rajashekhar and Ellingwood 1993). The rate of increase in accuracy reduces with the order of the polynomial but the computational effort increases exponentially since higher order polynomials involve greater numbers of unknown coefficients and require more structural analyses. The degree of $\bar{G}(\theta)$ is also upper-bounded by the shape of the exact response surface around the region of interest. A lower order of $\bar{G}(\theta)$ than the actual order of $G(\theta)$ results in a well-conditioned system

of linear equations to solve for the unknown coefficients of the polynomial, while a higher order of $\overline{G}(\theta)$ than the actual order of $G(\theta)$ yields an ill-conditioned system of equations (Engelund and Rackwitz 1992).

Generally, a second order polynomial is most often used for the response surface (Bucher and Bourgund 1990; Rajashekhar and Ellingwood 1993). In that case:

$$\overline{G}(\Theta) = A + \Theta^T B + \Theta^T C \Theta \tag{2.19}$$

Where, the undetermined coefficients are A, $B^T = [B_1, B_2, \ldots, B_m]$ and

$$C = \begin{bmatrix} C_{11} & \ldots & C_{1m} \\ \ldots & \ldots & \ldots \\ Sym & \ldots & C_{mm} \end{bmatrix}$$

A simplified form for Equation (2.19) is given in Equation (2.20) without the cross terms:

$$\overline{G}(\theta_1, \theta_2, ..., \theta_m) = a + \sum_{i=1}^{m} b_i \theta_i + \sum_{i=1}^{m} c_i \theta_i^2 \tag{2.20}$$

Where, a, b_i and c_i are unknown coefficients to be determined. And θ_i are the random variables that control the response function.

Because the best points for fitting the approximating response surface to the actual limit state function usually are not known a *priori*, an iterative search technique (Bucher and Bourgund 1990) is used to locate these points. These points might be mean point θ_m and points $\theta_i = \theta_{mi} \pm h_i \sigma_i$, where h_i is an arbitrary factor and σ_i is the standard deviation of Θ_i. Using these points, the approximating surface $\overline{G}(\overline{\theta})$ for the assumed mean point θ_m can be determined exactly. If the approximating surface is located in the optimal position, the mean point θ_m would coincide

with the point of maximum likelihood (the design point) and the distance from this point to the origin would be a minimum in standardized normal space. If θ_m is no the design point, some other point, say θ_d, can be found on the approximating surface $\overline{G}(\overline{\theta})$ which is closer to the origin and which is therefore the best estimate of the design point. Once θ_d is located, an additional numerical experiment is performed to evaluate the response surface and a new mean point θ_m^* can be obtained by linear interpolation between θ_m and θ_d.

$$\theta_m^* = \theta_m + (\theta_d - \theta_m)\frac{G(\theta_m)}{G(\theta_m) - G(\theta_d)} \tag{2.21}$$

The iteration process shown in Figure 2.4 is carried out using the new mean point until convergence is reached and the design point is identified. There are a lot of criteria that can be used to stop the iteration, such as steady value of β or identical values θ_m and θ_d. The process is illustrated in Figure 2.4.

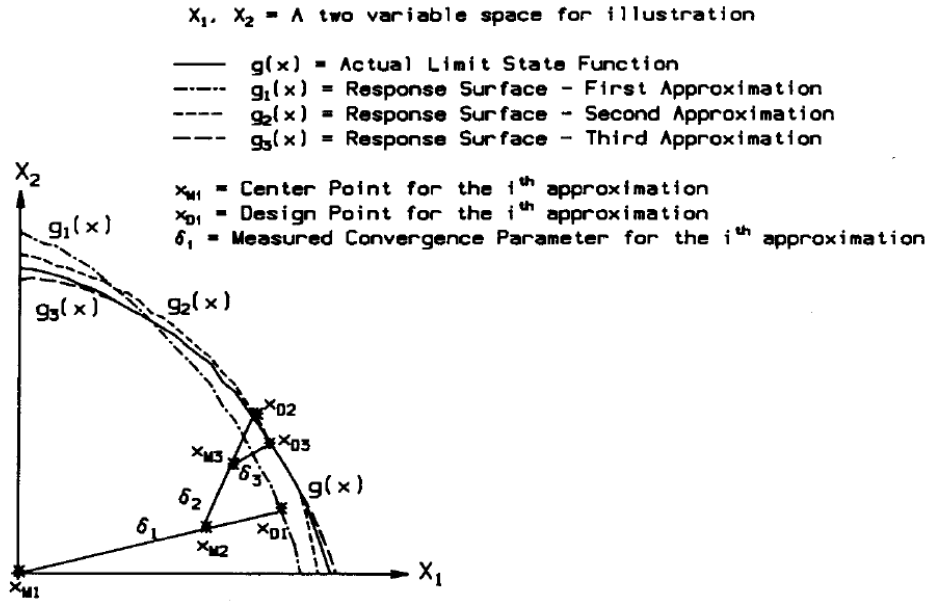

Figure 2.4 Illustration of iteration of Response Surface Method to find Design Point

Example:

The same example as used in FORM from Rajashekhar and Ellingwood (1993) is used to illustrate how to use Response Surface Method (RSM) to calculate the probability of structural failure.

The response surface is approximated by a second-order polynomial without cross terms and there are five unknown coefficients. The approximated response surfaces at the limit state for each iteration are given in Figure 2.5. The error for the distance from the center point to the design point as well as the design points are listed in Table 2.1.

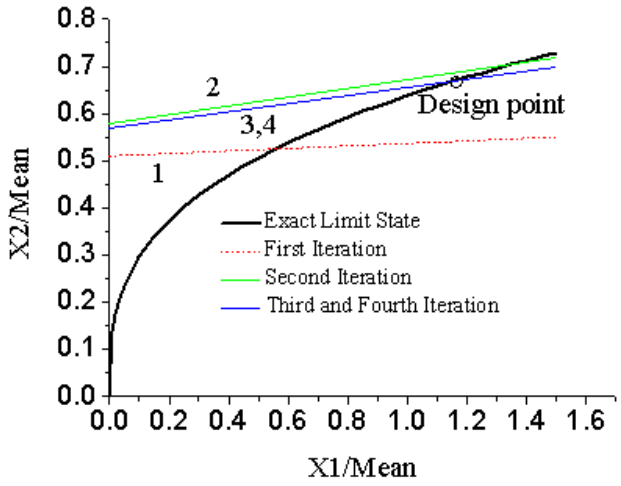

Figure 2.5 Approximation of the exact limit state (X1 and X2 are uniform load in Mpa and the depth of rectangular cross section in mm)

Table 2.1 Convergence of Design Points

Iteration	Error	θ_1 X1	θ_2 X2	Approximate Response surface
1	94.9116	1115.309	155.0884	-34.3182-8064.5925*X_1+0.3700*X_2-0.000583*$(X_2)^2$
2	5.1054	1114.591	171.0166	-190.1659-38514.6670*X1+2.1854*X2-2.1854*$(X2)^2$
3	0.1556	1139.212	165.9137	-261.442-52686.6*X1+3.1567*X2-0.00735*$(X2)^2$
4	0.001989	1136.576	166.3412	-167.294-21892.4*X1+1.9146*X2-0.00456*$(X2)^2$

At the final iteration, the reliability index β is 2.333 and the corresponding probability of failure is $9.824*10^{-3}$.

This example involves two random variables and five iterations are good enough to converge to the exact value. In actual structures, the number of random variables is much higher, which requires a large number of structural analysis and FORM iterations to get convergence. Response Surface Method works well provided the design point or the point of maximum likelihood can be identified and that reasonable decisions can be made about the points to be used for fitting the response surface. For large systems, design point cannot always be identified without subjective interference. Adaptive Response Surface methods are often used but convergence cannot be guaranteed (Guan and Melchers 2001).

2.3.3 Simulation Methods

In practice, limit state functions usually are of more not linear or second order functions. And the random variables are unlikely to be normally distributed. Although, the limit state

function may be approximated by linear and second order equations. For large systems with a high number of dimensions, FORM and RSM are not efficient. Simulation methods form a class of approximate numerical solutions to the probability integral Equation (2.8) applicable to problems for which the limit state function $G(\Theta)$ may have any form, and for which the probabilistic description of the random variables is unrestricted. The most basic simulation methods are based on the Monte Carlo approach. The following sections will describe the most commonly used simulation methods.

2.3.3.1 Monte Carlo Simulation (MCS)

The Monte Carlo (Fishman 1996; Rubinstein 1981) simulation method has been widely used in the past because of its robustness and its ability to solve problems with complex failure regions.

Monte Carlo Simulation techniques involve sampling at random to artificially simulate a large number of experiments and to observe the results. To evaluate the probability of structural failure, first, sample each random variable θ_i randomly to give a set of sample values $\hat{\theta}_i$. The limit state function $G(\hat{\theta})$ is then checked. If the limit state $G(\hat{\theta}) \le 0$, the structure fails. The experiment is repeated many times, each time with a randomly chosen vector $\hat{\theta}$. If N trials are conducted, the probability of failure for the limit state function of Equation (2.10) is given as:

$$\tilde{P}_f = J_1 = \frac{1}{N}\sum_{i=1}^{N} I_F[G(\hat{\theta}_i) \le 0] \qquad (2.22)$$

Equation (2.22) is an unbiased estimator of Equation (2.10).

Example:

The same example as used in FORM and Response from Rajashekhar and Ellingwood (1993) is used to illustrate how to use Monte Carlo Simulation method to calculate the probability of structural failure. Figure 2.6 shows how the probability of failure varied along with the number of samples. The result eventually reaches the exact solution $9.50*10^{-3}$ with 19000 samples.

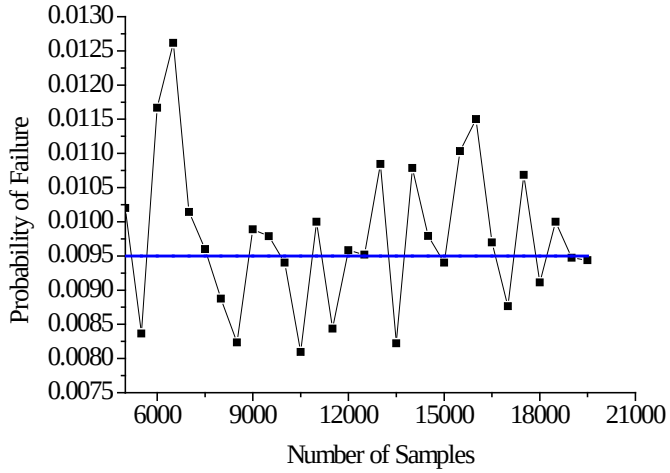

Figure 2.6 The probability of failure using different number of samples

The main disadvantage of MCS stems from its inefficiency when solving problems with large numbers of random variables and small probabilities. The number of samples must be proportional to $1/P_c$ (P_c is the probability of failure) in order for the Monte Carlo simulation to achieve an acceptable level of accuracy. Since the probability of failure, P_f, of structural systems is expected to be on the order of 10^{-6} or less and since each sample requires the nonlinear analysis of a complex structural system, it would require several days of computational effort for the Monte Carlo approach to yield accurate results for a realistic models of a structure despite current improvements in computer powers. Variations on the traditional Monte Carlo Simulation, such as

Importance Sampling, will be introduced in the following part.

2.3.3.2 Importance Sampling

In the integral Equation (2.8), for small probabilities P_f, very large sample sizes are required to get a reasonable confidence level, which means that the computational effort required to obtain a good estimate of probability of failure becomes excessive. Importance sampling techniques (Hammersley and handscomb 1964; Melchers 1989; Rubinstein 1981; Schueller and Stix 1987; Shinozuka 1983) have been developed over the past few decades to shift the underlying distribution towards the failure region so as to gain information from rare events more efficiently.

The integral Equation (2.10) can be equivalently written as:

$$P_f = P\{G(\Theta) \le 0\} = \int_{G(\Theta)} f(\Theta)d\Theta = \int I_F(\Theta) f(\Theta)d\Theta = \int I_F(\Theta)\frac{f(\Theta)}{h(\Theta)}h(\Theta)d\Theta \qquad (2.23)$$

Where, $h(\Theta)$ is the importance-sampling probability density function, then probability of failure P_f can be estimated by the following unbiased estimator :

$$\tilde{P}_f = \frac{1}{N}\sum_{j=1}^{N}\left\{I_F[G(V_j) \le 0]\frac{f_\theta(V_j)}{h_v(V_j)}\right\} \qquad (2.24)$$

Where V_j is a vector of samples taken from the importance sampling function $h_v()$. $h_v()$ should be selected such that most information is extracted from the sample points V_j used. This means that the samples should be taken in the vicinity of points of maximum likelihood of $f_\theta()$ and lying within $G(\theta) < 0$.

Generally speaking, it is difficult to derive optimal functions $h_v()$. However, appropriate functions may be selected on a priori grounds. In the n-dimensional reliability problem, the region of most interest is the hyperzone $G(\theta) < 0$. For a two-dimensional problem, this zone is just to the right of the point θ^* shown in Figure 2.7. The point θ^* is known as the point of "maximum likelihood". It is not difficult to recognize and it has been shown that this point corresponds to the so-called design or check point θ^* in first-order reliability method theory. A direct approach to get θ^* is to use a numerical maximization technique(Shinozuka 1983). This approach suggests that the point at which $f_\theta()$ is a maximum is a reasonable approximation to the region of most interest, namely the region of greatest probability mass contained by $f_\theta()$ within the failure region.

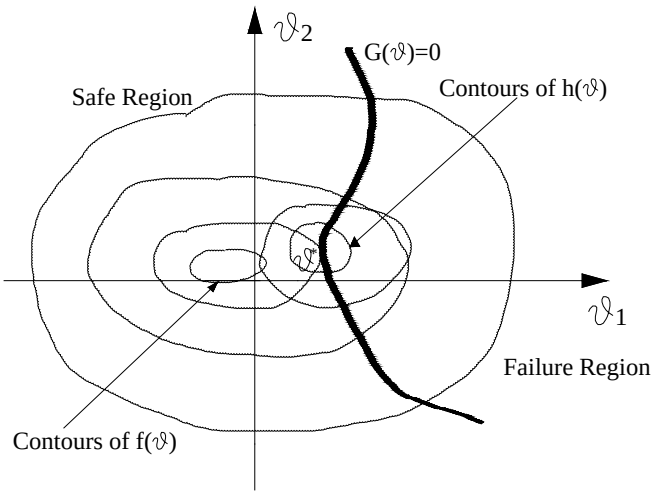

Figure 2.7 Importance sampling function $h_v()$

The success of the method relies on a prudent choice of the importance sampling density (ISD), which undoubtedly requires knowledge of the system in the failure region. When the dimension n of the uncertain parameter space is not too large and the failure region F is relatively simple to describe, many schemes for constructing the ISD, such as those based on design points

(Au et al. 1999; Der and Dakessian 1998; Harbitz 1983; Hohenbichler and Rachwitz 1988; Melchers 1989; Papadimitriou et al. 1997; Schueller and Stix 1987; Shinozuka 1983) or adaptive pre-samples (Ang et al. 1992; Au and Beck 1999; Bucher 1988; Karamchandani et al. 1989), are found to be useful. A simple example is used to show how a simple ISD is constructed based on the proposed method by (Melchers 1989).

Example:

The same example as used in FORM and Response from Rajashekhar and Ellingwood (1993) is used to illustrate how to use Importance Sampling Method to calculate the probability of structural failure.

Based on FORM, the design points are (1114.9 N/m^2, 165.3mm). These design points are then used to centre the importance sampling function $h_v()$ which is taken as:

$$h_v() = \prod_{i=1}^{5} h_{v_i}() \tag{2.25}$$

where h_{v_i} is a normal distribution with mean $\mu_{v_i} = \theta_i^*$ design point and Coefficients of Variation taken $2V_{\theta_i}$ where V_{θ_i} is the C.O.V. of θ_i (Melchers 1989). Based on Equation (2.24), the probability of failure is estimated as $9.50 \times 10^{(-3)}$ with 2000 samples.

When the dimension n is large and the complexity of the problem increases, however, it may be difficult to gain sufficient knowledge to construct a good ISD (Schueller et al. 1993).

2.3.3.3 Latin Hypercube Sampling

This technique was first described by McKay in 1979 (McKay et al. 1979). It was further

elaborated by Ronald L. Iman, and others in 1981 (Iman et al. 1981). Detailed computer codes and manuals were published in 1980 (Iman et al. 1980) and updated in 1998 by (Wyss and Jorgensen 1998).

Monte Carlo simulation typically picks points at random within the domain, Latin Hypercube sampling samples the entire domain more systematically.

Latin hypercube sampling begins by estimating each parameter's uncertainty using a probability distribution. Then we would break up the distribution into N equal probability segments and a value for the parameter would be generated from each segment. A visualization of a sample segmented pdf is below for N = 10 and assuming a normal distribution for the probable parameter values. Notice that each segment has equal area.

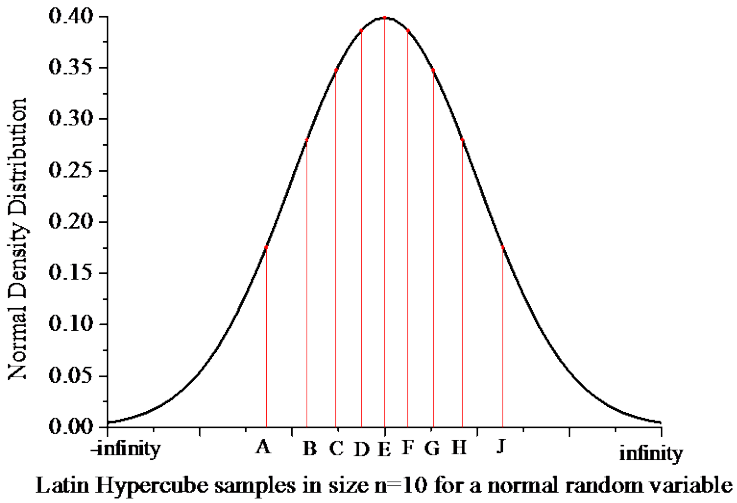

Latin Hypercube samples in size n=10 for a normal random variable

(a)

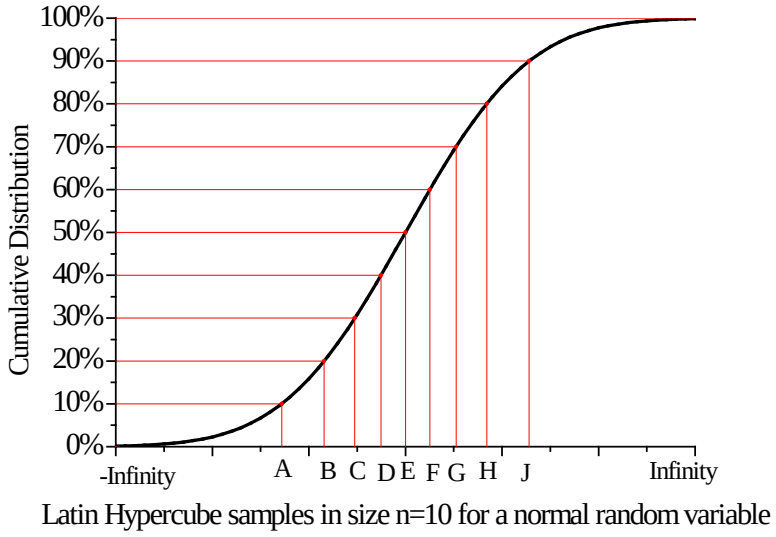

(b)

Figure 2.8 Intervals used with a Latin Hypercube Sample of size n=10 in terms of the Density Function and Cumulative Distribution Function for a Normal Random Variable

To help clarify how random samples are generated using Latin Hypercube Sampling method, consider the example used in Monte Carlo Simulation from Rajashekhar and Ellingwood (1993).

The failure equation $G = \dfrac{7.476923 * 10^{10} * \dfrac{\theta_1}{\theta_2^3}}{18.46154}$ and if G>=1, failure occurs.

Figure 2.9 indicates the empirical distribution of output G using four different numbers of samples: 10 samples in ①, 50 samples in ②, 100 samples in ③ and 500 samples in ④.

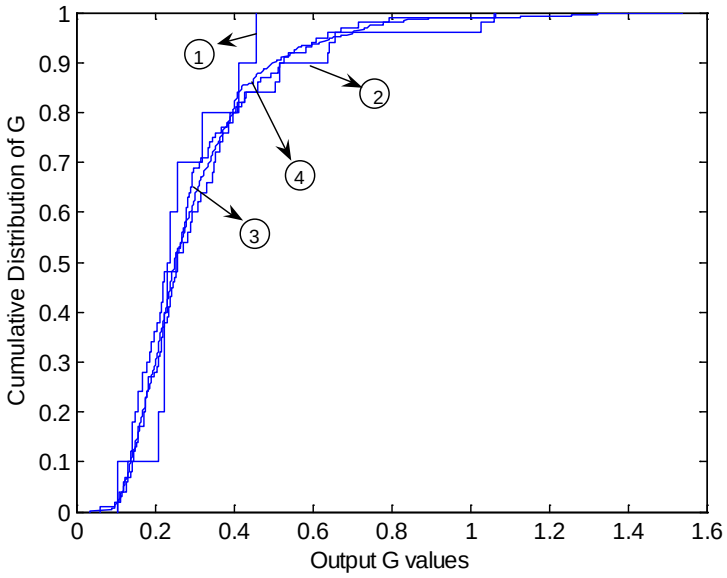

Figure 2.9 Empirical Distribution of G

From the empirical distribution curves of G, the mean, standard deviation and probability of failure can be obtained. Figures 2.10, 2.11 and 2.12 show how the mean, standard deviation of output G and the probability of failure varied along with number of samples.

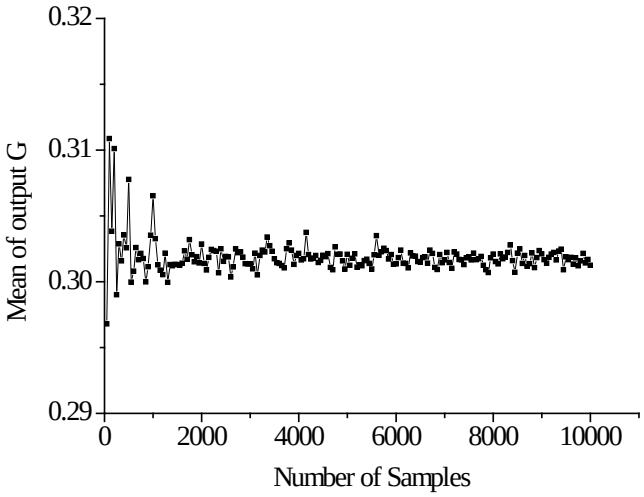

Figure 2.10 Mean of output G along with number of samples

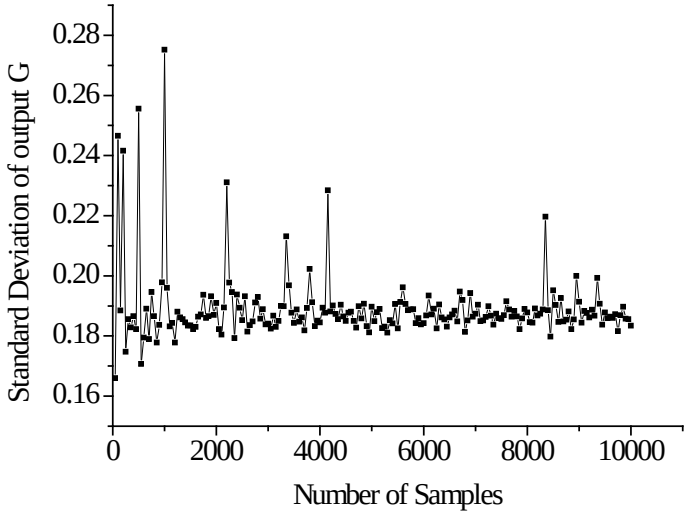

Figure 2.11 Standard Deviation of output G along with number of samples

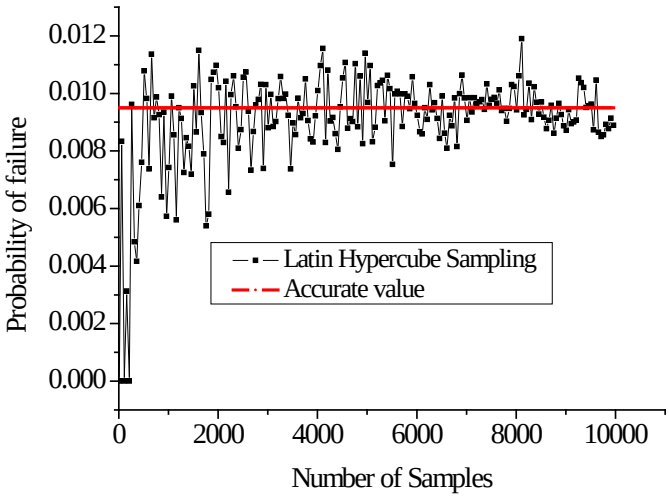

Figure 2.12 Probability of failure along with number of samples

We can see that LHS method can give a good estimate of the output, however, the standard deviation of output is greatly varied with the increasing of the number of samples. The failure of

failure pf =8.89x10$^{(-3)}$ using 10000 samples based on Latin Hypercube Sampling method is compared with the accurate pf=9.50x10$^{(-3)}$ in Figure 2.12.

2.3.4 Advanced Markov-chain Based Simulation Method

Recently, some Markov-chain based advanced simulation techniques have been developed to study the reliability of systems with large numbers of random variables and low probabilities of failure. These approaches include the Subset Simulation (SS) (Au and Beck 2001) and its variants (Ching et al. 2005a; Ching et al. 2005b). These and other similar approaches that include the Line Sampling-Stepwise estimation method (Koutsourelakis et al. 2004) and the Slice Sampling Algorithm (Katafygiotis and Cheung 2003) have been mainly applied for solving structural dynamic problems. A brief description of the Subset simulation method follows.

2.3.4.1 Markov Chain

A Markov chain is a stochastic process which is memory-less such that given the present state of a random variable or vector, the future states are independent of the past and are only a function of the present state. In other words, the description of the present state fully captures all the information that could influence the future evolution of the process.

Let X_t denote the value of a random variable, X, at time t, and let the state space refer to the range of possible values of X. The random variable is a Markov process if the transition probabilities between different values in the state space depend only on the random variable's current state, i.e.,

$$P_r(X_{t+1} = s_j \,|\, X_0 = s_k, \ldots, X_t = s_i) = P_r(X_{t+1} = s_j \,|\, X_t = s_i) \tag{2.26}$$

A Markov chain refers to a sequence of random variables $(X_0, \ldots, X_n)$ generated by a

Markov process. A particular chain is defined by its transition probabilities (or the transition kernel),

$$\mathbf{P(i, j)} = P(i \rightarrow j) = P_r(X_{t+1} = s_j \,|\, X_t = s_i) \tag{2.27}$$

We will often use the notation $P(i \rightarrow j)$ to imply a move from state i to j. The probability that the chain is in state j at time t, is defined as $\pi_j(t)$ where:

$$\pi_j(t) = P_r(X_t = s_j) \tag{2.28}$$

The vector $\boldsymbol{\pi}(\mathbf{t})$ includes all the state space probabilities $\pi_j(t)$ at step t.

We start the chain by specifying a starting vector $\boldsymbol{\pi}(\mathbf{0})$. Often all the elements of $\pi(0)$ are zero except for a single element equal to 1 assuming that to the process is starting in that particular state. As the chain progresses, the probability values spread out over the entire state space. The probability that the chain has state value s_i at time t+1 is given by the Chapman-Kolomogrov equation, which can be expressed as:

$$\pi_i(t+1) = P_r(X_{t+1} = s_i) = \sum_k P_r(X_{t+1} = s_i \,|\, X_t = s_k) \cdot P_r(X_t = s_k)$$

$$= \sum_k P(k \rightarrow i)\pi_k(t) = \sum_k P(k,i)\pi_k(t) \tag{2.29}$$

The successive application of the Chapman-Kolomogrov equation describes the evolution of the chain over time.

The Chapman-Kolomogrov equation can also be presented in matrix form by defining the probability transition matrix [**P**] as the matrix whose i, j element is $P(i, j)$. Then, the

Chapman-Kolomogrov equation becomes

$$\pi(t+1) = \pi(t)[\mathbf{P}] \tag{2.30}$$

Using the matrix form, we immediately see how to obtain the state of the variables at time t, given the state at time 0, $\boldsymbol{\pi}(0)$

$$\boldsymbol{\pi}(t) = \boldsymbol{\pi}(t-1)[\mathbf{P}] = (\boldsymbol{\pi}(t-2)[\mathbf{P}])[\mathbf{P}] = \boldsymbol{\pi}(t-2)[\mathbf{P}]^2 = \cdots = \boldsymbol{\pi}(0)[\mathbf{P}]^t \tag{2.31}$$

Defining the n-step transition probability $p_{ij}^{(n)}$ as the probability that the process is in state j given that it started in state i, n steps ago,

$$p_{ij}^{(n)} = P_r(X_{t+n} = s_j \,|\, X_t = s_i) \tag{2.32}$$

In the following, an example is given as an illustration of the evolution of the Markov chain process.

Example:

Suppose the state spaces are (Rain, Sunny, Cloudy) and the weather follows a Markov process. Thus, it is assumed that tomorrow's weather will only depend on today's weather, and not on any previous day's. If this is the case, the observation that it has rained for three straight days does not alter the probability of tomorrow's weather as compared to the situation where it rained today but was sunny for the last week. The probability transitions from state to state can be assembled based on collected weather data. For example, it is assumed that the probability transitions for tomorrow's weather given that today is rainy are

P (Rain tomorrow ｜ Rain today) = 0.5,

P(Sunny tomorrow | Rain today)=0.25,

P(Cloudy tomorrow | Rain today)=0.25,

The first row of the transition probability matrix becomes (0.5, 0.25, 0.25) and following a similar approach the rest of the transition matrix can be assembled. In this example we assume that the transition matrix is given by:

$$P = \begin{pmatrix} 0.5 & 0.25 & 0.25 \\ 0.5 & 0 & 0.5 \\ 0.25 & 0.25 & 0.5 \end{pmatrix}$$

Note that the sum of each row of the matrix **P** must always be equal to 1.0 to cover the whole range of possibilities.

Given that today is sunny or $\boldsymbol{\pi}(0) = (0 \quad 1 \quad 0)$, the transition matrix can be used to find the expected weather in two days $\boldsymbol{\pi}(2)$, or in seven days $\boldsymbol{\pi}(7)$ using:

$$\boldsymbol{\pi}(2) = \boldsymbol{\pi}(0)\mathbf{P}^2 = (0.375 \quad 0.25 \quad 0.375) \text{ and } \quad \boldsymbol{\pi}(7) = \boldsymbol{\pi}(0)\mathbf{P}^7 = (0.4 \quad 0.2 \quad 0.4)$$

Conversely, suppose that today is rainy, so that $\boldsymbol{\pi}(0) = (1 \quad 0 \quad 0)$. The expected weather becomes

$$\pi(2) = \boldsymbol{\pi}(0)\mathbf{P}^2 = (0.4375 \quad 0.1875 \quad 0.375) \text{ and } \quad \boldsymbol{\pi}(7) = \boldsymbol{\pi}(0)P^7 = (0.4 \quad 0.2 \quad 0.4)$$

It is easily observed that after a sufficiently long period of time (in this case after 7 days), the expected weather $\boldsymbol{\pi}(7)$ will be independent of the starting value. In other words, the chain will reach a stationary distribution $\boldsymbol{\pi}$ where the probability values are independent of the actual starting value.

For the Markov Chain to lead to a stationary distribution π(t), the chain must satisfy the reversibility condition which is given as:

$$\pi_j^* P(j,k) = \pi_k^* P(k, j) \qquad \text{for all all i, k} \tag{2.33}$$

For this example if j=2 and k=1 then $\pi_j^* P(j,k) = 0.2 \times 0.5 = 0.1$ and $\pi_k^* P(k, j) = 0.4 \times 0.25 = 0.1$.

The basic idea of discrete-state Markov chain can be generalized to a continuous state Markov process by having a probability transition kernel $P(\theta, \varepsilon)$ that satisfies $\int P(\theta, \varepsilon)\, d\varepsilon = 1$. The continuous extension of the Chapman-Kolomogrov equation becomes,

$$\pi_{(\varepsilon)}^{(t+1)} = \int \pi_{(\theta)}^{(t)} P(\theta, \varepsilon) d\theta \tag{2.34}$$

Equation (2.34) can be derived from the continuous form of the reversibility condition which can be represented by the detailed balance equation:

$$\boldsymbol{\pi}(\theta)\, \mathrm{P}(\theta, \varepsilon) = \boldsymbol{\pi}(\varepsilon)\, \mathrm{P}(\varepsilon, \theta), \quad \forall \theta, \varepsilon \tag{2.35}$$

The chain's stationary distribution $\boldsymbol{\pi}$ can be obtained by integrating both sides of Equation (2.35) with respect to θ or ε to obtain.

$$\int \pi(\theta)\, \mathrm{P}(\theta, \varepsilon) d\theta = \int \boldsymbol{\pi}(\varepsilon)\, \mathrm{P}(\varepsilon, \theta) d\theta \tag{2.36}$$

Given that $\int P(\varepsilon, \theta)\, d\theta = 1$, the right hand side of Equation (2.36) becomes $\boldsymbol{\pi}(\varepsilon)$ and by switching the right and left hand sides of Equation (2.36) we obtain:

$$\boldsymbol{\pi}(\varepsilon) = \int \boldsymbol{\pi}(\theta) P(\theta, \varepsilon) d\theta \tag{2.37}$$

2.3.4.2 Markov Chain Monte Carlo method

Markov Chain Monte Carlo Simulation (MCMC) is a class of powerful simulation techniques for generating samples according to any given probability distribution. In a traditional Monte Carlo, random samples are generated from their parent distributions and the outcome is checked to verify whether it falls within the safe or failure domains. The process is repeated independently. To minimize the number of samples that must be generated, (Metropolis et al. 1953) applied Markov Chains to generate a new sample for each random variable given the current value of the variable. Given that the complete set of samples must follow the probability distribution of the random variable, the stationary distribution π must be equal to the variable's Probability Distribution Function (PDF). To execute the sample generation process, a transition probability kernel P(.,.) is needed in order for the process to eventually reach the exact stationary distribution. The transition kernel $P(\cdot,\cdot)$ must also satisfy the detailed balance Equation (2.35).

Since P(.,.) is not known, we assume that we have a proposal probability density function $\mathrm{q}(\theta,\varepsilon)$ that can be used to generate a new candidate sample, ε, given the existing sample, θ. This density is to be interpreted as saying that when a process is at the point θ, the density generates a value ε from $\mathrm{q}(\theta,\varepsilon)$. Accordingly, the probability density function $\mathrm{q}(\theta,\varepsilon)$ must satisfy the condition that $\int q(\theta,\varepsilon)\,d\varepsilon = 1$. If it happens that $\mathrm{q}(\theta,\varepsilon)$ also satisfies the reversibility condition for all x and y values, then $\mathrm{q}(\theta,\varepsilon)$ is equal to the exact transition kernel $\mathrm{P}(\theta,\varepsilon) = \mathrm{q}(\theta,\varepsilon)$. However, in most situations, it is unlikely that the correct value for $\mathrm{P}(\theta,\varepsilon)$ can be determined a priori and we might find, for example, that for some θ, and ε,

$$\pi(\theta)\,\mathrm{q}(\theta,\varepsilon) > \pi(\varepsilon)\,\mathrm{q}(\varepsilon,\theta) \tag{2.38}$$

In this case, speaking somewhat loosely, the process moves from θ to ε too often and from ε to θ too rarely. A convenient way to correct this condition is to reduce the number of moves from θ to ε by introducing a probability $\alpha(\theta,\varepsilon)<1$ that can be applied to reduce the value of $\pi(\theta)\,\mathrm{q}(\theta,\varepsilon)$. We refer to $\alpha(\theta,\varepsilon)$ as the *probability of move*. Thus, transitions from θ to ε ($\varepsilon \neq \theta$) are made according to $p_{MH}(\theta,\varepsilon) = q(\theta,\varepsilon)\,\alpha(\theta,\varepsilon), \quad \theta \neq \varepsilon$. Where $\alpha(\theta,\varepsilon)$ is yet to be determined.

Inequality (2.38) tells us that the movement from y to x is not made often enough. We should therefore define $\alpha(\varepsilon,\theta)$ to be as large as possible. But since $\alpha(\varepsilon,\theta)$ is a probability function, its upper limit is 1. Therefore, in general $\alpha(\varepsilon,\theta)$ is selected to be exactly equal to $\alpha(\varepsilon,\theta)$=1.0. $\alpha(\theta,\varepsilon)$ is determined by requiring that $p_{MH}(\theta,\varepsilon)$ satisfy the reversibility condition:

$$\pi(\theta)\,\mathrm{q}(\theta,\varepsilon)\,\alpha(\theta,\varepsilon) = \pi(\varepsilon)\,\mathrm{q}(\varepsilon,\theta)\,\alpha(\varepsilon,\theta) = \pi(\varepsilon)\,\mathrm{q}(\varepsilon,\theta) \tag{2.39}$$

And $\alpha(\theta,\varepsilon)$ can then be calculated to be:

$$\alpha(\theta,\varepsilon) = \pi(y)q(y,\varepsilon)/\pi(\theta)q(\theta,\varepsilon) \tag{2.40}$$

Of course, if the inequality in (2.38) is reversed, we set $\alpha(\theta,\varepsilon)=1$ and derive $\alpha(\varepsilon,\theta)$ as above. The probabilities $\alpha(\theta,\varepsilon)$ and $\alpha(\varepsilon,\theta)$ are thus introduced to ensure that the two sides of (2.38) are in balance or, in other words, that $p_{MH}(\theta,\varepsilon)$ satisfies the reversibility condition and the probability of move must be set to:

$$\begin{aligned} \alpha(\theta,\varepsilon) &= \min\left[\frac{\pi(\varepsilon)q(\varepsilon,\theta)}{\pi(\theta)q(\theta,\varepsilon)},1\right], && \text{if } \pi(\theta)q(\theta,\varepsilon)>0 \\ &= 1, && \text{otherwise.} \end{aligned} \tag{2.41}$$

Equation (2.41) is the basic behind the classic scheme of MCMC. The

Metropolis-Hastings algorithm which will be introduced in the next section will help in selecting efficient candidate generating density functions $q(\theta, \varepsilon)$.

2.3.4.3 Subset Simulation

The basic concept behind the Subset Simulation approach developed by Au and Beck (2001) centers on the fact that a small probability of failure can be expressed as a product of large values of conditional failure probabilities by introducing several intermediate failure events. This would convert a rare event into a sequence of more frequent ones. During the simulation, conditional samples are generated from specially designed Markov Chains so that they gradually populate each intermediate failure region until they cover the whole failure domain.

Let F denote the failure domain. The subset failure regions F_i are arranged such that $F_1 \supset F_2 \supset ... \supset F_m = F$ to form a decreasing sequence of failure events. The probability of failure P_f can be represented as the probability of falling in the final subset F_m given that on the previous step, the event belonged to subset F_{m-1}. This can be represented by the equation:

$$P_f = P(F_m | F_{m-1}) P(F_{m-1}) \tag{2.42}$$

By recursively repeating the process Equation (2.43) is obtained.

$$P_f = P\left(F_m | F_{m-1}\right) P\left(F_{m-1}\right) = P\left(F_1\right) \prod_{i=2}^{m} P\left(F_i | F_{i-1}\right) \tag{2.43}$$

Equation (2.43) shows that instead of calculating P_f directly, P_f can be calculated as the product of several conditional probabilities. With a proper choice of the conditional events, the conditional failure probabilities can be made sufficiently large so that they can be estimated using

a small number of samples. Thus, the Subset Simulation avoids generating rare failure events to find small failure probabilities; instead it converts a problem involving rare events into a sequence of problems involving more frequent events. If failure domain F of a system is defined as the exceedance of the demand Y over a given capacity y, that is $F = (B > b)$, then the intermediate failure regions can be represented as:

$$F_i = (B > b_i) \tag{2.44}$$

The probability of failure can be rewritten as:

$$P_f = P(B > b) = P(B > b_1)\prod_{i=2}^{m} P(B > b_i | B > b_{i-1}) \tag{2.45}$$

Where $0 < b_1 < b_2 < ...b_m = b$ form an increasing sequence of intermediate threshold values.

Because it is difficult to know a priori what optimum intermediate threshold values to choose in order to get reasonable estimates of the conditional probabilities, the intermediate thresholds, b_i ,are chosen "adaptively" so that the conditional probabilities are approximately equal to a common specified value, p_0. Experience shows that p_0=0.1 is a prudent choice (Au and Beck 2001).

To compute P_f based on (2.43), one needs to compute the probabilities $P(F_1)$, $P(F_i|F_{i-1})$. The unconditional probability $P(F_1)$ for the first subset can be readily estimated by Monte Carlo Simulation (MCS). It is also possible to compute the conditional failure probabilities using MCS. This will necessitate verifying that each generated sample θ belongs to F_{i-1} before even checking whether θ belongs to F_i or not. Samples that do not satisfy F_{i-1} must be rejected which creates large inefficiencies.

To overcome the problem associated with generating samples that satisfy the conditional probability, a Markov Chain Monte Carlo simulation technique based on the M-H (Metropolis-Hastings) Algorithm (H(Hastings 1970; Metropolis et al. 1953) has been proposed by Au and Beck (2001). The M-H algorithm is based on the Markov Chain simulation approach using Equation (2.41). Accordingly, the approach requires generating a new sample ε given that θ already belongs to F_{i-1}. To execute the move, a proposal probability density function $q(\theta,\varepsilon)$ must be selected. The proposal distribution governs the choice of the candidate samples and consequently the efficiency of the M-H algorithm. $q(\theta,\varepsilon)$ can be selected as will be explained further below. Given $q(\theta,\varepsilon)$, the procedure consists of the following steps:

Given a current state $\tilde{\theta}_{i-1}=[\tilde{\theta}_{i-1}^{(1)},...,\tilde{\theta}_{i-1}^{(n)}]$ (n being the number of random variables) that belongs to the subset region F_{i-1}.

For each random variable, we generate a pre-candidate component $\varepsilon_i^{(j)}$ from the proposal probability density function (PDF) $q_j\left(\cdot\middle|\theta_{i-1}^{(j)}\right)$ (j=1,…,n)

Compute the move probability $\alpha(\theta,\varepsilon)$ also known as the acceptance probability:

$$\alpha_i^{(j)}=\frac{\pi_j\left(\varepsilon_i^{(j)}\right)q_j\left(\theta_{i-1}^{(j)}\middle|\varepsilon_i^{(j)}\right)}{\pi_j\left(\theta_{i-1}^{(j)}\right)q_j\left(\varepsilon_i^{(j)}\middle|\theta_{i-1}^{(j)}\right)} \tag{2.46}$$

1. Set the j-th component of $\tilde{\theta}_i$ according to

$$\tilde{\theta}_i=\begin{cases}\varepsilon_i^{(j)} \text{ with } \textit{probability } \min\left(1,\alpha_i^{(j)}\right)\\ \theta_{i-1}^{(j)} \text{ with } \textit{probability } 1-\min\left(1,\alpha_i^{(j)}\right)\end{cases} \tag{2.47}$$

Generate an independent random variable, u, from the uniform probability distribution

U(0,1). If $u \le \alpha_i$, the move is accepted and if $u > \alpha_i$, the move is not allowed.

Accept the candidate $\tilde{\theta}$ if it belongs to F_{i-1}; otherwise reject it and take the current state as the new sample so that $\theta_i = \theta_{i-1}$.

The procedure for adaptively generating samples of θ conditional on $F_i (i = 1,..., m)$ is summarized as follows.

Generate N sample vectors $\left(\theta_{0,k} : k = 1,..., N\right)$ by direct Monte Carlo simulation such that they are i.i.d. from the proposal PDF q. The subscript '0'here denotes that the samples that belong to "Conditional Level 0" or the "Unconditional" case.

1. Use $\left(\theta_{0,k} : k = 1,..., N\right)$ to obtain the N responses $\left(B_{0,k} : k = 1,...N\right)$for each vector θ_0.

2. The value of b_1 is chosen such that $[(1 - p_0)N]$ responses lie outside the subset F_1 and p_0N samples belong to $F_1 = \left(B > b_1\right)$.

3. The $p_0 N$ samples among the original $\left(\theta_{0,k} : k = 1,\cdots, N\right)$that lie within F_1 are the conditional samples at 'Conditional Level 1'.

4. Starting from each of the samples that belong to F_1, the M-H algorithm is used to simulate an additional $[(1 - p_0)N]$ conditional samples so that there are a total of N conditional samples at Conditional Level 1.

5. The value of b_2 is then chosen such that the responses of $[(1-p_0)N]$ samples of those generated in step 5 lie outside $F_2 = (B > b_2)$. Note that the sample estimate for $P(F_2|F_1) = P(B > b_2|B > b_1)$ is automatically equal to p_0.

6. Again, there will be $p_0 N$ samples within F_2. These samples are conditional on F_2 and provide 'seeds' for applying the M-H algorithm to simulate an additional $[(1-p_0)N]$ conditional samples so that there is a total of N conditional samples at Conditional Level 2.

7. The procedure is repeated for higher conditional levels until the samples at Conditional Level (m-1) have been generated.

The approach used for generating the samples for the subset simulation method is schematically illustrated in Figure 2.13. Figure 2.13.a shows the unconditional N samples generated at level 0 and the corresponding probability distribution curve of the response B. Figure 2.13.b illustrates how failure region F_1 is defined to contain NP_0 samples, where P_0 is a preset conditional probability. Figure 2.13.c shows how the NP_0 samples are augmented by generating additional samples to obtain a total of N samples in F_1. Figure 2.13.d shows how F_2 is subdivided from F_1 such that NP_0 samples are included in F_2. The process of regenerating new samples in F_2 and dividing F_2 into new subsets is continued using the same approach.

Note that the proposal PDF affects the generation of the candidate samples given the current samples, and controls the efficiency of the Markov chain in populating the failure region (Au and Beck, 2001). Some commonly used special methods for selecting the proposal PDF are discussed below.

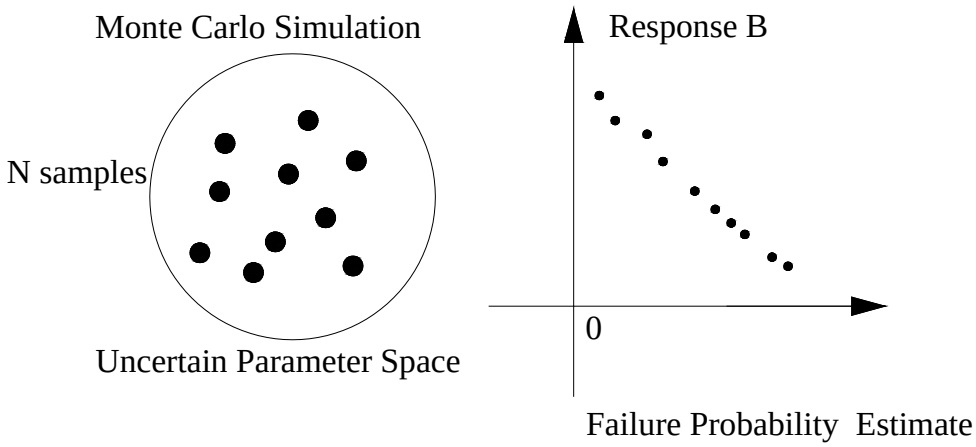

(a) Level 0: Monte Carlo Simulation

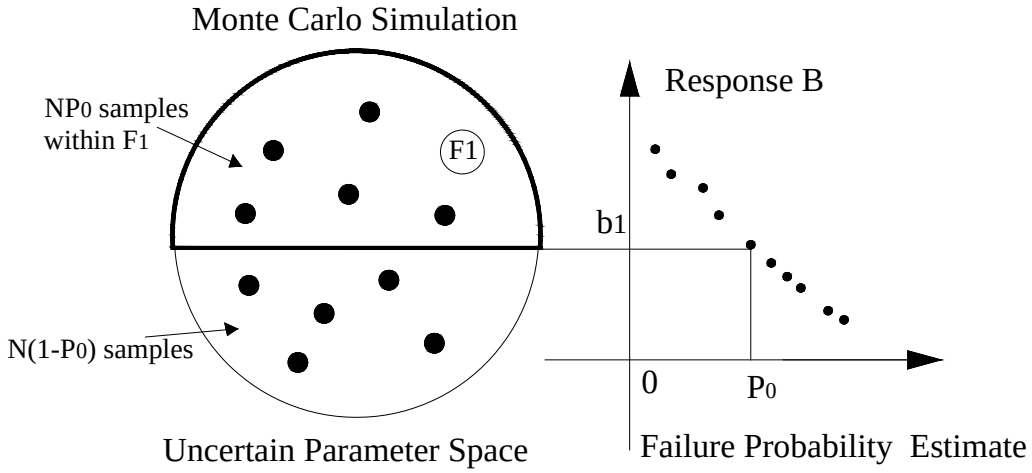

(b) Level 0: selection of first intermediate threshold level

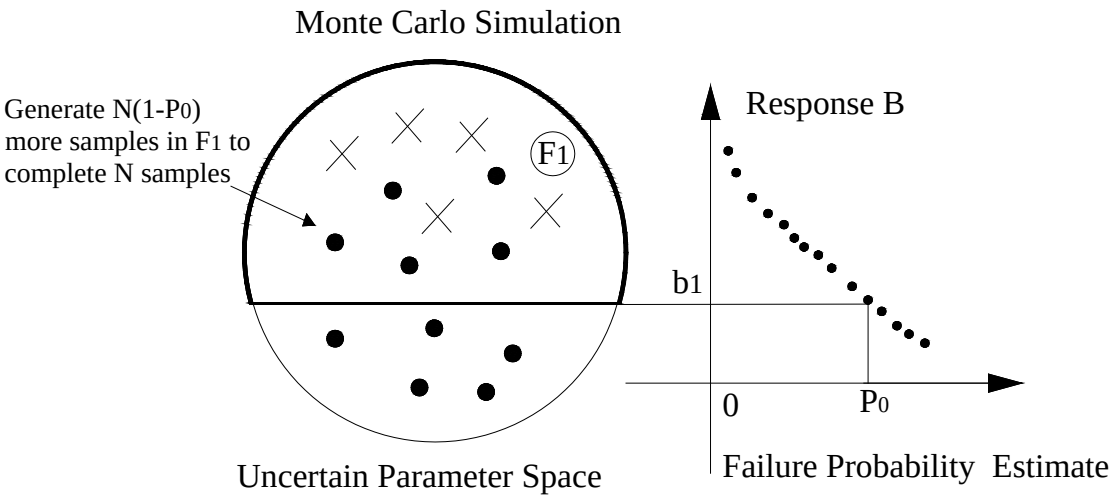

(c) Level 1: conditional samples generated using M-H algorithm

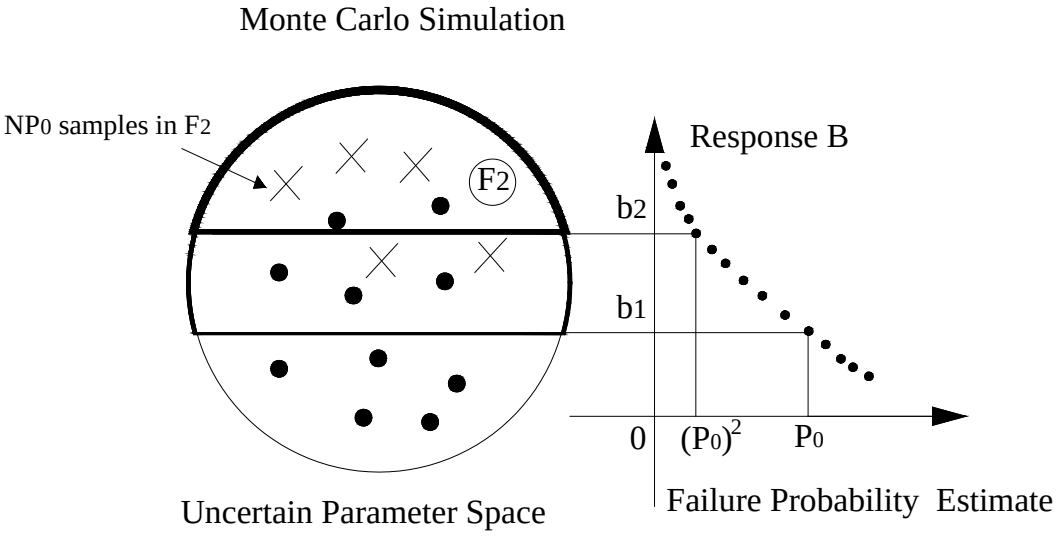

(d) Level 1: selection of second intermediate threshold level

Figure 2.13 Illustration of Subset Simulation Procedure

Symmetric Chain (Metropolis method)

The simplest case for selecting the proposal PDF q(.,.)is the Metropolis sampler, which is based on the use of a symmetric proposal with $q(\theta,\varepsilon) = q(\varepsilon,\theta)$. In this case, as discussed earlier, the acceptance probability becomes $\alpha(\theta,\varepsilon) = \min\left\{1, \frac{\pi(\varepsilon)}{\pi(\theta)}\right\}$. Hence, the process does not involve the proposal density at all. Consequently, proposed moves which will take the chain to a region of higher density are always accepted, while moves which take the chain to a region of lower density are accepted with a probability proportional to the ratio of the two densities $\frac{\pi(\varepsilon)}{\pi(\theta)}$.

Random Walk Chains

In this case, the proposed sample ε_j at stage j is $\varepsilon_j = \theta^{(j-1)} + w_j$ where w_j are iid random variables which are completely independent of the state of the chain. Suppose that the w_j have density $f(.)$, which is easy to simulate from. We can then simulate a random innovation, w_j, and set the candidate sample to $\varepsilon_j = \theta^{(j-1)} + w_j$. The proposed PDF is then $q(\theta,\varepsilon) = f(\varepsilon - \theta)$, which can be used to compute the acceptance probability. Of course, if $f(.)$ is symmetric about zero, then we have a symmetric chain, and the acceptance probability does not depend on $f(.)$ at all.

Independence chains

In this case, the proposed PDF is formed independently of the previous position of the chain, such that $q(\theta,\varepsilon) = f(\varepsilon)$ for probability density function $f(.)$. Here the acceptance probability becomes $\alpha(\theta,\varepsilon) = \min\left\{1, \frac{\pi(\varepsilon)}{\pi(\theta)} \Big/ \frac{f(\varepsilon)}{f(\theta)}\right\}$, and we see that the acceptance probability can be

increased by making $f(.)$ as similar to $\pi(.)$ as possible.

Summary

Au & Beck (2001) illustrated the application of the Subset Simulation method to solve structural dynamic problems. In these cases, the Subset Simulation was found to be capable of handling large numbers of random variables while remaining efficient in evaluating small probabilities of failure. Although Au and Beck (2001) demonstrated that their approach for selecting proposal PDF and accepting or rejecting sample candidates works well for the problems they solved, their approach has several limitations. These limitations include:

It is often not easily adaptable for determining the probability of failure of complex structural systems since the failure domain cannot be determined a priori. That is to say, the failure region F of structural systems cannot always be defined as the exceedance of the demand B of a given capacity b, which can be easily expressed as $F = (B > b)$.

The M-H algorithm is known to have problems with convergence. This is sometimes known as the "burn-in problem". One does not generally know how long it takes before the chain is sufficiently close to its limiting distribution. (Nummelin 1984). A standard approach to dealing with this issue is to simply discard some initial portion of the chain, labeling it as a "burn-in" component. However, without the ability to start the chain with a set of samples that belong to the proper target distribution π, by discarding the burn-in components the problem, although reduced, still remains.

Another problem is the inherent correlation between the successive sample elements of the chain, which makes it difficult to estimate the variance of the simulation.

According to Au & Beck (2001), the Subset Simulation is insensitive to the type of the proposal PDF and a Uniform PDF centered at the current sample is usually chosen. However, it is hard to choose the *spread* of the proposal Uniform PDF. The *spread* of the proposal PDF affects the size of the region covered by the Markov chain samples, and consequently it controls the efficiency of the method.

The next Chapter of this proposal will propose solutions for the above stated problems.

2.4 Conclusion

This chapter reviewed the current state of the art related to the analysis of the redundancy, robustness and resistance to progressive collapse of structural systems and examined recently developed structural reliability analysis techniques. It has been observed that traditionally these properties that can be placed under the umbrella term of "Structural redundancy" have been evaluated using deterministic methods. However, the high levels of uncertainty associated with estimating material properties, member strengths, applied loads, and the response of the system justify the use of probabilistic measures of redundancy and the use of reliability-based criteria to evaluate the safety of structural systems. Specifically, although several studies have analyzed the progressive collapse of structural systems, the development of acceptable safety criteria has generally eluded the structural design community. Ghosn & Moses (1998) have proposed a method to assess the redundancy and robustness of bridge systems using reliability criteria extracted from structural configurations which have generally been known to provide sufficient levels of redundancy and robustness. These reliability criteria were subsequently used to propose a set of system factors that penalize non-redundant and non-robust structures by requiring that their members be more conservatively designed than those of redundant structures. A similar

approach can be used to develop reliability-based criteria for assessing the capacity of bridge systems to resist the possibility of progressive collapse. This will require the availability of reliability methods capable of handling complex structural systems with multiple modes of failures and low probabilities of collapse.

Many reliability analysis methods have been developed during the last three decades. The most commonly used methods include FORM (or SORM), Response Surface Method, as well as basic simulation methods like Monte Carlo and its variants. More recently, Markov Chain-based simulation methods such as the Subset Simulation method have been proposed. FORM and SORM are often very efficient. However, they both require the availability of an explicit formulation of the failure function. Also, neither method is robust when solving complex limit-state equations, such as a highly non-linear failure points or a combination of failure functions (Melchers 1999).

The Response Surface method has been used when the explicit limit state function is not available such as when the problem requires the use of a Finite Element analysis. RSM works well provided the design point or the point of maximum likelihood can be identified and that reasonable decisions can be made about the points to be used for fitting the response surface. For large systems with large number of random variables, a large number of structural analyses and FORM iterations are needed for the solution to converge and in many cases the design point cannot be identified without subjective interference. Also, convergence problems may often arise when dealing with systems having multiple failure modes (Melchers 1999).

The Monte Carlo simulation method has been widely used in the past because of its robustness and its ability to solve problems with complex failure regions. Its main disadvantage

stems from its inefficiency when solving problems with large numbers of random variables and small probabilities. The number of samples must be proportional to $1/P_f$ in order for the Monte Carlo simulation to achieve an acceptable level of accuracy. Since the probability of failure, P_f, of complex structural systems is expected to be on the order of 10^{-6} or less and since each sample usually requires the nonlinear analysis, it would require several days of computational effort for the Monte Carlo approach to yield accurate results for realistic structural models despite current improvements in computer powers (Au and Beck 2001).

The recently developed Markov Chain-based advanced simulation method known as the Subset Simulation is efficient and is able to handle structural dynamic systems with large numbers of random variables, and small probabilities of failure. However, the Subset Simulation cannot always be directly used in evaluating the probability of structural system failure because the failure region F may not always be defined as the exceedance of the demand Y over a given capacity y, that is $F = (Y > y)$. Also, the coefficient of variation of the probability of failure calculated by the Subset Simulation is found to be relatively large, especially for small probability of failure, which means that the method is not always stable(Au and Beck , 2001).

In the next chapter, the latest advances in Markov Chain simulation theories will be reviewed in an attempt to improve the efficiency and the stability of the subset simulation methods by replacing the M-H algorithm with improved methods for generating conditional samples. Subsequent chapters will illustrate how this improved simulation algorithm can be used to evaluate the redundancy, robustness and the resistance to progressive collapse of bridge systems. Furthermore, this Dissertation will illustrate how the results of such analyses can be used to develop reliability-based criteria for the progressive collapse analysis of bridge systems that cen be

implemented in engineering practice.

CHAPTER THREE: PROPOSED SIMULATION METHOD

3.1 Introduction

In Chapter 2, the Subset Simulation was found to be capable of solving structural reliability problems involving large numbers of random variables while remaining efficient in evaluating small probabilities of failure. Several limitations in the method were noted including its inability of solving problems where the failure domain cannot be determined a priori. Also, the M-H algorithm used in the Subset Simulation has some known limitations such as the "burn-in problem" and the difficulty of estimating the error. In this chapter, a Regenerative Adaptive Subset Simulation (RASS) method will be proposed to overcome the limitations of the original Subset Simulation. The proposed improvements include a more efficient advanced Markov Chain sample generation algorithm and an adaptive algorithm to improve the convergence of the method.

3.2 Formulation Of Subset Simulation for structural systems

As mentioned above, the Subset Simulation can not be directly used in evaluating the probability of failure of complex structural systems where both member strengths and loads are random variables and where failure may not be directly defined as the probability of exceeding a limiting displacement or other response level. In most cases, the structural analysis process involves an incremental loading technique to determine the load at which failure occurs. The failure domain, F, may then be defined as:

$$F = \left(LL^* > LL\right) = \left(\frac{LL^*}{LL} = B > 1\right) \tag{3.1}$$

Where, LL^* is the random applied load and LL is the load that leads to the collapse of the structural system.

The intermediate failure regions can be represented as

$$F_i = \left(\frac{LL^*}{LL_i} = B > y_i \right) \tag{3.2}$$

The probability of failure of the structure can then be rewritten as:

$$P_f = P\left(\frac{LL^*}{LL} = B > 1 \right) = P(B > b_1) \prod_{i=2}^{m} P\left(B > b_i \middle| B > b_{i-1}\right) \tag{3.3}$$

Where $0 < b_1 < b_2 < ... b_m = 1$ form an increasing sequence of intermediate threshold values. The values of LL can then be obtained from an incremental structural analysis of the finite element model using as input generated samples from the random variables that model the properties of the structural members and the permanent loads. The subset simulation can then be used to compare the samples of LL* to LL for each simulated analysis step. Although the original subset will be able to handle this problem much more efficiently and accurately than most existing reliability analysis methods as discussed in Chapter 2. The nonlinear analysis of a complex structural system will still require a considerable amount of computational time. For this reason along with the previously discussed problems with the stability of the original SS, this Chapter will introduce improvements to the Subset Simulation method that utilize some of the latest advances in Markov Chain simulation algorithms.

3.3 Advanced Markov Chain Simulation Algorithms

To resolve the issues with the stability and burn in issues of the subset simulation method

four mechanisms are proposed in this Report based on recent advances in the theory and application of Markov Chains for simulation. These mechanisms are known as the Regeneration algorithm, The Adaptive Markov Chain process, the Delayed Rejections algorithm and the Component wise sampler.

3.3.1 Regeneration

The advantage of the Subset Simulation method relies on efficiently generating the conditional intermediate samples. For this reason, instead of using a standard Monte Carlo procedure to generate the conditional samples, Au and Beck (2001) recommended using a Markov Chain simulation technique based on the M-H (Metropolis-Hastings) Algorithm. However, as pointed out in Chapter 2, the M-H has a "burn-in" problem which may delay the convergence of the generated samples to the stationary distribution π. Also, the correlation between the samples generated at each step makes estimating the standard error rather difficult. One approach that can help reduce these problems is to establish *regeneration times* at which the chain restarts itself (Mykland et al. 1995). The set of samples between two successive regeneration times are called tours. The different tours are independent and identically distributed. Consequently, after a fixed number of tours, the initialization issues (including the "burn-in" problem) are eliminated, and the standard errors in the final results can be estimated. This approach is known as "regenerative simulation" and the procedure to implement it is described by Mykland et al. (1995) and summarized next.

The samples generated up to step n, $\{\theta_n : n = 0, 1, ...\}$ form an irreducible Markov chain on a state space (E, λ) with transition kernel $P = P(\theta, \varepsilon)$ and invariant distribution π. Suppose that we can find a set of samples $A \in \lambda$ with $\pi(A) > 0$ such that θ_{n+1}, θ_{n+2},…is conditionally

independent of θ_1, $\theta_2, \ldots \theta_n$ given $\theta_n \in A$. Then A is called a *"proper atom"* for the Markov Chain. Whenever the chain enters A, the chain is said to regenerate itself. Regeneration times divide the chain into sections, called *tours*, and the future of the process after regeneration is independent of the past but all the samples are identically distributed. For a discrete state-space Markov Chain, any individual state can be chosen to represent A. However, in continuous state spaces, proper atoms are difficult to identify. Nevertheless, regeneration times might still be defined using a technique due to Nummelin (1984) called *splitting*. Splitting includes a decomposition of the transition kernel of the chain P(.,.) into two components, one of which does not depend on the current state of the chain.

To apply the splitting method, we assume that it is possible to find a function $s(\theta)$ and a probability measure $v(\varepsilon)$ such that $\pi(s) = \int s(\theta)\pi(\theta) > 0$ and

$$P(\theta, A) \geq s(\theta)v(A) \tag{3.4}$$

for all $\theta \in E$ and all $A \in \lambda$. A pair (s, v) satisfying these conditions is called an atom for the transition kernel $P(.,.)$. Therefore, the transition probability P can be split into two parts (Nummelin 1984):

$$P(\theta, A) = s(\theta)\, v(A) + (1 - s(\theta))\, Q(\theta, A) \tag{3.5}$$

This expression indicates that a new sample can be generated from a probability distribution $v(.)$ which does not depend on θ, with probability $s(.)$. The new sample is generated by the distribution $Q(.)$ with probability 1- $s(.)$.

The Regeneration Algorithm constructs the Markov chain using the splitting method of Equation (3.5). We assume that the chain is currently at θ_n and we generate a candidate sample ε which is obtained from the proposal PDF $q(.,.)$. As mentioned earlier, $q(.,.)$ approximates the actual transition kernel P_i where P can be represented by Equation (3.5) such that v and s satisfy Equation (3.4).

If the candidate sample ε is accepted, then, a random splitting variable S_{n+1} is generated from a Bernoulli distribution with retrospective success probability $\gamma_i^A(\theta_n, \varepsilon)$ given in Equation (3.6). If $S_{n+1} = 1$, a regeneration is undertaken, and we discard ε and we sample a new θ_{n+1} from v which is totally independent of θ_n. If $S_{n+1} = 0$, then we take $\theta_{n+1} = \varepsilon$ which was earlier generated from $q(.,.)$.

$$\gamma_i^A(\theta_n, \varepsilon) = \frac{s_i(\theta_n)v_i(\varepsilon)}{P_i(\theta_n, \varepsilon)} \tag{3.6}$$

In order to generate a Bernoulli splitting variable S_{n+1} with retrospective success probability $\gamma_i^A(\theta_n, \varepsilon)$, we can generate a random variable, u_i, from a Uniform distribution U(0,1). If u_i is less than $\gamma_i^A(\theta_n, \varepsilon)$, then $S_{n+1} = 1$, otherwise, $S_{n+1} = 0$.

Two general approaches for obtaining the atom (s, v) that replaces $q_n(.,.)$ at step n are available (Mykland et al, 1995). One option is known as the independence sampler and the other as the random-walk sampler. The Random Walk Sampler is used because it is believed to be the more efficient of the two approaches.

Random-Walk Sampler (Mykland et al. 1995)

To split the random-walk sampler, we first need to find an atom (s_q, v_q) for the transition kernel P. In the Random Walk Sampler, we can choose $\tilde{\theta}$ at the mode which is the most common of the previously generated samples, $\tilde{\theta} \in E$ and we generate a candidate sample $\varepsilon \in D$ (we can set D=E), we define $s_q(\theta)$ and $v_q(\varepsilon)$ as:

$$s_q(\theta) = \text{infimum}\left(\frac{q(\theta,\varepsilon)}{q(\tilde{\theta},\varepsilon)} : \varepsilon \in D\right) \text{(infimum means greatest lower bound)}$$

$$v_q(\varepsilon) = q(\tilde{\theta},\varepsilon) \tag{3.7}$$

Then the atom (s,ν) is obtained from

$$s(\theta) = s_q(\theta)\min\left(\frac{\pi(\tilde{\theta})}{\pi(\theta)},1\right), \quad v(d\varepsilon) = v_q(\varepsilon)\min\left(\frac{\pi(\varepsilon)}{\pi(\tilde{\theta})},1\right) \tag{3.8}$$

3.3.2 Adaptive Algorithm

In most cases, an effective proposal distribution is very difficult to select since the kernel is not known. According to Au & Beck (2001), the Subset Simulation is insensitive to the type of the proposal PDF and a Uniform PDF centered at the current sample is usually chosen. However, it is difficult to choose the spread of the Uniform proposal PDF. A possible remedy is provided by the Adaptive Metropolis (AM) (Haario et al. 2001), which uses the history of the chain to update the variances or the spread of the proposal distribution.

The basic idea of the approach proposed by Haario et al (2001) it to create a Gaussian proposal distribution with a covariance matrix calibrated using the sample path of the chain. Haario (2001) assumes that the Gaussian proposal is centered at the current position of the Markov chain θ_n and that its covariance is set as:

$$C_n = \omega_d Cov(\theta_0,...,\theta_{n-1}) + \omega_d \xi\, I_d \tag{3.9}$$

Where ω_d is a parameter that depends only on the dimension d of the state space on which π is defined and $\xi > 0$ is a constant that we may choose to be very small. Here I_d denotes the d -dimensional identity matrix. In order to start the adaptive procedure, an initial arbitrary strictly positive definite initial covariance, C_0, is chosen a priori. This initial arbitrary choice may be quite poor. But, the selection will improve as the process evolves as will be explained later below. A time index $n_0 > 0$ defines the length of the initial period such that:

$$C_n = \begin{cases} C_0 & \text{n} \le \text{n}_0 \\ \omega_d Cov(\theta_0,...,\theta_{n-1}) + \omega_d \xi\, I_d & \text{n} > \text{n}_0 \end{cases} \tag{3.10}$$

The covariance matrix may be defined as:

$$Cov(\theta_0,...,\theta_k) = \frac{1}{k}\left(\sum_{i=0}^{k} \theta_i \theta_i^T - (k+1)\bar{\theta}_k \bar{\theta}_k^T \right) \tag{3.11}$$

Where $\bar{\theta}_k = \frac{1}{k+1}\sum_{i=0}^{k} \theta_i$ and the elements $\theta_i \in R^d$ are considered as column vectors. For $n>n_{0,}$ the covariance C_n satisfies:

$$C_{n+1} = \frac{n-1}{n} C_n + \frac{s_d}{n}(n\bar{\theta}_{n-1}\bar{\theta}_{n-1}^T - (n+1)\bar{\theta}_n \bar{\theta}_n^T + \bar{\theta}_n \bar{\theta}_n^T + \xi\, I_d) \tag{3.12}$$

The choice for the length of the initial segment $n_0>0$ is arbitrary, but the bigger it is the more slowly the effect of the adaptive algorithm is felt. The role of the parameter ε is just to ensure that C_n will not become singular. In most cases, ξ can be safely set to zero. Following (Gelman et al. 1996), a basic choice for the scaling parameter ω_d is $2.4^2 / d$.

In summary, at each regeneration time, the spread of the proposal PDF of the chain is modified, based on the history of the chain. Although Haario (2001) proposed the application of Equation (3.12) for Gaussian proposal PDF, the approach is also valid for any distribution type and in particular to the Uniform distribution which was favored by Au and Beck (2001).

3.3.3 Delayed Rejection

The rejection of proposed moves is an intrinsic part of the regeneration algorithm ensuring that the chain converges to the intended target distribution. However, persistent rejections in particular parts of the state space may indicate that, locally, the proposal distribution is badly calibrated to the target. The basic process can then be modified by introducing a "Delayed Rejection" algorithm so that on rejection, a second attempt to move is made (Mira 2001; Tierney 1994). The basic idea is that, when a reject decision is taken, instead of turning to the next transition, a second proposal is made, using a different distribution possibly dependent on the rejected value and accept or reject that second attempt using a suitably computed probability. The following section will give details of DR.

Suppose that the current position of the Markov chain is $\theta_n = x$. Then, a candidate y_1 is generated from a proposal $q(x,\cdot)$ and accepted with the acceptance probability

$$\alpha_1(x, y_1) = \min\left(\frac{\pi(y_1)q(y_1, x)}{\pi(x)q(x, y_1)}, 1\right) \tag{3.13}$$

Upon rejection, instead of retaining the same position, $\theta_{n+1} = x$, a second stage move, y_2 is proposed. The second stage proposal is allowed to depend not only on the current position of the

chain but also on what we have just proposed and rejected: $q(x, y_1, \cdot)$. The second stage proposal is accepted with probability

$$\alpha_2(x, y_1, y_2) = \min\left(\frac{\pi(y_2)q(y_2, y_1)q(y_2, y_1, x)[1-\alpha_1(y_2, y_1)]}{\pi(x)q(x, y_1)q(x, y_1, y_2)[1-\alpha_1(x, y_1)]}, 1 \right) \tag{3.14}$$

This process of delaying rejection can be repeated. the acceptance probability at that stage is (Mira 2001):

$$\alpha_i(x, y_1, \ldots, y_i) = \min\left(\frac{\pi(y_i)q(y_i, y_{i-1})q(y_i, y_{i-1}, y_{i-2})\ldots q(y_i, y_{i-1}, \ldots, x)}{\pi(x)q(x, y_1)q(x, y_1, y_2)\ldots q(x, y_1, \ldots, y_i)}, 1 \right) \tag{3.15}$$

The process of delaying rejection can be iterated for a fixed or random number of stages. Higher stage proposals are allowed to depend on the candidates so far proposed and rejected. Thus, DR allows partial local adaptation of the proposal within each time step of the Markov chain while still retaining the Markovian property and reversibility.

3.3.4 Componentwise Regeneration

The original Regeneration Algorithm has been demonstrated to work well in practice for low dimensional problems. Unfortunately, as the dimension of the state space increases, the Regeneration Algorithm described above becomes inefficient due to the increase in the dimension of the proposal distribution q(..,…)(Cowles and Rosenthal 1996). In this paper, the Componentwise Algorithm is used to solve this problem by choosing a separate proposal PDF's for each random variable (Haario et al. 2005). The Componentwise approach can be used in high dimensional problems or for the cases where the full multidimensional conditional distributions are not known and they have to be approximated at each step and for each parameter.

3.4 Proposed Regenerative Adaptive Subset Simulation

In this paper, a MCMC-based simulation called Regeneration Algorithm Subset Simulation method is proposed, which combines the benefits of the Regeneration Algorithm (Gilks et al. 1998), the Delayed Rejection process (Mira 2001; Tierney 1994) and the Adaptive Metropolis (Haario et al. 2001) and Componentwise Algorithm (Haario et al. 2005) for evaluating small failure probabilities in high-dimensional structural analysis problems.

The procedure for a d-dimensional problem is summarized as follows:

Suppose that the chain is currently at $\theta_n^{(j)} = x^{(j)}$ $(j = 1,\ldots,d)$ with current proposal probability density function $q_n^{(j)}$ at state n and an atom (s_n, v_n) . Roughly speaking, the spread of $q_1^{(j)}$ may be chosen as some fraction of the standard deviation of the corresponding component $\theta^{(j)}$. $q_n^{(j)}$ at state n will be updated though the variance v_t^j which is computed from previous samples in the chain. Since we are using the Componentwise approach, the matrix of Equation (3.11) reduces to d scalars where the variances of each proposal distribution depends on time and can be calculated as follows:

$$v_t^j = \begin{cases} v_o^j, n \le n_o \\ \omega\, Var\left(\theta_o^{(j)},...,\theta_{n-1}^{(j)}\right), n > n_o \end{cases} \tag{3.16}$$

Here, v_o^j denotes an initial variance of the proposal distribution for random variable j; ω denotes the scaling factor taken to be ω=2.4 as suggested by (Gelman et al. 1996)

First, generate sample $y^{(j)}$ using the proposal PDF $q_n^{(j)}(\theta_n,\cdot)$. Then perform the Metropolis-Hasting acceptance test:

1. Sample $u_1^{(j)}$ from uniform distribution density $U(0,1)$ .and check if $u_1^{(j)} \le \alpha_1\left(x^{(j)}, y^{(j)}\right)$(Equation (3.14)) .Then perform a regeneration test: Sample $u_2^{(j)}$ from uniform distribution density $U(0,1)$. Compare $u_2^{(j)}$ to the retrospective success probability γ_n^A.

a. If $u_2^{(j)} \le \gamma_n^A\left(x^{(j)}, y^{(j)}\right)$ (Equation (3.6)), then regeneration is executed and we discard y. Instead we sample θ_{n+1} from v rather than $q_n(.,.)$. Keep sampling y^* from v and also sample $u_3^{(j)}$ from the uniform distribution density $U(0,1)$ accept $\theta_{n+1}^{(j)} = y^*$ untill $u_3^{(j)} \le \min\left(\frac{\pi(y^*)v(y^*, x^{(j)})}{\pi(x^{(j)})v(x^{(j)}, y^*)}, 1\right)$.

b. Else if $u_2^{(j)} > \gamma_n^A\left(x^{(j)}, y^{(j)}\right)$, then accept the current candidate $y^{(j)}$: $\theta_{n+1}^{(j)} = y^{(j)}$.

2. Else if $u_1^{(j)} > \alpha_1\left(x^{(j)}, y^{(j)}\right)$ (Equation (3.14)), perform the Delayed Rejection Algorithm. Instead of retaining the same position, $\theta_{n+1}^{(j)} = \theta_n^{(j)}$, a second stage move, $y^{(j)}$ is proposed and will be rejected and accepted based on Equation (3.15). This process of delaying rejection can be repeated and we only perform three stages in my research. If at *ith* stage, the candidate $y^{(j)}$ is accepted, then regeneration occurs. Otherwise, reject the candidate samples and let $\theta_{n+1}^{(j)} = \theta_n^{(j)}$. The whole procedure is also shown in a flowchart Figure 3.1.

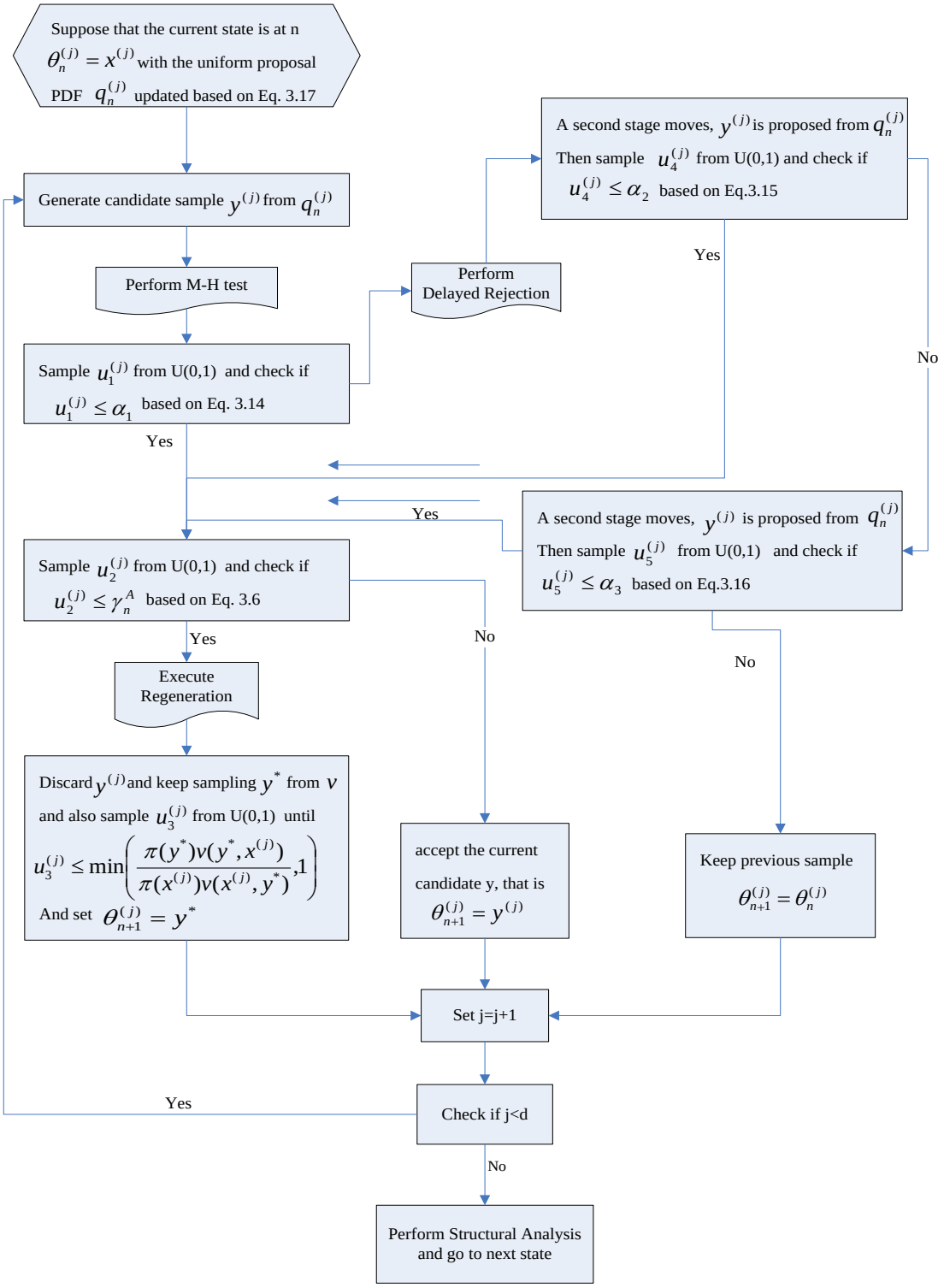

Figure 3.1 The flowchart for generating samples

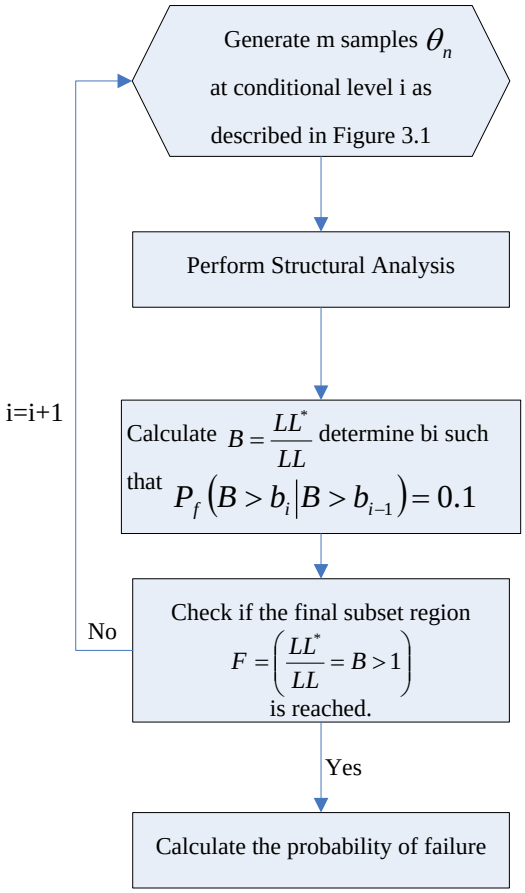

Figure 3.2 The flowchart for calculating probability of failure

based on Subset Simulation

In this chapter, for simplicity, we take the known limit state functions for examples to verify the proposed RASS method in next chapter.

3.5 Application and Verification of RASS Method

To verify the validity of the RA-SS approach, the algorithm described in the previous section is used to estimate the probability of failure for a set of widely used Limit State Functions (LSF) of various levels of complexity. The following six problems labeled LSF1 through LSF6 were collected from the published literature and are solved using the proposed algorithm. The

results are compared with those obtained using the classical Monte Carlo simulation and the original Subset Simulation.

LSF1--Noisy limit state function with six random variables (Engelund and Rachwitz 1993)

The noisy equation is given as a function of six Normal random variables X_1 through X_6:

$$LSF_1 = X_1 + 2X_2 + 2X_3 + X_4 - 5X_5 - 5X_6 + 0.001\sum_{i=1}^{6}\sin(100X_i)$$

$$X_1 = X_2 = X_3 = X_4 \sim N(120,12)$$

$$X_5 \sim N(50,15)\,, \quad X_6 \sim N(40,12)$$

LSF2--Multiple failure points with two random variables (Engelund and Rachwitz 1993)

In this case, the limit state function is a hyperbola and has two design points which makes difficult to solve using the FORM algorithm.

$$LSF_2 = X_1X_2 - PL$$

P and L are deterministic parameters with

$$P = 14.614\,, \quad L = 10.0$$

While X_1 and X_2 are Normal random variables.

$$X_1 \sim N(78064.4, 11709.7)$$

$$X_2 \sim N(0.0104, 1.56*10^{-3})$$

LSF3--Quadratic Limit State Function with Mixed term, Convex LSF (Borri and Speranzini 1997)

The convex limit state function is given as:

$$LSF_3 = 0.1(x_1 - x_2)^2 - \frac{(x_1 + x_2)}{\sqrt{2}} + 2.5$$

$$X_1 \sim N(0,1)$$

$$X_2 \sim N(0,1)$$

LSF4--Concave LSF (Borri and Speranzini 1997)

This limit state function is represented by the equation

$$LSF_4 = -0.5(x_1 - x_2)^2 - \frac{(x_1 + x_2)}{\sqrt{2}} + 3$$

$$X_1 \sim N(0,1)$$

$$X_2 \sim N(0,1)$$

LSF5--Nonlinear LSF with saddle point (Kiureghian et al. 1987)

The presence of the saddle point complicates the identification of the design point.

$$LSF_5 = 2 - x_2 - 0.1{x_1}^2 + 0.06{x_1}^3$$

$$X_1 \sim N(0,1)$$

$$X_2 \sim N(0,1)$$

LSF6--Quadratic Limit State Function with Mixed term, Convex LSF (Au and Beck 1999)

This highly nonlinear equation is given as:

$$LSF_6 = 3 - x_2 + (4x_1)^4$$

$X_1 \sim N(0,1)$

$X_2 \sim N(0,1)$

The results in Table 3.1 demonstrate the efficiency of the proposed RASS algorithm that was capable of providing good accuracy for the probability of failure up to the order of 10^{-7} within a maximum of 27760 samples. The values listed in Table 3.1 are the average values based on 20 independent runs. Table 3.1 has shown that the COV (coefficient of variance) of probability of failure based on the proposed RASS is much smaller than the original SS.

Table 3.1- Results of RASS for six Limit States

	Original Subset Simulation			Proposed RASS			
LSF No.	P_f	No. of samples	COV of Pf	P_f	No. of samples	COV of Pf	Accurate P_f
1	1.34×10^{-2}	2705	0.13	1.28×10^{-2}	2180	0.08	1.22×10^{-2}
2	2.73×10^{-7}	34970	0.45	1.86×10^{-7}	27760	0.31	1.46×10^{-7}
3	4.75×10^{-4}	6760	0.24	4.39×10^{-4}	5280	0.16	4.16×10^{-4}
4	0.0965	2160	0.07	0.0960	1966	0.07	0.105
5	0.0351	2815	0.12	0.0340	2431	0.09	0.0347
6	2.09×10^{-4}	8182	0.25	1.88×10^{-4}	6338	0.14	1.80×10^{-4}

In addition, an adaptive method is used to determine how many samples are needed in order to obtain good accuracy. That is, in each conditional level, keep increasing the number of samples until the error of intermediate threshold value b_i is sufficiently small. Applying this approach to solving LSF_6 for an example shown in Table 3.2, we observe that if the b_i are set to reach an accuracy of 5% the average number of samples needed to converge is 6000. In this case, the P_f is $1.84\text{x}10^{-4}$ which is compared to the exact solution provided by Grooteman (2008) is $1.80\text{x}10^{-4}$.

Table 3.2 – Adaptive method for number of samples

Conditional Level	No. of samples	No. of samples	No. of samples	No. of samples	No. of samples	Pf
Level 1	800	900(7.5%)	1200(5.4%)	1400(1.6%)		
Level 2	800	900(2.8%)	1200(6.6%)	1400(5.1%)	1600(1.8%)	1.84×10^{-4}
Level 3	800	900(6.9%)	1200(5.5%)	1400(2.5%)		
Level 4	800	900(4.6%)	1200(8.2%)	1400(6.8%)	1600(2.2%)	

When the final subset region $F_m = \left(\frac{LL^*}{LL} = B > 1 \right)$ is reached, the samples generated in the last subset are the points that will be close to the failure curve. These samples are plotted in Figures 3.3 to 3.7 for the results of LSF_2 through LSF_6 and compared to the limit state functions shown in red. The plots show how well these generated samples define the failure domain. The plot for LSF_1 is not possible to represent due to the high dimensions of the problem.

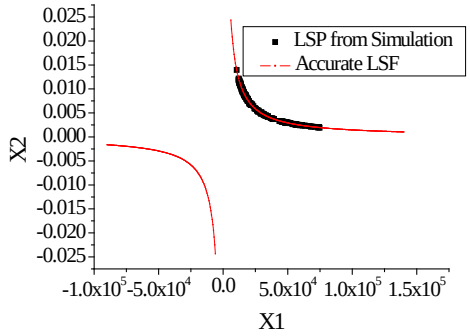

.

Figure 3.3---LSF_2 with failure points

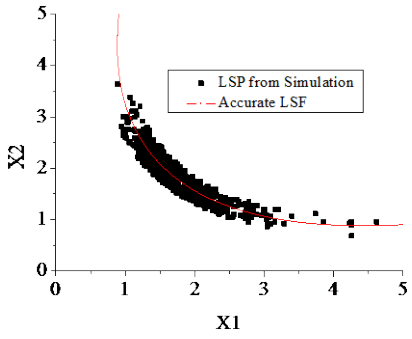

Figure 3.4---LSF_3 with failure points

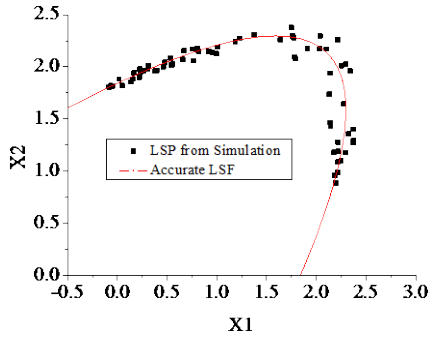

Figure 3.5- LSF_4 with failure points

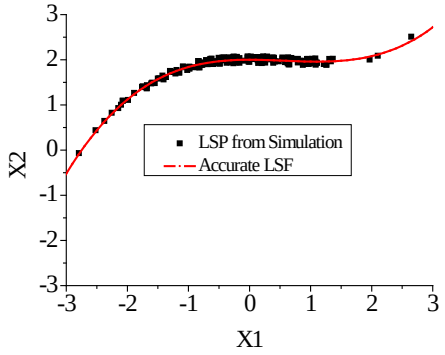

Figure 3.6- LSF_5 with failure points

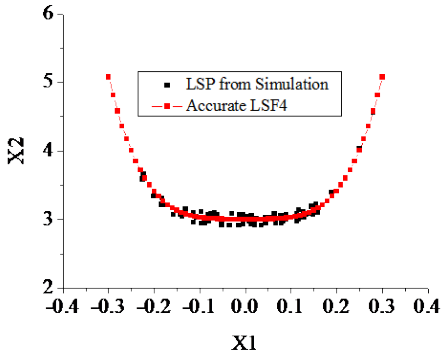

Figure 3.7- LSF_6 with failure points

3.6 Analysis of high dimensional dynamic problem

This example is used to verify the efficiency of RASS in dealing with high-dimensional problems. In this example, we solve the same problem described by (Au and Beck 2001) that consider a single degree of freedom oscillator with natural frequency $\omega = 1.25HZ$ and damping ratio $\zeta = 2\%$ subjected to white noise excitation:

$$\ddot{X}(t) + 2\zeta\omega\,\dot{X}(t) + \omega^2 X(t) = W(t) \tag{3.17}$$

The system is assumed to start from rest, so that $X(0) = 0$ and $\dot{X}(0) = 0$. In this example, the input $W(t)$ is a Gaussian white noise process with spectral intensity S. The response of the system is computed at the discrete time instants $\{t_k = (k-1)\Delta t : \mathrm{k} = 1,..., \mathrm{n}\}$, where the sampling interval is assumed to be $\Delta t = 0.02$ s and the duration of the study is T=30s, so that the number of time steps is $n = T/\Delta t + 1 = 1501$. The uncertain state vector θ then consists of the sequence of i.i.d. (independent and identically distributed) standard Gaussian random variables which generate the white noise input at the discrete time instants, $\{W(t_k) = \sqrt{2\pi S/\Delta t}\theta_k\}$. Hence, the number of uncertain parameters involved in the problem is n=1501. The spectral intensity for the white noise is assumed to be S=1. Failure is defined when the displacement response exceeds a threshold level b within the first 30s. Fig 3.8 shows the failure probability estimates for different threshold levels b. As an example, for threshold level b=1.6, the probability of failure is 4.23 x 10^{-3} using the proposed method with a total number of samples equal to 2880. For comparison, when a Monte Carlo simulation is used, the probability of failure is obtained as 4.21x10^{-3} using a total of 200,000 samples. It is seen that the proposed simulation result agrees well with the Monte Carlo simulation, but the proposed simulation can greatly reduce the number of samples and the computational effort.

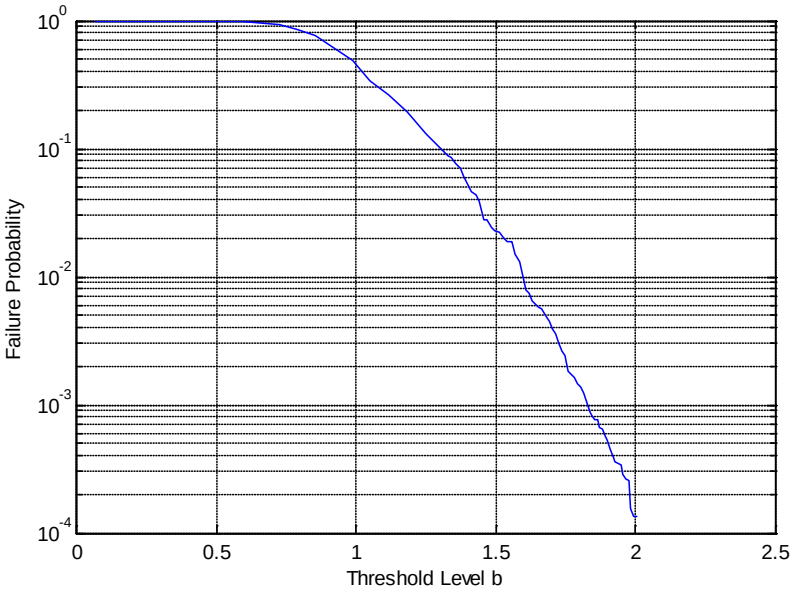

Figure 3.8 Estimation for the probability of failure for different threshold levels

3.7 Reliability Analysis of Simplified Two-Girder Bridge System

This example consists of a simplified bridge model formed by two girders and two continuous spans as shown in Figure 3.9 (Ghosn and Frangopol 1999). Assuming plastic behavior, two different collapse mechanisms are possible for this bridge as shown in Figure 3.9. Each collapse mechanism can be represented by a Limit State Function (LSF), Z_i, which can be written as:

$$Z_1 = 2(M_1 - D_1) + (M_2 - D_2) - \frac{P \times L_1}{2} \tag{3.18}$$

$$Z_2 = 2(M_3 - D_3) + (M_2 - D_2) - \frac{P \times L_2}{2} \tag{3.19}$$

Where M_i is the moment capacity at section *i*, D_i is the dead load moment at section *i*, P is the applied maximum lifetime truck load, and L_j is the length of span j. The concentrated load P is used

to model the weight of the HS-20 design truck (320 kN) with a dynamic amplification factor equal to 1.15 and a load distribution factor equal to 0.5. Table 3.3 gives the properties of the random variables. The results of the reliability analysis are obtained using the proposed RASS for each failure mode separately and for the system as provided in Table 3.4. The Table also shows the results from the original subset and the Monte Carlo simulations. The results show how for the same number of samples, the RASS leads to significantly improvement in the accuracy compared to the original SS method. The RASS method can be used to obtain the probability of system failure by performing the incremental analysis using the formulation of Equation (3.1) through (3.3).

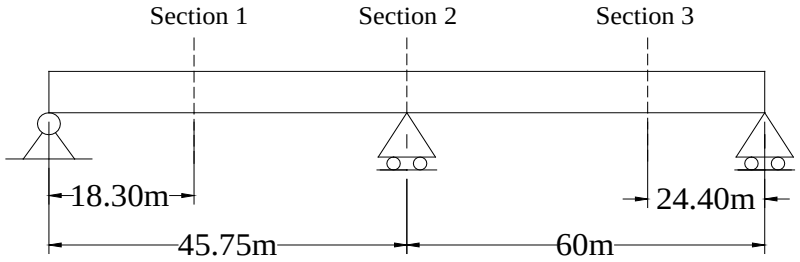

Figure 3.9 -- Two-girder continuous bridge configuration

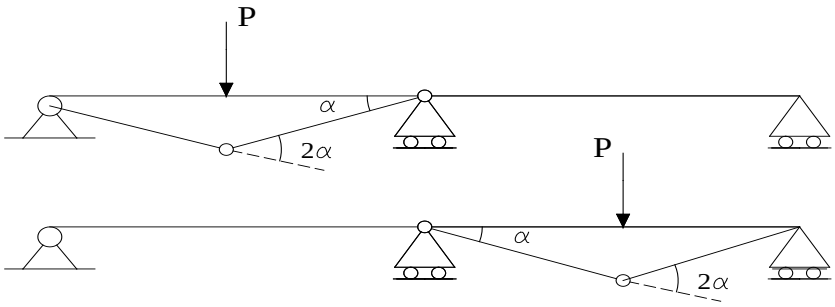

Figure 3.10 -- Two span bridge collapse mechanism

Table 3.3- Random variables for two-girder bridge example

	Variable	Nominal value	Bias	COV	Distribution Type
Section 1	Moment Cap. (kN-m)	8190	1.12	10%	Lognormal
	Dead Load (kN-m)	3640	1.05	9%	Normal
	Live Load	HS-20	2.07	19%	Extreme I
Section 2	Moment Cap. (kN-m)	23400	1.12	10%	Lognormal
	Dead Load (kN-m)	13755	1.05	9%	Normal
	Live Load	HS-20	2.07	19%	Extreme I
Section 3	Moment Cap. (kN-m)	19217	1.12	10%	Lognormal
	Dead Load (kN-m)	10750	1.05	9%	Normal
	Live Load	HS-20	2.07	19%	Extreme I

Table 3.4 - Comparison of results for continuous bridge system

Simulation Method	Reliability Index Z_1	Reliability Index Z_2	Probability of Failure Z_1	Probability of Failure Z_2	Probability of system failure
Original SS	3.75 (6830)	3.75 (7326)	8.74×10-5	8.86×10-5	N/A
Proposed RASS	3.69 (5420)	3.71 (6096)	1.13×10-4	1.04×10-4	2.12×10-4
Monte Carlo	3.71 (3.3×106 runs)	3.73 (3.5×106 runs)	1.04×10-4	9.57×10-5	2.06×10-4

3.8 Conclusion

This chapter proposed an improved subset simulation method herein referred as Regenerative Adaptive Subset Simulation (RASS). The proposed algorithm is based on advanced Markov Chain Simulation Algorithms combining the benefits of a Regeneration process, the Delayed Rejection and Adaptive algorithms and the Componentwise Algorithm. The Delayed Rejection allows partial local adaptation of the generated candidate samples at each time step of the Markov chain. The Adaptive Algorithm uses the history of the chain to update the variances of the proposal distribution function and can help in choosing the spread of the proposal samples. The Regeneration process helps in reducing the correlation between the generated samples and help in solving the burn-in problem. Additionally, a componentwise generation of samples is used to reduce the computational effort associated with multivariate input. Several illustrative examples verified the validity and stability of the proposed simulation method. The advantages of this proposed method include its accuracy, efficiency and its ability to handle structural systems with complex failure regions, large numbers of random variables, and small probabilities of failure.

CHAPTER FOUR: PROBABILISTIC ANALYSIS OF REDUNDANCY AND ROBUSTNESS OF BRIDGES

4.1 Introduction

As explained in Chapters 1 and 2, the redundancy analysis of structural systems should be performed using reliability methods in order to properly take into consideration the uncertainties in evaluating the system's behavior and overall capacity. Because most existing algorithms are not able to accurately evaluate the reliability of complex structural systems, Chapter 3 proposed an improved subset simulation method and presented several illustrative examples to verify the validity and stability of the proposed method. This Chapter will illustrate how to apply this method to analyze the redundancy and the robustness of typical bridge configurations. In particular, the method is applied to investigate the redundancy and robustness of a truss bridge and a pre-stressed I-girder bridge. Section 2 of this Chapter will describe the probability models that will be used in the reliability analysis. Section 3 will demonstrate the application of the methodology for the redundancy analysis of intact bridges. Section 4 will apply the methodology for the robustness analysis of damaged bridges. As explained in Chapter 2, according to the terminology adopted in this Dissertation, structural redundancy refers the ability of an originally intact system to continue to carry load after its members reach their ultimate carrying capacities. Robustness refers to the ability of a damaged system that has lost one or more members to continue to carry some load. The analysis of the possibility of progressive collapse due to the sudden occurrence damage and the associated release of the embedded strain energy will be discussed in a subsequent chapter.

4.2 Bridge Modeling

Bridge systems come in a variety of categories in this study the analysis of the reliability of bridge systems will be demonstrated for the most common bridge configurations consisting of multi-beam and truss bridges. The procedures outlined herein are however applicable to all other bridge types. To perform the reliability analysis, statistical models for member strengths and loads must be available. This section will present the models that will be used in this study.

4.2.1 Member Properties for Trusses

Generally, when modeling structures, most attention is paid to the main structural members. However, a preliminary report by the Federal Highway Administration (FHWA) (Holt and Hartmann 2008) suggests that the I-35W Minnesota bridge failure initiated at a gusset plate of the bridge. Therefore, in this study, the reliability analysis of truss bridges will model structural members and connections. The connections consist of the bolts and gusset plates.

4.2.1.1 Structural Steel Members

Figure 4.1 gives a typical stress-strain curve for structural steel. The stress-strain curve can be divided into have four parts: a) Elastic region, b) plastic region, c) strain-hardening region, and d) descending necking region. Because data on the necking segment is difficult to obtain, this study will use the simplified model shown in Figure 4.2.

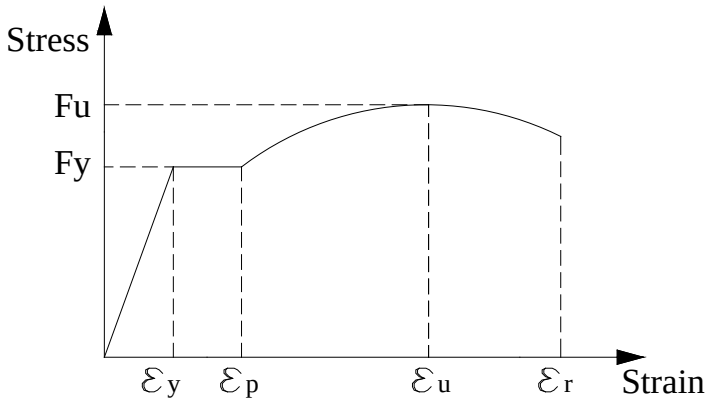

Figure 4.1 Steel Stress-Strain test Curve

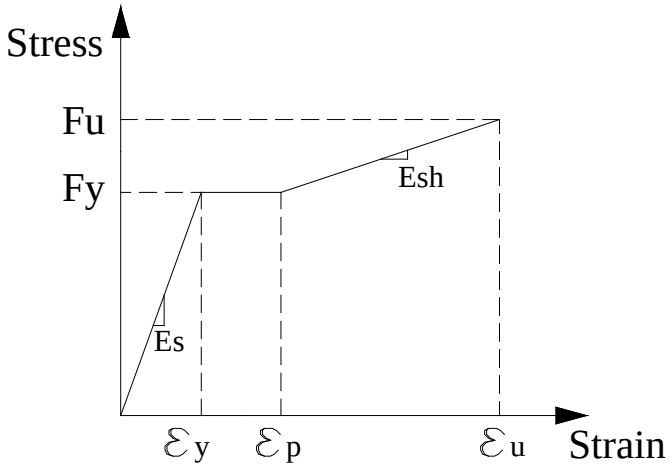

Figure 4.2 Simplified Model

During the calibration of the LRFD Steel Design Manual, Galambos and Ravindra (1978) studied the behavior of steel structural members. The steel properties they investigated included the modulus of elasticity, yield stress, and strain hardening properties. The statistical data for the yield strength and ultimate strength are summarized by Ellingwood et al. (1980) and Galambos and Ravindra (1978) . Accordingly, the bias and coefficient of variation (COV) for the yield strength and ultimate strength are 1.10 and 0.11. Both of these random variables are assumed to be log-normally distributed. based on collected data from (Johnson and Opila 1941; Julian 1957; Tall and Alpsten 1969). The

bias and coefficient of variation for the modulus of elasticity which is assumed to be normally distributed are found to be 1.08 and 0.060.

The only directly measured strain-hardening property is the strain-hardening modulus. Doane (1969) made an analysis of strain-hardening modulus data , E_{sh} , for ASTM A7, A36 and A441 steel. He found the mean value to be 600 ksi and the COV to be 0.25. However, 600 ksi seems to be too high. Laboratory tests performed at the City College of New York, show that the mean of the strain hardening modulus is 104 ksi and the COV is 0.06. The other property related to the nonlinear behavior of the steel material is the length of the plastic plateau. From tests done at the City College of New York, the plastic strain is found to be consistently 15 times the yield strain. This value is assumed to be deterministic. Table 4.1 summarizes the statistics of the random variables used in this study for structural steel.

Table 4.1 Statistics of random variables – steel members

Random Variable	Nominal	Bias	COV	Distribution Type	Reference
F_y	36 ksi	1.10	0.11	Log-normal	(Ellingwood et al. 1980; Galambos and Ravindra 1978)
F_u	58 ksi	1.10	0.11	Log-normal	(Ellingwood et al. 1980; Galambos and Ravindra 1978)
E_s	29000 ksi	1.08	0.06	Normal	(Johnson and Opila 1941; Julian 1957; Tall and Alpsten 1969)
E_{sh}	104 ksi (mean)	N.A.	0.06	Normal	City College

4.2.1.2 Steel Connections

Bolts

Based on collected data from research performed at Lehigh University (Fisher et al. 1978; Fisher and Kulak 1968; Rumpf and Fisher 1963; Wallaert and Fisher 1965), a tri-linear shear stress-deformation model is proposed to model the behavior of bolts as shown in Figure 4.3. The bias for the ultimate shear stress is 1.20 (Fisher et al. 1978). Given a nominal tensile strength for A325 bolts of 120 ksi, the nominal ultimate shear stress is 74.4 ksi, which is 62% of the tensile strength (Kulak et al. 1987). However, in lap splices transmitting an axial force between members with more than two bolts in the line of the force, non-uniform deformations of the connected material between fasteners causes a non-uniform distribution of the shear forces in the bolts. Consequently, the strength of the joint decreases (Kulak et al. 1987). Figure 4.4 describes how the average strength is affected by the increasing number of fasteners. Rather than provide a decreasing function that reflects this decrease in average strength with joint length, a single reduction factor of 0.80 is applied to the 0.62 multiplier with joint length on the order of 30 in. Based on the

data provided in references (Fisher et al. 1978; Fisher and Kulak 1968; Rumpf and Fisher 1963; Wallaert and Fisher 1965), the statistics of the random variable $\sigma_1, \sigma_2, \sigma_3$ and Δ_1, Δ_2, Δ_3 that describe the behavior of bolts in steel connections are provided in Table 4.2.

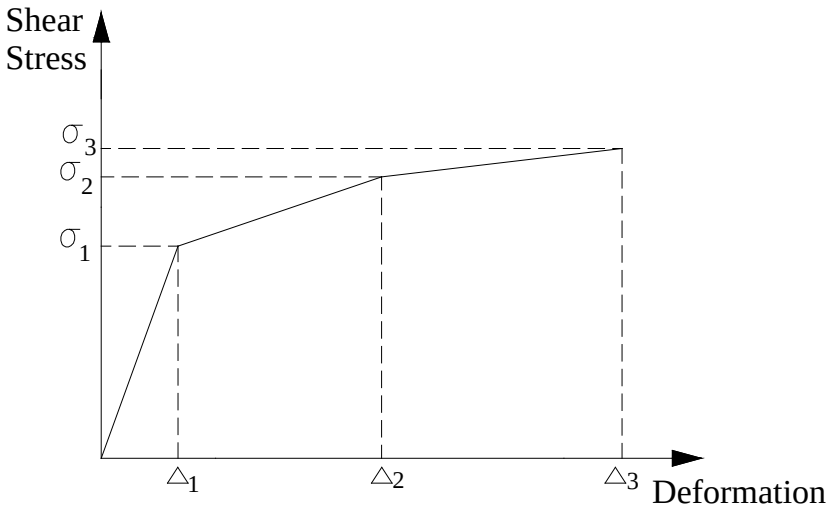

Figure 4.3 Simplified Tri-linear model

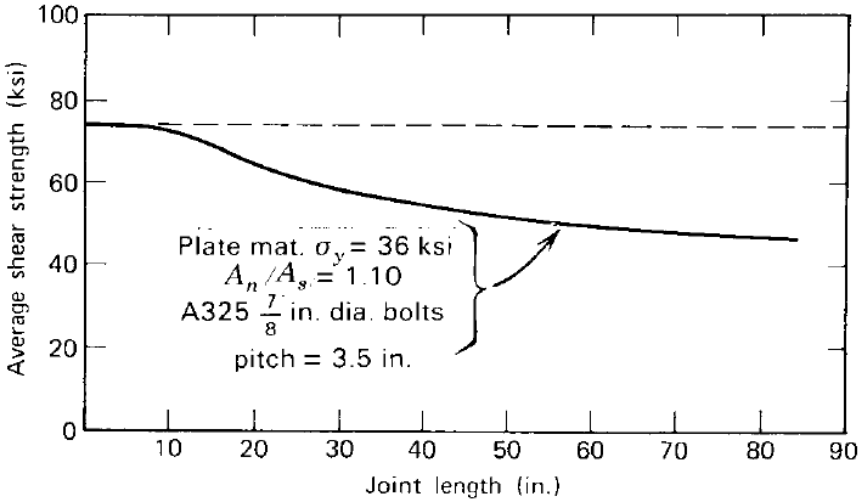

Figure 4.4 Effect of joint length on ultimate shear strength

Table 4.2 Statistics of random variables – steel connection

Random Variable	Mean	COV	Distribution Type	Reference
σ_1	41.30 ksi	0.10	Normal	(Fisher et al. 1978; Fisher and Kulak 1968; Rumpf and Fisher 1963; Wallaert and Fisher 1965)
σ_2	64.54 ksi	0.10	Normal	(Fisher et al. 1978; Fisher and Kulak 1968; Rumpf and Fisher 1963; Wallaert and Fisher 1965)
σ_3	71.42 ksi	0.10	Normal	(Fisher et al. 1978; Fisher and Kulak 1968; Rumpf and Fisher 1963; Wallaert and Fisher 1965)
Δ_1	0.036 in	0.08	Normal	(Fisher et al. 1978; Fisher and Kulak 1968; Rumpf and Fisher 1963; Wallaert and Fisher 1965)
Δ_2	0.12 in	0.08	Normal	(Fisher et al. 1978; Fisher and Kulak 1968; Rumpf and Fisher 1963; Wallaert and Fisher 1965)
Δ_3	0.23 in	0.08	Normal	(Fisher et al. 1978; Fisher and Kulak 1968; Rumpf and Fisher 1963; Wallaert and Fisher 1965)

Bearing Capacity of Gusset Plates

Rex and Easterling (2003) and Kim and Yura (1999) performed a large number of experiments to provide data about the strength and load-deformation behavior of a single plate bearing on a single bolt or two bolts. A normalized Load-Deformation relationship for the bearing capacity of connection plates was proposed by Rex and Easterling (2003) as given in Equation (4.1):

$$\frac{P}{P_n} = \frac{1.74\,\overline{\Delta}}{\left(1+\overline{\Delta}^{0.5}\right)^2} - 0.009\,\overline{\Delta} \tag{4.1}$$

Where, P=plate load; P_n=nominal plate strength; $\overline{\Delta}$ =normalized deformation= $\Delta\beta K_i / P_n$; Δ =hole elongation; β =steel correction

factor=30%/%Elongation (for typical steels taken as one); and K_i=initial stiffness.

Nominal Plate Strength

The most common strength model for predicting the bearing strength F_b of plates was developed by Fisher and Struik (1974):

$$F_b = \frac{P_n}{d_b t_p} = 1.4F_u\left(\frac{L_e}{d_b} - \frac{1}{2}\right) \leq 3.0F_u \tag{4.2}$$

Where, d_b=diameter of bolts; t_p=the thickness of plate; L_e= the end distance; F_u=ultimate strength of plate

In addition to Equation (4.2), Fisher and Struik (1974) also recommended a simpler expression that was adopted by the AISC Specification (LRFD, 1993):

$$F_b = F_u \frac{L_e}{d_b} \leq 2.4F_u \tag{4.3}$$

More recently, the AISC Specification (LRFD 1999) has adopted an equation that is based on a physical model similar to that used by Fisher and Struik (1974) and is given as:

$$F_b = 1.2F_u \frac{L_c}{d_b} \leq 2.4F_u \tag{4.4}$$

Where L_c=minimum distance from the edge of the bolt hole to the edge of the plate.

The Eurocode (Eurocode3 1993) has a slightly different expression for the bearing strength. If it is assumed that the bolt steel tensile strength is greater than the plate steel tensile strength, the Eurocode expression (Eurocode3 1993) can be written as:

$$F_b = \frac{2.5}{3} F_u \frac{L_c}{d_h} \le 2.5 F_u \tag{4.5}$$

Where d_h=hole diameter

After statistical comparisons of the existing models for evaluating nominal plate strength, Rex and Easterling (2003) pointed out that the AISC Specification (LRFD 1993) provided the best correlation with experimental results and is therefore used in our analysis.

Based on the data from Rex and Easterling (2003) and Hyeong J. Kim (1999), a bilinear force-displacement model for bearing is developed as shown in Figure 4.5.

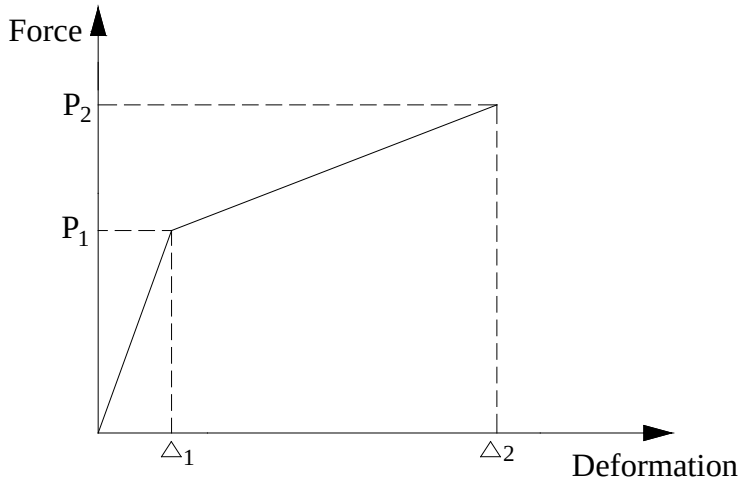

Figure 4.5 Bilinear force-displacement model for bearing plates

Several factors can influence the ultimate deformation Δ_2, such as the distance between the edge of the plate and the bolt L_e, the ultimate strength F_u, and the diameter of the bolts d_b. Regression analysis gives the following relationship between Δ_2 (mm), L_e (mm), F_u (kN/mm) and d_b (mm).

$$\Delta_2 = -7.9462 + 1.1315 * L_e - 0.0129 * F_u + 0.1331 * d_b - 0.0137 * L_e^2 \tag{4.6}$$

Δ_1 is approximated to be $\frac{1}{6}\Delta_2$ based on the data provided by Rex (2003).

The initial stiffness is predicted using the model provided by Rex and Easterling (2003).

$$K_i = \frac{1}{\frac{1}{K_{br}} + \frac{1}{K_b} + \frac{1}{K_v}} \tag{4.7}$$

Where K_{br} is bearing stiffness=$120 t_p F_y (d_b / 25.4)^{0.8}$;

K_b is bending stiffness= $32 E t_p (L_e / d_b - 1/2)^3$;

K_v is shearing stiffness= $6.67 G t_p (L_e / d_b - 1/2)$ where G is shear modulus of elasticity.

Once Δ_1, Δ_2 and K_i are determined, P_1 and P_2 can be obtained from Equation (4.1).

The bias giving the ratio of the experimental result for P_2 to the predicted P_2 is defined as γ_p. Assuming that the bias and coefficient of variation for the shear modulus of elasticity G are the same as those for the modulus of elasticity E, the random variables that describe the behavior of gusset plates are summarized as shown in Table 4.3.

Table 4.3 Statistics of random variables – gusset plate

Random Variable	Nominal	Bias	COV	Distribution Type	Reference
F_y	36ksi	1.10	0.11	Log-normal	(Ellingwood et al. 1980; Galambos and Ravindra 1978)
F_u	58ksi	1.10	0.11	Log-normal	(Ellingwood et al. 1980; Galambos and Ravindra 1978)
E_s	29000ksi	1.08	0.06	Normal	(Ellingwood et al. 1980; Galambos and Ravindra 1978)
G	11153.85ksi	1.08	0.06	Normal	(Rex and Easterling 2003)
γ_p	N.A.	1.05 (mean)	0.05	Normal	(Rex and Easterling 2003)

4.2.1.3 Member Properties for Beams

For the bending moment resistance of bridge members, the mean and COV are given by Nowak (1999) as:

$\overline{R} = 1.12\ R_n$ $V_R = 10\%$ For steel beams

$\overline{R} = 1.05\ R_n$ $V_R = 7.5\%$ For prestressed concrete beams

$\overline{R} = 1.14\ R_n$ $V_R = 13\%$ For reinforced concrete beams

For the shear resistance, the mean and COV are given by Nowak (1999) as:

$\overline{R} = 1.14\ R_n$ $V_R = 10.5\%$ For steel beams

$\overline{R} = 1.15\ R_n$ $V_R = 14\%$ For prestressed concrete beams

$\overline{R} = 1.20\ R_n$ $V_R = 15.5\%$ For concrete beams with steel

$\overline{R} = 1.40\ R_n$ $V_R = 17\%$ For concrete beams without steel

4.2.2 Load Models

Based on the recommendation of Ghosn and Moses (1998), the live load is evaluated for three traffic conditions: a) Extreme loading condition with a 75-year exposure period for the redundancy analysis of intact bridges, LL_{75}; b) Regular loading condition with a 2-year exposure period for the robustness analysis of damaged bridges, $LL_{2;}$. These factors can be expressed in terms of equivalent AASHTO HS-20 truck loads. Table 4.4 gives the mean and COV of live loads as function of the effect of AASHTO HS-20 trucks. LL_{75} and LL_2 values in Table 4.4 are the same values used by Nowak (Nowak 1999) and follow lognormal distribution.

Table 4.4 Mean and COV of live loads as function of the effect of two side-by-side AASHTO HS-20 trucks

Span length (ft)	LL_{75}	LL_2	V_{LL}
45	1.67	1.53	19%
60	1.72	1.60	19%
80	1.81	1.67	19%
100	1.89	1.75	19%
120	1.98	1.84	19%
150	2.01	1.87	19%

In addition to the live loads, the random variables that control the safety of bridges include the applied dead loads. Using Nowak's (1999) recommendation, the total dead load, DL is divided into the dead load of pre-fabricated members, DC1, the dead load of cast-in-place members, DC2, and the dead load of the wearing surface, Dw, such that the mean total dead load is given by:

$$\overline{DL} = \overline{D_{c1}} + \overline{D_{c2}} + \overline{D_w} \tag{4.8}$$

Nowak (1999) provided models to represent the mean values as a function of the nominal values and the COV's or standard deviations of these dead load random variables that can be summarized as follows:

$$\begin{aligned} \overline{D_{C1}} &= 1.03\, D_{C1} \qquad & V_{DC1} &= 8\% \\ \overline{D_{C2}} &= 1.05\, D_{C2} \qquad & V_{DC2} &= 10\% \\ \overline{D_W} &= 1.0\, D_W \qquad & V_{DW} &= 25\% \end{aligned} \tag{4.9}$$

4.3 Analysis of the Redundancy in Bridge Systems

In this section, two simple examples describing the analysis of a prestressed concrete bridge and a thru-truss bridge are analyzed to illustrate the procedure of evaluating the redundancy and reliability of bridge systems. The first example consists of a 100-ft 6-beam prestressed concrete bridge having the configuration shown in Figure 4.6. The moment curvature relationship for the composite main girders and transverse beams are shown in Figure 4.7. In the reliability analysis, the variable Capacity R is modeled by increasing the moment in the Figure 4.7 by the same amount for M1 to M4.

Bridge failure is assumed to occur when concrete crushes at a maximum nominal rotation θ_{max}=0.047 with a bias of 1.15 and a COV of 40%

assuming a Lognormal distribution.

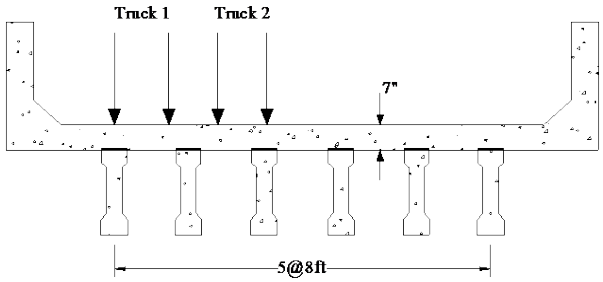

Figure 4.6 Cross Section of Prestressed Concrete Bridge

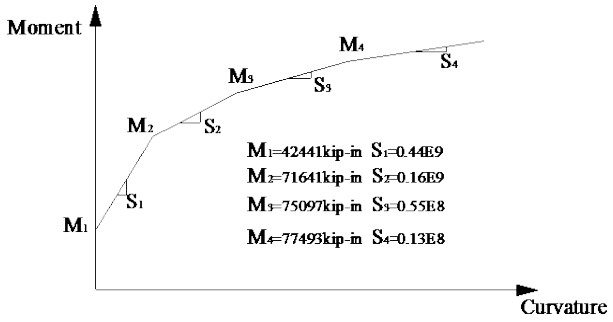

(a) Moment-Curvature Relationship for longitudinal beams

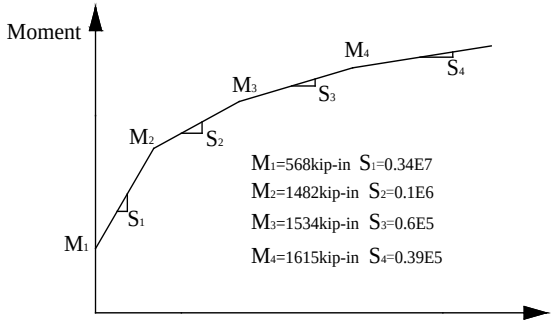

(b) Moment-Curvature Relationship for transverse slab beams

Figure 4.7 Typical Moment-Curvature Relationship for Prestressed Concrete Members

The second example consists of the truss bridge having the configuration shown in Figure 4.8. The through-truss bridge selected has two parallel trusses. Table 4.5 gives a listing of the truss members along with their cross sectional areas. The two parallel trusses are connected by cross beams and diagonals supporting a concrete deck. In this preliminary example, the nonlinear behavior of the steel truss members is modeled using the bilinear stress strain curve shown in Figure 4.9 which is used to illustrate the procedure. In this chapter, the analysis is based on the model described in section 4.2.

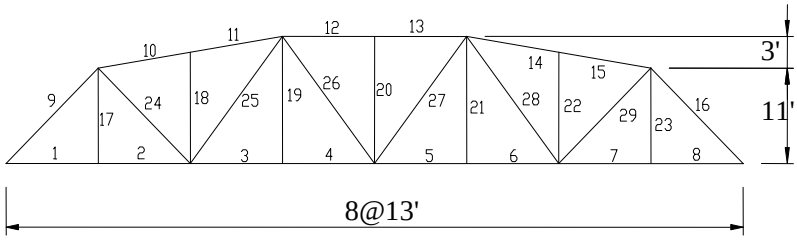

Figure 4.8 Layout of Bridge Truss

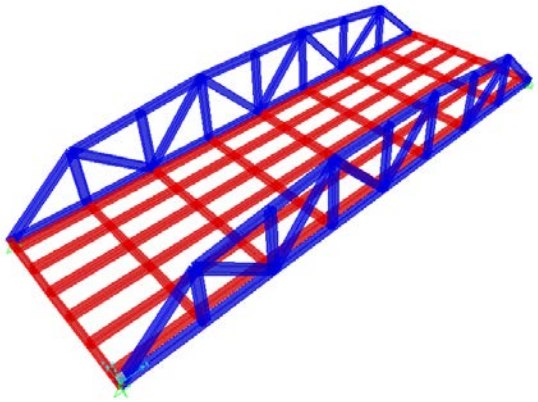

Figure 4.9 3D model of Truss Bridge

Table 4.5 Truss Members' Cross Sectional areas

No.	Area (in2)	No.	Area (in2)	No.	Area (in2)
1	25.2	11	40.4	21	19.1
2	25.2	12	43.4	22	13.2
3	38.3	13	43.4	23	15.6
4	38.3	14	40.4	24	17.0
5	38.3	15	40.4	25	13.2
6	38.3	16	38.0	26	13.2
7	25.2	17	15.6	27	13.2
8	25.2	18	13.2	28	13.2
9	38.0	19	19.1	29	17.0
10	40.4	20	13.2		

4.3.1 Redundancy Analysis

According to the NCHRP 406 study by Ghosn and Moses (1998), redundancy is defined in terms of the difference between the reliability index of the bridge system and the reliability index of the members. The analysis of bridge system safety includes checking the redundancy of intact bridges under the effect of overloads. In order to analyze the safety of bridge systems, three limit states are defined to ensure adequate bridge redundancy and safety as well as functionality. These limit states include: a) Member failure; b) Ultimate limit state; c) Functionality limit state.

In this study, conditional probabilities of failure are calculated for specific values of the live load, LL. The unconditional probability of failure can then be obtained given the probability distribution of LL. This approach is adopted herein to provide sufficient flexibility to account for different loading conditions. Accordingly, the probability of bridge failure can be obtained from:

$$P_c = \sum_i P\left(C\middle|LL_i\right)P\left(LL_i\right) \tag{4.10}$$

Where, Pc is the probability of failure of the bridge. P(C|LLi) is the conditional probability of failure given the occurrence of specific values of LL_{75}. P(LLi) is the probability distribution of LL_{75}.

The calculation of the probability of failure is performed for all of the limit states using the modified Subset Simulation method described in Chapter 3 with a conditional failure probability at each level equal to p_0=0.1 and with the number of samples set to N=500 at each conditional level. The proposal PDF for each uncertain parameter is chosen as a uniform PDF centered at the current sample.

4.3.1.1 Calculation of Conditional Probabilities

The conditional probabilities of failure for the prestressed concrete bridge are shown in Fig 4.10 to Fig 4.12 for the three limit states. For the truss bridge, the probabilities of failure given the occurrence of particular truck loads are shown in Figures 4.13 to Fig 4.15.

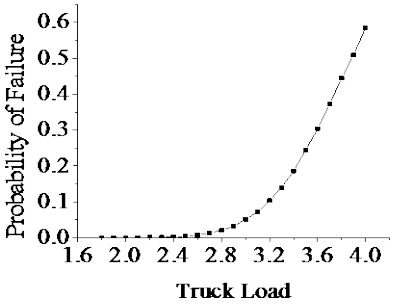

Figure 4.10 Conditional Probability of Member Failure of P/C bridge

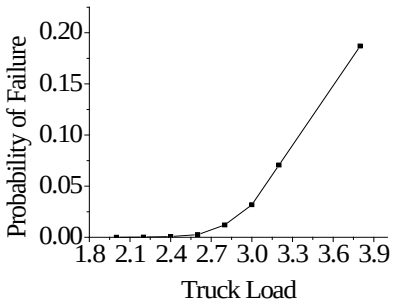

Figure 4.11 Conditional Probability for Functionality Limit of P/C bridge

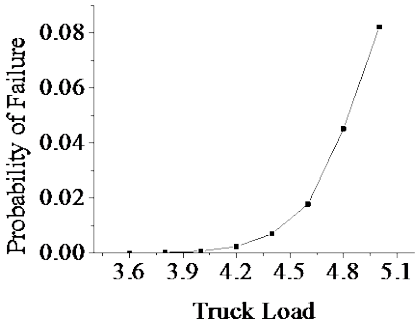

Figure 4.12 Conditional Probability for Ultimate Limit State of P/C bridge

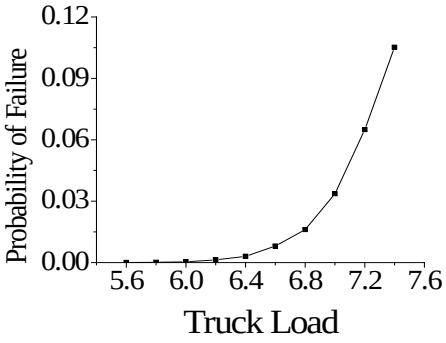

Figure 4.13 Conditional Probability of Member Failure of truss bridge

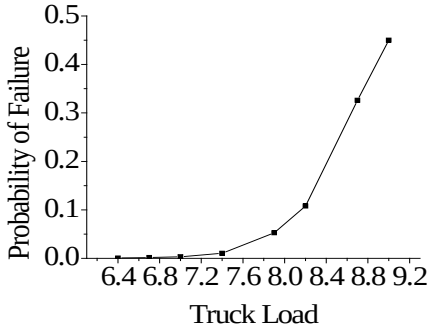

Figure 4.14 Conditional Probability for Functionality Limit State of truss bridge

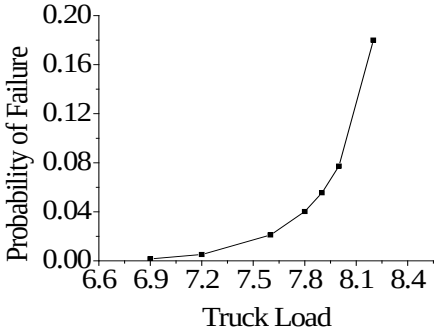

Figure 4.15 Conditional Probability for Ultimate Limit State of truss bridge

The results in Figures 4.10 thru 4.15 describe the vulnerability of the bridge systems to different types of failures when subjected to specific values of the live load. These values are presented as multipliers of the effect of the HS-20 truck and are listed as LF_1, LF_f, and LF_u, respectively for the Member Failure, Functionality, and Ultimate limit states respectively. For example, at the mean value of 75-year maximum load, when $LL_{75} = 1.89$, the results of the Subset Simulation for the 100-ft Prestressed Concrete bridge show that the conditional probability of failure for the most critical member is equal to

$P(C|LL_{75})=5.2*10^{-5}$ corresponding to a conditional reliability index for the member $\beta_{mem}=3.88$. Similarly the conditional probabilities of exceeding the functionality limit state defined as the point at which the maximum vertical displacement reaches a value equal to span length/100 and the corresponding reliability index are obtained as $P(C|LL_{75})=8.1*10^{-6}$ corresponding to a reliability index $\beta_{funct}=4.31$ for the functionality limit state. The failure of the entire system due to overloading is associated with a probability $P(C|LL_{75})= 5.8*10^{-10}$ with a conditional reliability index $\beta_{ult}=6.08$.

4.3.1.2 Redundancy Analysis of Prestressed Concrete Bridge

Because the live loads may exceed or be less than their mean values, the overall unconditional probabilities of failure are obtained by summing over all the possible values of the applied load and the load probabilities as described in Equation (4.8). Table 4.6 lists the probabilities of failure under the three limit states mentioned above for the Prestressed Concrete Bridge.

Table 4.6 Probability of failure for prestressed concrete bridge

P(member)	P(functionality)	P(ultimate)
2.19*10-3	1.12*10-4	7.20*10-9
βmember	βfunctionality	□ultimate
2.85	3.69	5.67

Using the reliability-based criteria for redundancy set by Ghosn and Moses (1998), the results of Table 4.6 show that

$\Delta\beta u=\beta ult-\beta mem=5.67-2.85=2.82>0.85;$

$\Delta\beta f=\beta funct-\beta mem=3.69-2.85=0.84>0.25;$

Where the margin target reliability indexes of 0.85 and 0.25 for the ultimate and functionality limit states were determined by Ghosn and Moses (1998) to indicate acceptable levels of redundancy. Therefore, this bridge has sufficient levels of redundancy since the reliability indices satisfy the criteria suggested in NCHRP Report 406. However, the member reliability index is less than the 3.50 standard value used by the AASHTO LRFD even-though the bridge members are designed to satisfy the criteria of the standard AASHTO specifications.

Section 4.3.2 of this chapter will provide an illustration on how to select an appropriate safety factor that should be used to strengthen this particular bridge's members in order to provide overall system reliability levels that will take into consideration the fact that this bridge's members are under designed and the fact that the bridge's configuration provides sufficient levels of redundancy.

4.3.1.3 Redundancy Analysis of Truss Bridge

Table 4.7 lists the unconditional probability of failure under the three limit states mentioned above for the truss bridge. Specifically, Table 4.7 shows that

$\Delta\beta u=\beta ult-\beta mem=7.67-6.80=0.87>0.85;$

$\Delta\beta f=\beta funct-\beta mem=7.43-6.80=0.63>0.25;$

Since the target reliability index criteria are met, this bridge is classified as redundant.

Table 4.7 Probability of failure for truss bridge

P(member)	P(functionality)	P(ultimate)
5.13*10-12	5.1*10-14	8.9*10-15
βmember	βfunctionality	βultimate
6.80	7.43	7.67

4.3.2 System Safety Factor

A bridge system that is adequately redundant may still be unsafe if its members are inadequately designed (and vice versa). AASHTO LRFD (2002) was calibrated to provide a reliability index β_{member}=3.50 for bridge members. The prestressed concrete bridge example analyzed in Section 4.3.1 showed that its member reliability index is β_{member}=2.85 which is lower than the target 3.50. Similarly, the reliability index for the functionality limit state is $\beta_{functionality}$=3.69, which is less than the target $\beta_{functionality}$=3.50+0.25=3.75. On the other hand, the redundancy analysis shows that the system is adequately redundant. However, to verify that the bridge system provides minimum levels of overall system safety an analysis of the system reliability must be performed.

Assume that the member resistance is represented by the load factor LF_1 and the applied maximum lifetime live load represented by the factor LL_{75}. A plot of the results of Figure 4.10 on a lognormal probability scale is provided in Figure 4.16. Figure 4.16 shows that LF_1 can be reasonably well represented by a Lognormal distribution with a mean value $\overline{LF_1} = 3.69$ and a COV V_{LF}=12%. Given that LL_{75} also follows a Lognormal distribution with a mean $\overline{LL_{75}} = 1.89$ and V_{LL}=19%. An approximate evaluation of the reliability index β_{member} for the failure of the first member can then be expressed as

$$\beta_{member} = \frac{\ln \dfrac{\overline{LF_1}}{\overline{LL_{75}}} \dfrac{\sqrt{1+V_{LL}^2}}{\sqrt{1+V_{LF}^2}}}{\sqrt{\ln\left(\left(1+V_{LF}^2\right)\left(1+V_{LL}^2\right)\right)}} \tag{4.11}$$

Which gives β_{member}=3.05 which is reasonably close to the β_{member}=2.85 obtained by the Markov Chain. Similarly, Figure 4.17 gives the probability plot of the functionality limit state. Once again the results show that LF_f follows a lognormal distribution with a $\overline{LF_f} = 4.31$ and V_{LF}=12% and the reliability index $\beta_{functionality}$ can be expressed as:

$$\beta_{functionality} = \frac{\ln \dfrac{\overline{LF_f}}{\overline{LL_{75}}} \dfrac{\sqrt{1+V_{LL}^2}}{\sqrt{1+V_{LF}^2}}}{\sqrt{\ln\left(\left(1+V_{LF}^2\right)\left(1+V_{LL}^2\right)\right)}} \tag{4.12}$$

If the designer wishes to strengthen the bridge members to satisfy a target β_{member}=3.50, and assuming that the probability plot is parallel to that for β_{member}=2.85, then the new required mean value for LF_1 should be $\overline{LF_{1req}} = 4.15$.

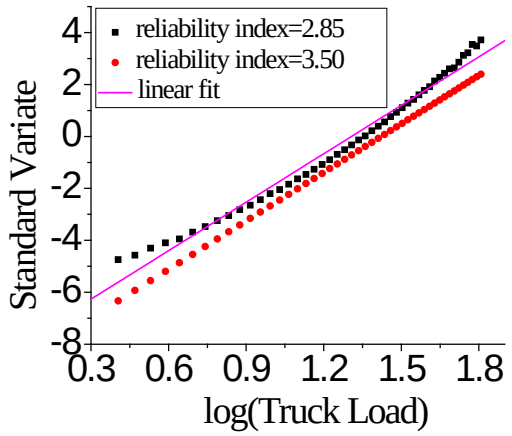

Figure 4.16 Lognormal probability plot for LF_1

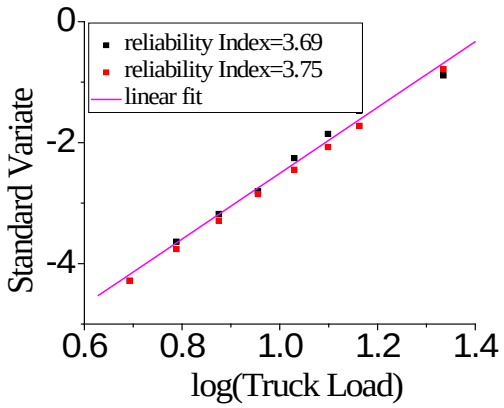

Figure 4.17 Lognormal probability plot for LF_f

For the functionality limit state, the current design produces a reliability index $\beta_{functionality}$=3.69. If the $\beta_{functionality}$ needs to be changed to match the required target 3.75, then the bridge system must satisfy an average functionality capacity represented by $\overline{LF_{freq}} = 4.39$. Following Ghosn Moses (1998), the system reserve ratios are defined as $r_1 = \overline{LF_1} / \overline{LF_{1req}}$ =0.89 for first member failure, while $r_f = \overline{LF_f} / \overline{LF_{f\,req}}$ =0.98 for the functionality limit state. The redundancy factor ϕ_{red} can then be calculated using the following equation:

$$\phi_{red} = \min(r_1, r_f) = \min(0.89, 0.98) = 0.89 \tag{4.13}$$

A redundancy factor $\phi_{red} = 0.89$ indicates that this bridge's member strengths must be increased by a factor $1/\phi_{red}$ to improve the overall system safety of this bridge. This can be executed using the equation:

$$R' - D' = \frac{R - D}{\phi_{red}} \tag{4.14}$$

Where, R' is the member resistance required to satisfy the redundancy criteria. D' is

the updated dead load corresponding to the member with resistance R'. R is the original resistance in the member, and D is the original dead load. For the prestressed bridge, the members have a resistance capacity, R=84993 kips-in, and a dead load D=34200 kips-in. If we assume that the strengthened member's dead load remains at 34200 kips-in, then the new required member strength that will satisfy all the redundancy and overall system safety criteria should be R'=91270 kips-in.

4.4 Illustrative Examples for Robustness Analysis

As mentioned in Chapter 2, for the purposes of this Dissertation structural robustness is defined as the ability of a damaged bridge that has lost a main load carrying member or component to continue to carry some level of live load. Criteria for the reliability level that a damaged bridge should satisfy have been established by Ghosn and Moses (1998). In this section, we will illustrate how the subset simulation method can be used to check the robustness of bridge structures. For that purpose, the same example bridges described in Section 4.3 will be used to analyze their structural robustness.

For the prestressed concrete bridge example, the most critical member of the intact structure was chosen as the damaged girder. For example, the damage may be due to fatigue failure of the prestressing tendons. For the truss bridge example, the most critically loaded tension member was chosen as the damaged member and removing it from the structural model simulates a possible fatigue failure. The conditional probabilities of failure of the damaged prestressed concrete bridge and truss bridge are shown in Fig 4.18 and Fig 4.19. The probabilities of failure under damaged condition are listed in Table 4.8.

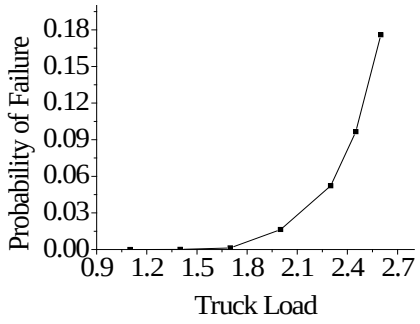

Figure 4.18 Damaged Limit State of P/C bridge Figure

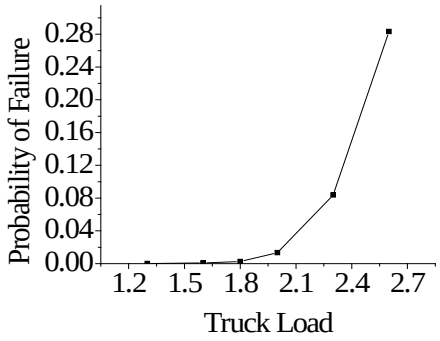

Figure 4.19 Damaged Limit State of Truss bridge

Table 4.8 Probabilities of failure

	Prestressed Concrete Bridge	Truss Bridge
P(ultimate)	0.0425	1.355*10-2
□damaged	1.72	2.21

The differences between the reliability indexes of the damaged bridges are compared to the reliability index of the members to yield:

$\Delta\beta d=\beta damaged-\beta mem=1.72-2.85=-1.13>-2.70$ for the prestressed concrete bridge

$\Delta\beta d=\beta damaged-\beta mem=2.21-6.80=-4.59<-2.70$ for the truss bridge

Based on the criteria set by Ghosn and Moses (1998) that damaged bridges should provide a difference in the reliability index of -2.70 or higher, the results of the analysis show that the prestressed concrete bridge has sufficient level of robustness and the truss bridge is not robust. However, since the member reliability index of the truss is $\beta_{member}=6.80$ which is much higher than the target AASHTO LRFD $\beta_{member}=3.5$, then the

overall system safety may still be satisfactory. Thus, a bridge which may not have a configuration that allows for a sufficient redistribution of loads should one of its members fails may still provide sufficient system safety to accommodate some minimum level of live load if the bridge members are overdesigned. In this sense, optimizing the design of non-redundant bridge configurations is not recommended while the application of additional safety factors will generally help increase overall system safety.

4.6 Conclusions

This Chapter illustrated the application of the modified Markov Chain simulation for evaluating the system reliability, redundancy of originally intact bridges and the robustness of bridge systems subjected to local failures. A prestressed concrete bridge and a truss bridge were used to illustrate the methodology. The examples demonstrate how the application of system factors can enhance the system safety of bridges whose configurations may not be providing sufficient levels of redundancy or robustness. A methodology for calibrating the necessary system factors is presented.

CHAPTER FIVE: PROBABILISTIC ANALYSIS OF REDUNDANCY, ROBUSTNESS OF BOX-GIRDER BRIDGES

5.1 Introduction

In Chapter 4, the proposed simulation approach is applied to evaluate the redundancy, robustness of truss bridge and prestressed I-girder bridge. This Chapter will illustrate how to perform probabilistic redundancy analysis of steel box-girder bridges. Section 2 of this Chapter will verify the grillage model for the analysis of box-girder bridges. Section 3 will demonstrate the application of the methodology for the redundancy and robustness analysis of a steel box-girder bridge.

5.2 Verification of Grillage Model for the Analysis of Box-Girder Bridges

In this section, the grillage model is used to analyze a box-girder bridge and demonstrate the validity of the approach by comparing it with the results of experimental tests on a concrete box girder bridge as reported by Kurian and Menon (2007).

5.2.1 Modeling of Box Girder Bridges

The program SAP2000 is used in the paper to perform a grillage analysis of a bridge system where the girders and the deck are modeled as equivalent beam elements. For the analysis of spread box girder bridge superstructures, longitudinal box beams are placed to coincide with the centerline of each web of the box and each beam represents half of the box girder section. The transverse beams consist of two types. The first type is used for the section falling outside the box girders. In this case, the transverse beam properties are based only on the slab thickness and corresponding material behavior. The second type of

transverse beams is used to model the transverse properties of the box beam section along with the slab. The transverse properties are based on the transverse bending inertia of the box and an equivalent shear area to account for the in-plane distortions of the box. The properties of the transverse element are proportional to the element width.

The elastic properties required by the grillage analysis for each beam element include: (1) the modulus of elasticity, E, (2) the moment of inertia, I, (3) the shear modulus, G, and (4) the torsional constant, J. While the elastic bending properties are easy to calculate from basic strength of materials concepts, the torsional properties are most important for the analysis of box girder bridges and methods for their calculations are provided by Hambly (1991).

For the transverse beams representing the contribution of the slab alone with thickness t, the torsional constant is obtained as:

$$J = t^3 / 6 \qquad \text{per unit length of slab} \tag{5.1}$$

As proposed by Hambly (1991), the value used for the torsion constant is only half $J = t^3 / 3$ that would be used for a thin rectangular section to account for the continuity between the slab elements.

The torsional constant of the beams modeling the transverse properties of the box is given as:

$$J = 2h^2 \frac{t_1 \times t_2}{t_1 + t_2} \quad \textit{per unit width of cell} \tag{5.2}$$

Where t_1 and t_2 are the thicknesses of the top and bottom flange and h is the height of

the section.

The pure torsional constant of the box section is determined by the following equations given by Hambly (1991).

$$J = \frac{4A^2}{\sum \frac{s_i}{t_t}} \tag{5.3}$$

Where S_i and t_i are respectively the length and thickness of each segment of the closed box as shown in Figure 5.1, while A is the area of the box enclosed within the center-line of the webs and flanges. When the section is composite, the concrete slab is transformed into an equivalent thickness of steel by dividing by the modular ratio.

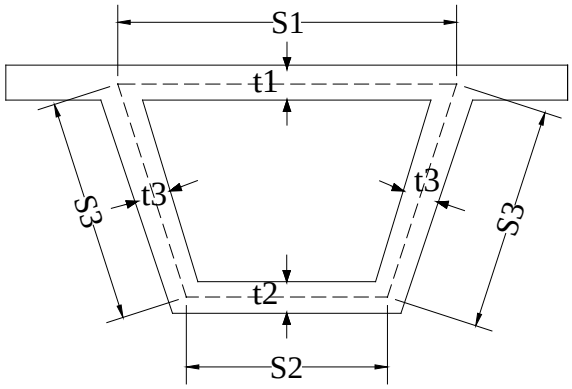

Figure 5.1 Geometrical Parameters corresponding to torsional constant of a box girder

To include the effect of the distortion of the box frame and the contributions of the bracings in reducing the in-plane deformations of the box, the distortion of the box can be simulated by an equivalent torsion constant C_d according to Hambly (1991). Thus, the total torsion constant C_{dt}, which would account for the pure torsion rotations as well as the distortion, is given by

$$\frac{1}{C_{dt}} = \frac{1}{C_d} + \frac{1}{J} \tag{5.4}$$

The distortion component, C_d is obtained from:

$$C_d = \frac{S_1^{\,2} l\, I_c\, \beta^3}{1.6w} \tag{5.5}$$

with

$$\beta = \left\{ \frac{1}{EI_c \delta_1} \right\}^{0.25} \tag{5.6}$$

$$\delta_1 = \frac{S_1 S_2}{24(S_1 + S_2)} \left\{ \frac{S_3}{D_c} \left[\frac{2S_1 S_2}{S_1 + S_2} - v(2S_1 + S_2) \right] + \frac{S_1^{\,2}}{D_a} \left[\frac{S_2}{S_1 + S_2} - v \right] \right\} \tag{5.7}$$

Where, S_1, S_2 , S_3 are shown in Figure 1; l is the span length; I_c is the moment of inertia of the box section; v is Poisson's ratio; $D_a = \frac{Et_1^{\,3}}{12(1-v^2)}$ and $D_c = \frac{Et_2^{\,3}}{12(1-v^2)}$, where t_1 and t_2 are the thickness of the top and bottom flanges of the box section, respectively; E is the modulus of elasticity. Wright and Abdel Samad (1968) provide charts of w versus the dimensionless panel length βl.

If the box girder is provided with cross bracings, then Wright and Abdel Samad (1968) define a dimensionless stiffness for bracing, q:

$$q = \frac{E_b A_b}{L_b} \frac{\delta_b^{\,2}}{l \delta_1} \tag{5.8}$$

$$\delta_b = \frac{2\left[1+\frac{S_1}{S_2}\right]}{\left[1+\left\{\frac{S_1+S_2}{2h}\right\}^2\right]^{0.5}} \tag{5.9}$$

Where, A_b is the area of bracing; L_b is the length of bracing; l is distance between bracings; E_b is Young's modulus of bracing; h is the height of the box section.

Given q and βl, the value of w can be obtained from the charts are provided by Wright and Abdel Samad (1968).

The stiffness of a plate diaphragm is approximated by replacing it with an equivalent pair of cross braces. A rectangular plate diaphragm in pure shear would have the same stiffness as cross bracing of area provided by Wright and Abdel Samad (1968):

$$A_b = \frac{G_p t_p L_b^{\,3}}{2E_p A_p} \tag{5.10}$$

Where, t_p and A_p are the thickness and middle surface area and and G_p, E_p are the shear modulus and the modulus of elasticity of the plate diaphragm.

For trapezoidal diaphragms,

$$A_b = \frac{G_p t_p h^2}{E_p (S_1+S_2)}\left[1+\left(\frac{S_1+S_2}{2h}\right)^2\right]^{3/2} \tag{5.11}$$

In addition to the typical elastic properties, the grillage analysis requires information on the nonlinear section properties of each beam element. In this study, uncoupling

between the torsional and bending properties is assumed and the linear torsion properties remain in effect throughout the loading process. The nonlinear bending behavior is modeled using a moment versus plastic rotation curve for each beam element.

Since no experimental relationships are available for steel box girders, the moment versus plastic rotation curve of a box-girder member is obtained by first calculating the moment versus curvature relationship using strength of material principles. A plastic hinge length equal to the depth of the section is assumed as long as the depth is less than ½ the beam element length. Otherwise, ½ the element length is used for the plastic hinge length.

5.2.2 Verification of the Validity of the Grillage Model for the Analysis of Concrete Box-Girder Bridges

To verify the validity of the grillage model for the analysis of box-girder bridges, the results obtained by SAP2000 are compared with available experimental results. Specifically, the grillage analysis is performed for four concrete box-girder bridge models that were tested by Kurian and Menon (2007). All four models had the same dimensions and reinforcement. The difference was in the positioning of the loads during testing.

Figure5.2 shows the cross section of the concrete box girder with the details of reinforcement. The total length of the specimen was 5300 mm with a simply supported span of 5000 mm. The compressive strength of concrete is 40 Mpa. Mild steel rods of 6 mm diameter were used for the reinforcement. Tension tests were carried out on six samples and the average value of the yield stress was found to be 636 Mpa with an ultimate stress of 725 Mpa. Young's modulus of the steel was obtained as 2.01×10^5 Mpa. The reinforcements are provided in two layers at a spacing of 100 mm center-center in the

longitudinal as well as in the transverse directions. The minimum clearance to the face of the transverse reinforcement was provided as 6 mm.

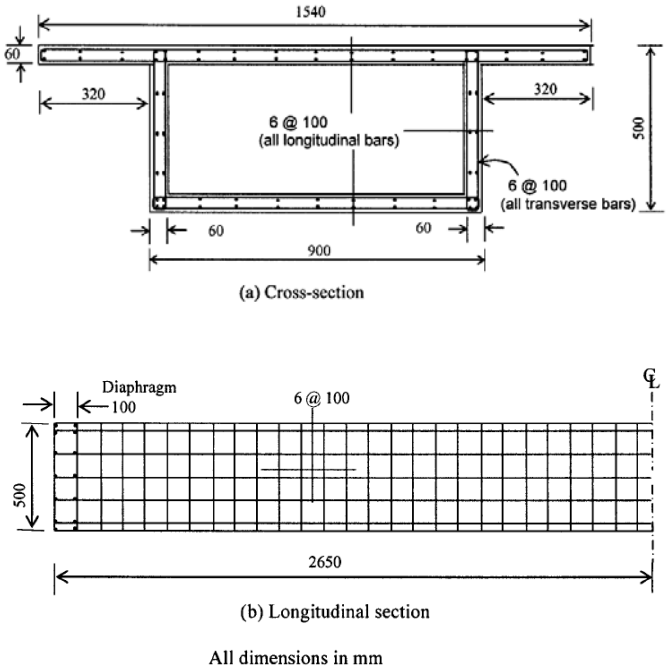

Figure 5.2 Cross section and the details of reinforcement [Kuiran and Menon, 2007]

The bridge is discretized as shown in Figure5.3. The longitudinal grillage beams L1 are placed to coincide with the centerline of each web of the box. T1 represent the transverse box beam section and T2 represent the transverse slab beam section.

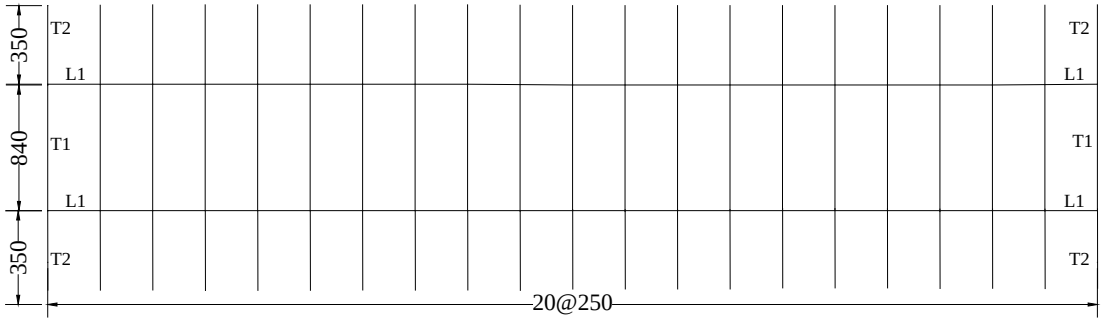

Figure 5.3 Grillage model (all dimensions in mm)

The dead load entered as a distributed load over the longitudinal beam elements is equal to 2.258 N/mm.

Four live load positions, as shown in Figure5.4, were considered. The location of the load on the top flange of the box girder was varied to study the effects of eccentricity of the loads and the torsion they produced on the behavior of box-girder bridges. In all four models, the loads were applied at the mid-span location of the box girder.

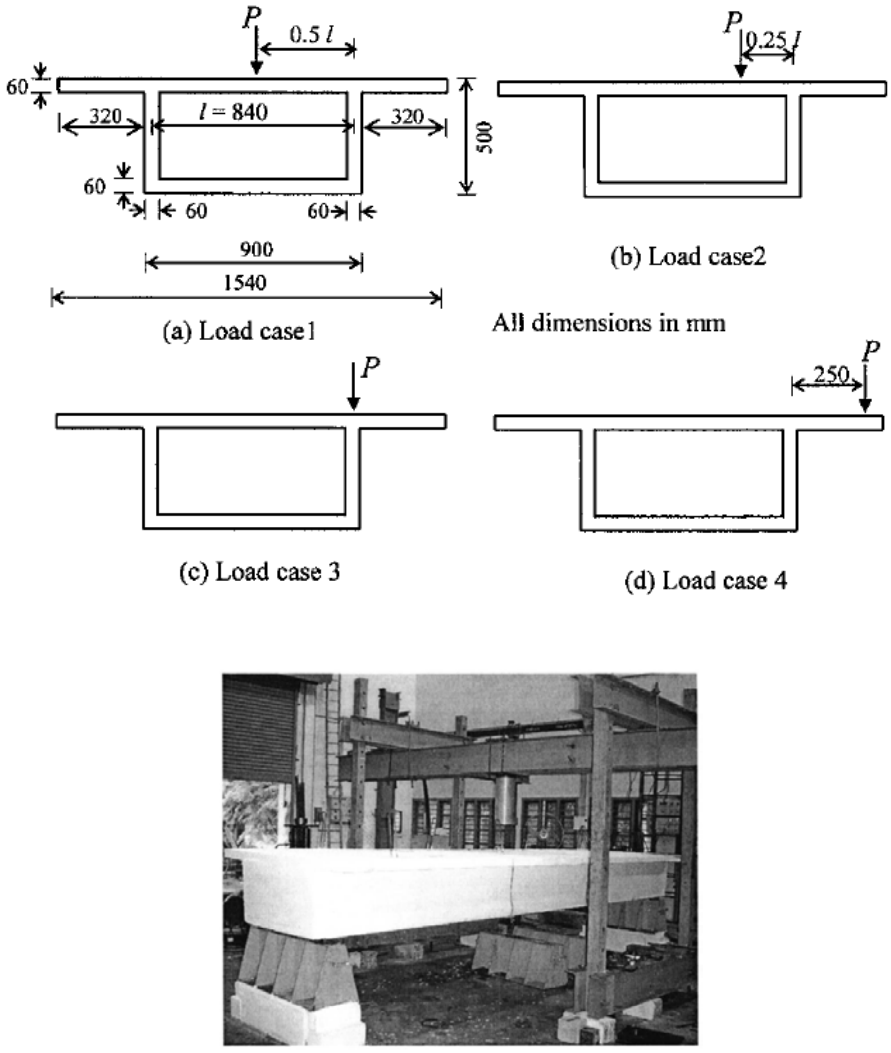

Figure 5.4 Load cases and experimental setup [Kuiran and Menon, 2007]

The moments of inertia and torsional constant for each of the beams in the grillage models are listed in Table 5.1.

Table 5.1 - Elastic properties

	Moment of Inertia I (mm4)	Torsional Constant J (mm4)
longitudinal beams	3.63e9	1.52e9
Transverse box beams	1.46e9	2.90e9
Transverse slab beams	4.5e6	9.0e6

Figure 5.5(a) shows the moment versus curvature plots obtained for the longitudinal beam section with hinge length 125 mm which is half of the element length. Figure 5.5(b) shows the moment versus curvature plots for transverse box members with hinge length equal to 420 mm which is equal to half of the element length. In these cases half the element length is used because it is smaller than the section depth d. Figure 5(c) shows the moment versus curvature plots for transverse slab members with hinge length equal to 60 mm which is equal to the depth of the section element length.

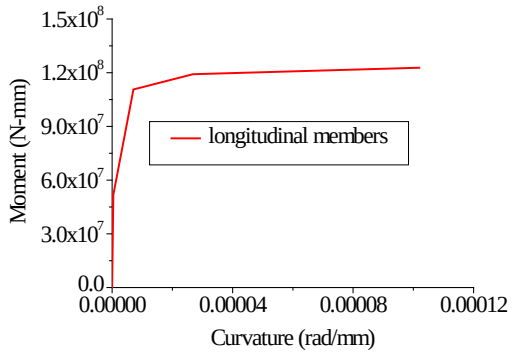

(a) M-curvature for longitudinal beams

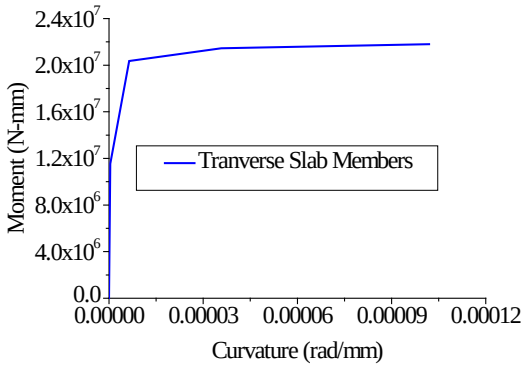

(b) M-curvature for Transverse Box beams

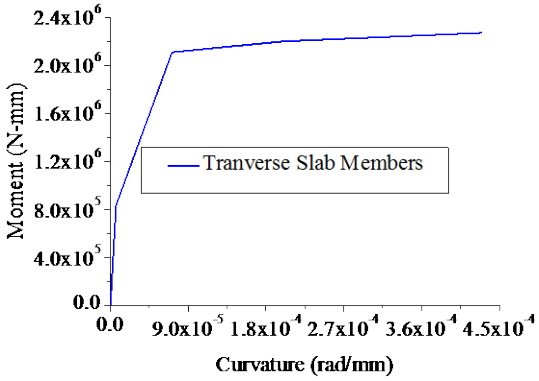

(c) M-curvature for Transverse Slab beams

Figure 5.5 Moment-curvature for longitudinal members and transverse members

The collapse loads for all four load cases obtained by the grillage model analysis are tabulated in Table 5.2 and compared with the experimental results. The results are within 4.6% demonstrating that the grillage model can be used to predict the collapse loads of box girder bridges with good accuracy.

Table 5.2 Comparison of collapse load

Load Case	Case 1(N)	Case 2(N)	Case 3(N)	Case 4(N)
Grillage Analysis	185,214	184,639	183,107	184,770
Experimental results	191,000	185,000	175,000	186,000
Difference	-3.03 %	-0.19%	4.63%	-0.66%

5.2.3 Verification of the Validity of the Grillage Model for the Analysis of Texas Steel Box-Girder Bridge

In this section, the approach proposed in Section 4.2 to model box-girder bridges using the grillage analysis method is applied to evaluate the redundancy of twin tub steel box girder bridges that was tested at the University of Texas at Austin as reported by Hovell (2007) and Neuman (2009).

The bridge consists of two trapezoidal box girders with a very slight horizontal curvature. The interior girder has a centerline length of 119.5 ft and the exterior girder has a centerline length of 120.5 ft. The centerline length of the bridge is 120 ft. The picture of the bridge along with the cross sectional dimensions are given in Figure 5.6.

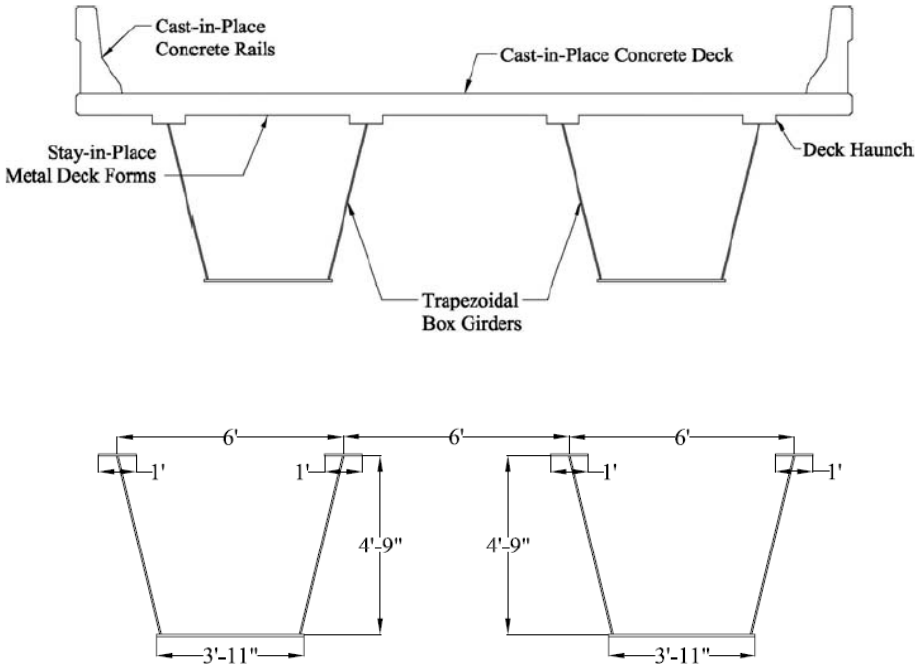

Figure 5.6 - Elevation and cross-section of twin steel box-girder bridge (Hovell, 2007)

The girder webs and flanges are made up of constant-thickness plates with the dimensions given in Table 5.3. The average measured thickness is used in this study to find the section properties.

Table 5.3 Steel box dimensions

	Average Measured Thickness (in)	Plan Thickness (in)	Difference
Top Flange	0.646	0.625	3.3%
Web	0.503	0.500	0.5%
Bottom Flange	0.757	0.750	0.9%

The overall deck dimensions are 23ft-8in. width and 120 ft in length. The design depth is 8 in. with a 3 in. haunch over each flange. The concrete deck is reinforced with two layers of rebar placed transversely and longitudinally. The rebar profile can be found in Figure 5.7.

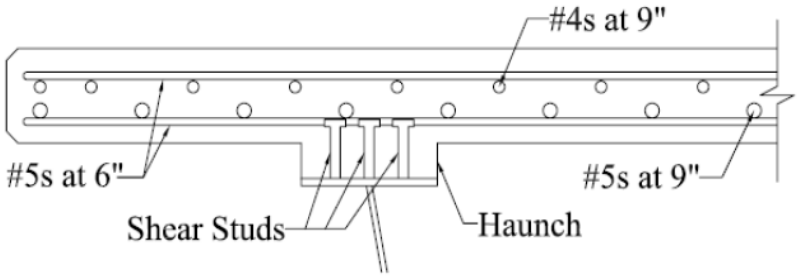

Figure 5.7 Rebar profile in cast-in-place concrete deck [Hovell, 2007]

Each girder has a solid 0.5-in plate internal diaphragm at the end supports. In addition, internal K-frame braces are used down the length of each girder with one placed every twelve feet, as shown in Figure 5.8. The effects of bracing and diaphragm are taken

into account when evaluating the distortion of transverse box members as described in Equation (5.13)-(5.14).

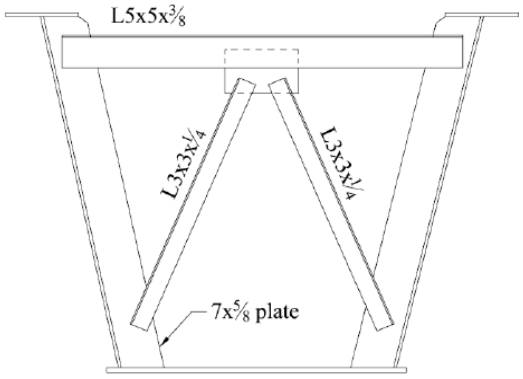

Figure 5.8 - Internal brace configuration

The properties of the concrete used in the full-scale test were obtained using 6 in. by 12 in. test cylinders. Each cylinder made from concrete designed to be 4000 psi in compressive strength, tested above 4600 psi after 28 days (Hovell, 2007). Similarly, the rebars were tested to have a modulus of elasticity of 30,000 ksi and yield stress of 70 ksi. For the steel box, the yielding stress is 50 ksi.

The dead load consists of the weight of the steel boxes and the concrete deck and barriers. In this full-scale test, the wet concrete is assumed to have very little stiffness and strength when the dead load was first applied on the bridge. Therefore, initially all members are considered to be non-composite sections.

The intact bridge is discretized as shown in Figure 5.9 to study the deformations under dead loads. The longitudinal grillage beams L1 are placed to coincide with the centerline of each web of the box and each beam represents half of the noncomposite steel box section. The transverse beams S1 represent the contributions of the deck in transferring the load laterally. The beams labeled T1 represent the transverse box beam section.

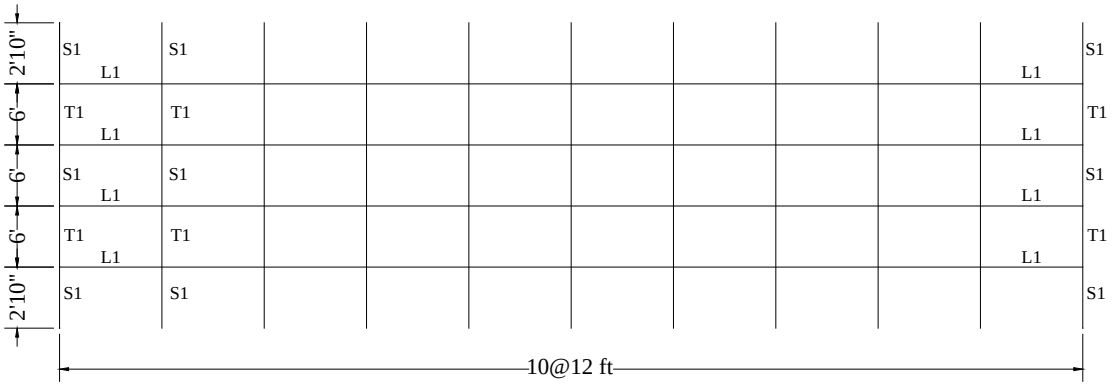

Figure 5.9 - Grillage model of intact bridge under dead load

The dead load is entered as a distributed load over the longitudinal beam elements. The weight of the steel box is W1=0.015 kips/in, the weight of the concrete deck is W2=0.0532 kips/in and the weight due to the rail W3=0.0137 kips/in are applied on each longitudinal beam element.

The moments of inertia and torsional constants for each of the beams are listed in Table 5.4 for the grillage model of Figure 5.9. All the longitudinal beams are assumed to have the same properties. The end transverse beams are assumed to have half the values of the properties of the middle transverse beams.

Table 5.4 Elastic properties of intact bridge under dead load

Dead load testing	Moment of Inertia I (in4)	Torsional Constant J (in4)
Non-composite longitudinal beams	27485	14360
Transverse box beams	5.21	250
Transverse slab beams	6144	12288

Full-scale live load test 1

A custom steel blast-shield was used to induce a 0.25 in. wide fracture in the bottom flange near the mid-span of one girder. This fracture cuts all the way through the 0.757 in. thickness and across the 47 in. length of the bottom flange, as shown in Figure 5.10.

Figure 5.10 - Fracture view in the bottom flange

The bridge was loaded with concrete girders and blocks, representative of the AASHTO HS-20 truck. The HS-20 truck is shown in Figure 5.11 and a picture of the concrete girders that provide essentially the same load is provided in Figure 5.12.

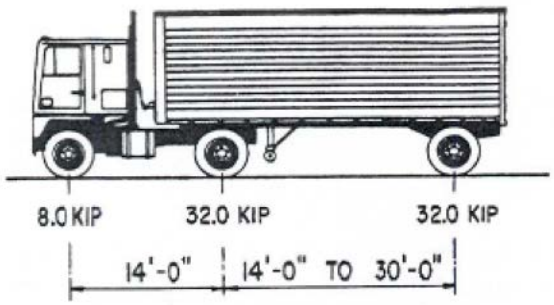

Figure 5.11 AASHTO HS-20 Truck

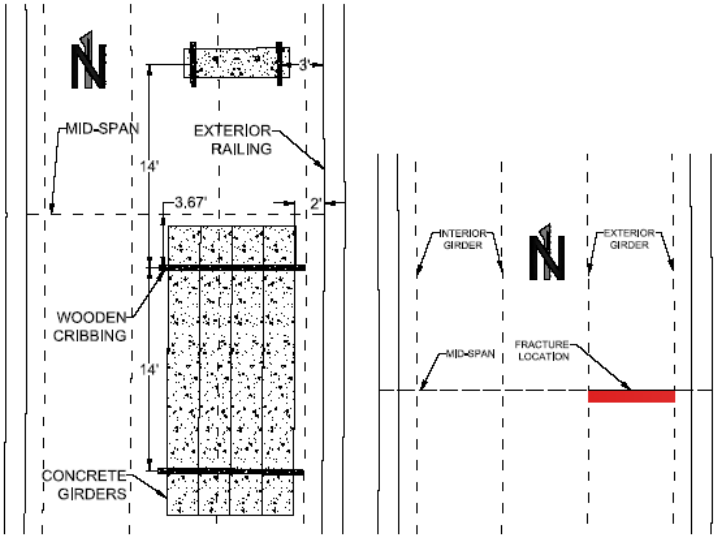

Figure 5.12 Live load location for the full load test [Hovell, 2007]

For the grillage analysis, the fractured bridge is discretized as shown in Figure 5.13. The beam elements labeled C1 represent the fractured section where only the slab is assumed to carry the longitudinal load. The fractured portion of the beam is assumed to be 6 inches to account for the damage incurred by the section close to the fracture. A sensitivity analysis is performed further below to study the effect of the damaged length. The 6 in fractured length is applied on one side of the centerline following the observation made by Hovell (2007) on the location of the crack as depicted in Figure 5.12. The longitudinal grillage beams L1 are composite box sections including the effects of the deck. S1 represents the properties of the slab and T1 the transverse properties of the box girder.

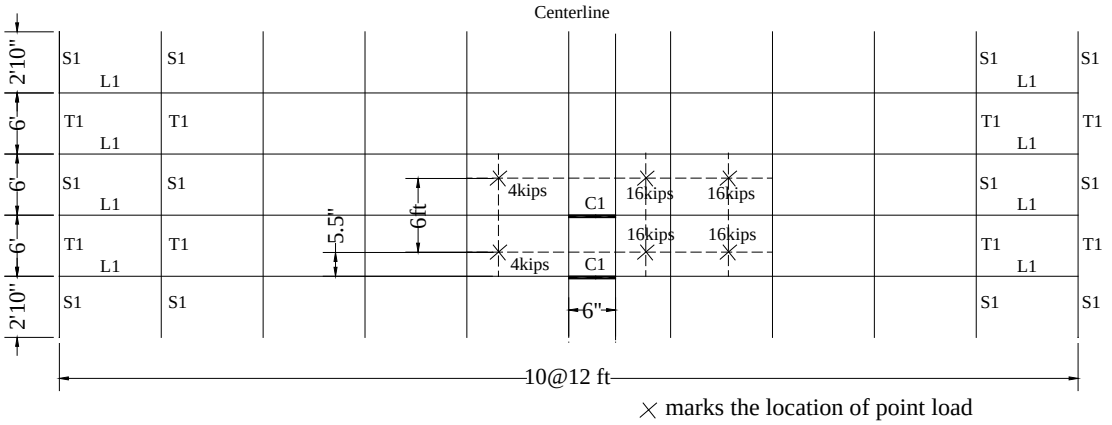

Figure 5.13 Live Load position and mesh discretization of fractured girder

The moments of inertia and torsional constants for each of the beams are listed in Table 5.5 for grillage model shown in Figure 5.13. The applied loading during test 1 was designed to simulate the effect of the HS20 truck. Therefore, during the analysis process, the point loads in Figure 5.13 were used.

Table 5.5 Elastic properties of fractured bridge in test 1

	Moment of Inertia I (in4)	Torsional Constant J (in4)
Composite longitudinal beams	82182	17248
Cracked Longitudinal beams	3122	6144
Transverse box beams	261304.	932279
Transverse slab beams	6144	12288

Full-scale live load test 2

In test 2, the bridge is incrementally loaded to determine the ultimate load required to induce a total collapse of the bridge [Neuman, 2009]. A custom steel blast-shield was used to induce fracture in the bottom flange near the mid-span of one box girder. This fracture cut all the way through the bottom flange and the whole web as shown in Figure 5.14. For the analysis, the fracture was still modeled by the 6-inch long element C1 as done for test 1.

Figure 5.14 - Fracture view with the bin loaded on the top [Neuman, 2009]

The five concrete girders used in the previous full-scale tests to simulate the design truck load were rearranged with a sixth additional girder to form a rectangular bin on the bridge deck weighing a total of 82,100 lbs (Figure 5.15). The open rectangle was designed as a receptacle for the incremental load so that it could be accurately placed and analyzed. The bin was shaped by pairing the four 20-ft long pre-stressed girders as the bin edges along the length of the bridge and by using the two concrete blocks as the ends of the bin spanning in the transverse direction of the bridge [Neuman, 2009].

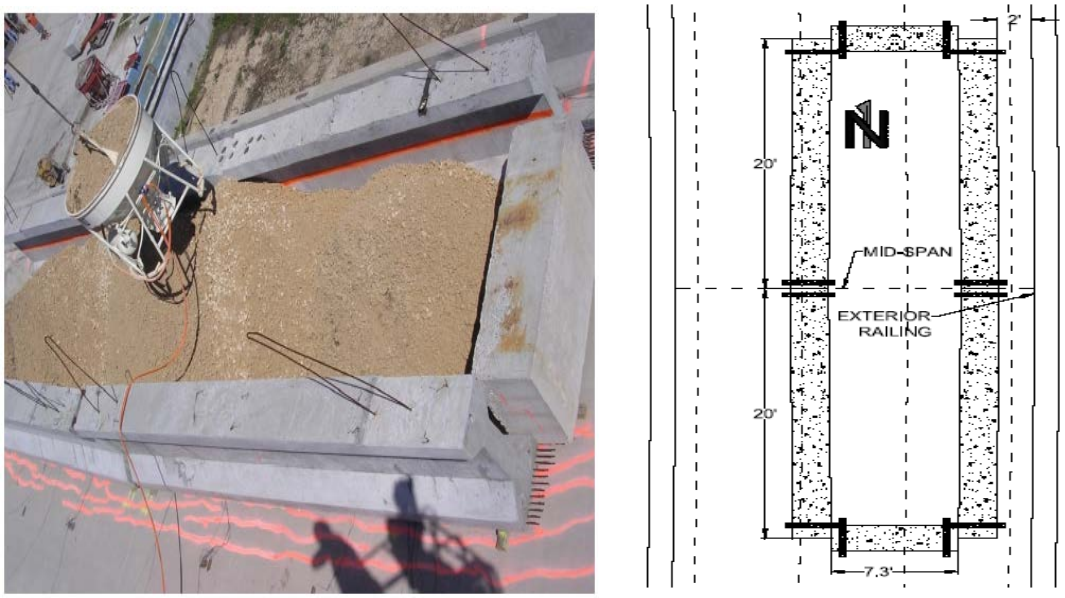

Figure 5.15 Live load location for the full load test [Nueman, 2009]

When the bin was being positioned on the deck, it can be seen from Figure 5.15 that the top deck had already separated from the box girder near mid-span. At the beginning of loading the road base, the top flange of the fractured girder separated from the concrete deck across a substantial central portion of the bridge span. When the total applied load reached 161,500 lbs, the cracks separating the exterior flange of the fractured girder and

the deck extended 20 ft in both directions from the fracture location as shown in Figure 5.16 (Neuman, 2009).

To account for the deck separation in the grillage analysis the longitudinal members, are modeled as non-composite for a length of 24-ft on either side of the centerline. Thefractured bridge is discretized for the incremental loading as shown in Figure 5.17. The elements labeled C1 represent the 6-inch fractured section of the box and the properties of these elements correspond to the properties of the slab alone. The elements labeled Lnon1 represent the zone having the properties of the non-composite steel box. L1 represents the composite steel longitudinal members; T1 represents transverse box beams; S1 represents the transverse slab beams.

(a) close-up view

(b) wide view

Figure 5.16 - Initial separation between the fractured girder and the concrete deck [Neuman, 2009]

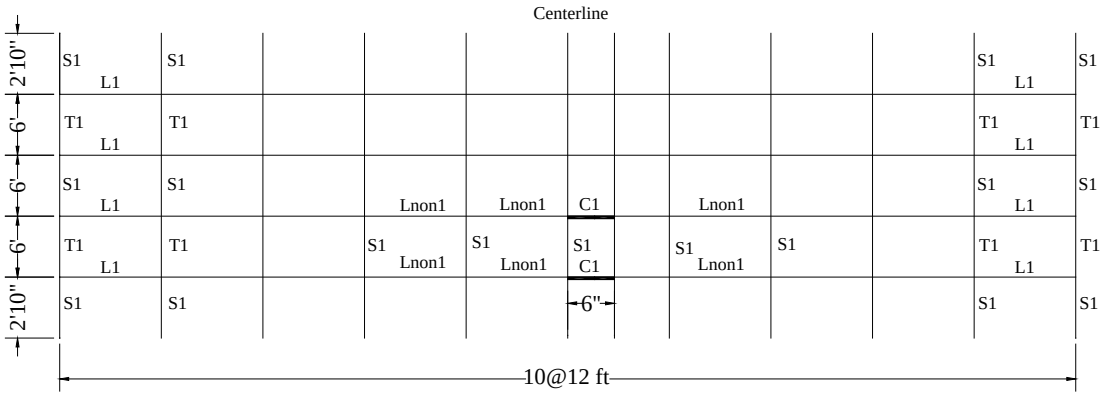

Figure 5.17 Mesh discretization under live load

The elastic section properties of the members shown in Figure 5.17 are listed in Table 5.4 and Table 5.5.

Figure 5.18 shows the moment versus curvature plots obtained for the non-composite and composite longitudinal sections. The hinge length is assumed to be equal to half the beam element length. Figure 5.19 shows the moment versus curvature plots for transverse slab members with hinge length equal to 8 in which is equal to the depth of the slab. As mentioned earlier, half the element length is used as an upper limit when the section depth exceeds that value.

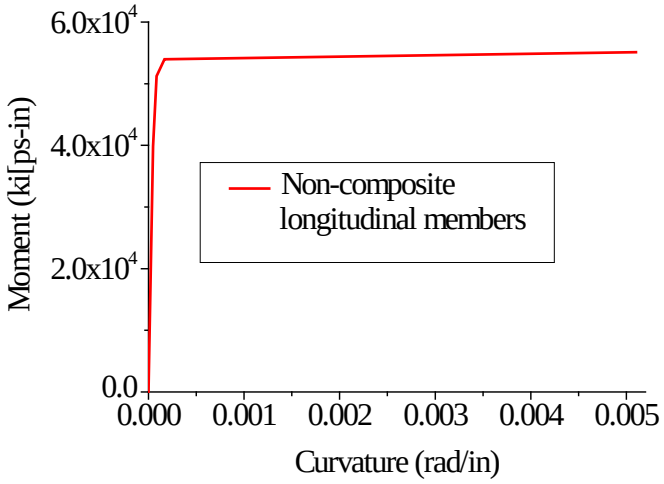

(d) M-curvature for Non-composite longitudinal beams

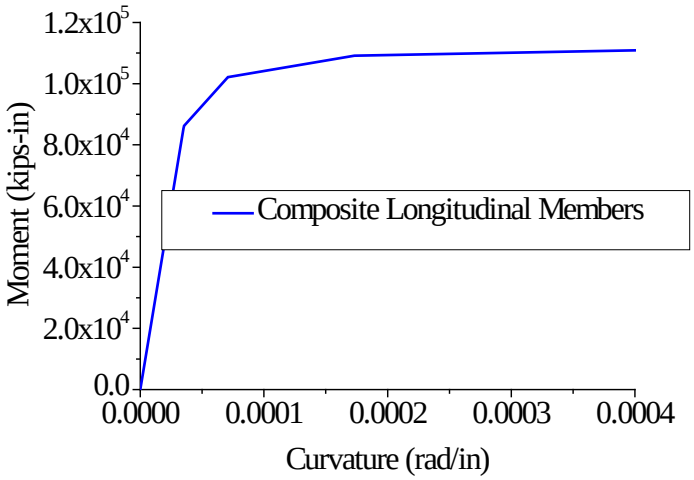

(e) M-curvature for composite longitudinal beams

Figure 5.18 Moment-curvature for longitudinal members

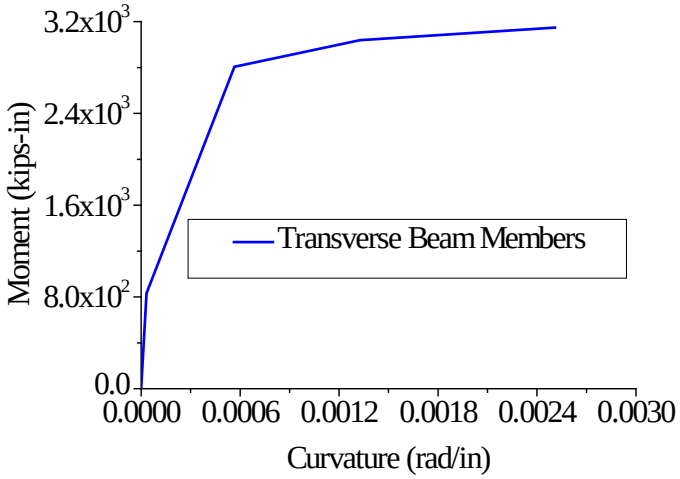

Figure 5.19 Moment curvature of transverse slab members

5.2.3.1 Comparison of Results

Test 1

The deflections obtained from the grillage analysis of the bridge under dead load and HS20 live load are shown in Figure 5.20. Figure 5.20 gives the deflections along the bridge length and compares the results of the grillage analysis with the deflections measured during the test. Also, the results are compared to those obtained by a nonlinear 3-D finite element performed by Hovell (2007).

The plots in Figure 5.20 labelled Deck_T, Deck+rail_T, Deck+rail+Live_T are for the test results under the deck dead weight, deck plus rail dead load and deck plus rail plus live load. The plots labeled Deck_G, Deck+rail_G and Deck+rail+Live_G give the results of the analysis performed in this report using the grillage model for the deck load, deck plus rail load and deck plus rail plus live load; The plot labeled FEM_Hovell gives the results of the 3-D finite element analysis as performed and reported by Hovell (2007).

The top set of plots in Figure 5.20(a) gives the deflections measured in the undamaged box (exterior box). The lower set of plots in Figure 5.20(b) gives the deflections along the length of the fractured box (interior box).

The plots presented in Figure 5.20 show that the grillage analysis provides acceptable level of accuracy considering the simplicity of the grillage analysis approach. The largest levels of discrepancies appear to occur for the deflections due to the weights of the deck and the rail in the damaged box where the grillage analysis predicted larger deformations than observed during the test. Similarly, larger deformations were predicted by the grillage analysis for the undamaged box when loaded by the deck weight, the barrier and the equivalent of the HS-20 live load. These larger deformations may be due to the fact that the grillage model did not account for the contributions of the barrier to the inertia of the undamaged box. The separation of the deck from the damaged box when the live load was placed may have eliminated the stiffening contributions of the barrier that is located over the damaged box and thus the deflections of the damaged box under live load predicted by the grillage analysis are closer to those observed from the measurements.

Overall, at this stage, the grillage analysis seems to provide a better representation of the bridge deflections than the preliminary full-fledged non-linear 3-D finite element performed a part of the Texas study, although the Texas researchers are still working on improving their model. The grillage analysis seems to be reasonable for predicting the overall global behavior of box girder bridges even though some difference between the test results and the grillage analysis will always exist. The 3-D finite element analysis, however, should provide a better representation of the stresses at critical points in the

bridge.

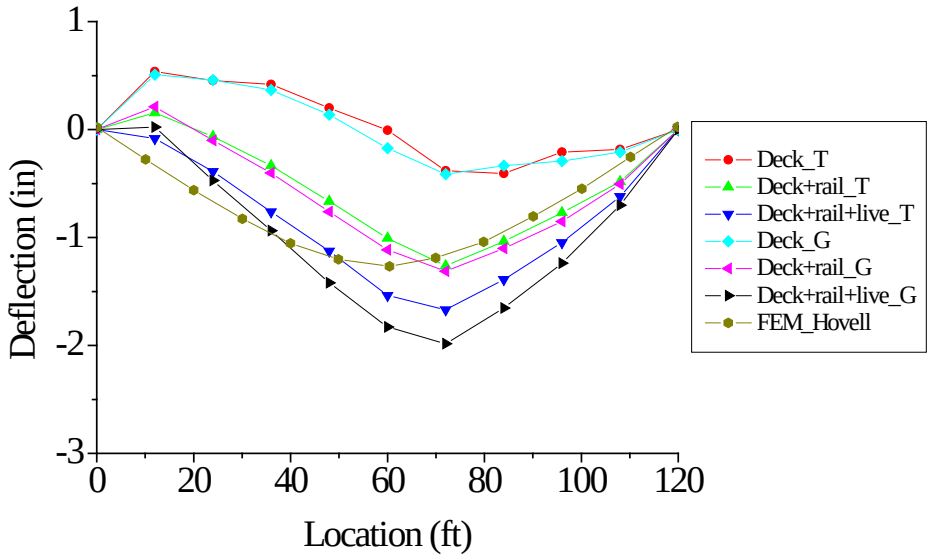

(a) undamaged box girder

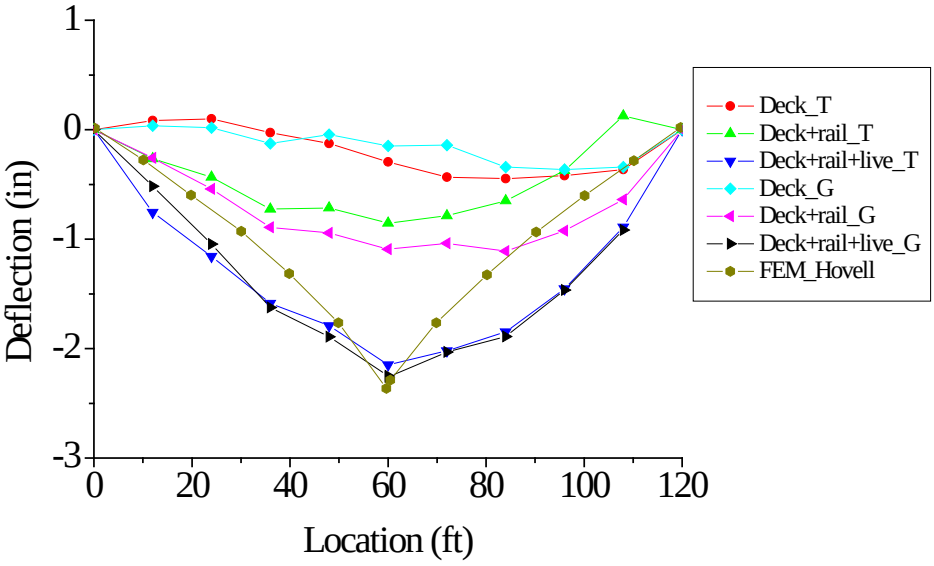

(b) damaged box girder

Figure 5.20 Deflections of damaged bridge under dead load and HS20 truck load

Test 2

The complete load-deflection curves for the incremental loading (test 2) are shown in Figure 5.21. For test 2, the deflections were taken as the average deflection along the bottom flange of each cross-section, 18-ft south of the mid-span since there is no complete mid-span deflection data (Neuman, 2009). The damaged bridge collapses when the longitudinal cracked section C1 in Figure 5.17 reaches the maximum plastic hinge rotation. Figure 5.17 compares the results of the grillage analysis to those measured during the test. No 3-D finite element results have been provided for this test by either Hovell (2007) or Neuman (2009).

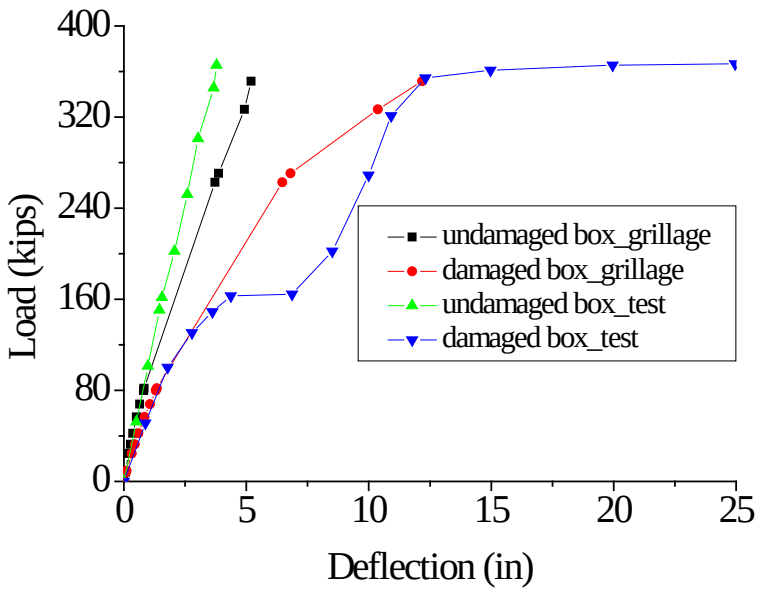

Figure 5.21 - Load deflection curve for test 2

Figure 5.21 shows that the modeling of the damaged bridge using the grillage

analysis provides reasonable results up to a load of about 160 kips. At that load Hovell (2007) and Neuman (2009) report that the shearing studs broke off. At that load, the damaged segment of the box exhibited plastic deformations and eventually transferred much of the load to the barrier. When the barrier started taking additional load, the load versus deflection curve for the damaged box becomes stiffer and the system was able to carry additional load until failure. The Texas investigators report that when the shear studs ripped off, significant spalling of concrete cover on the rail was observed in the test but that the railing did not unload with the loss of the concrete cover before the collapse of the bridge (Neuman, 2009).

In the grillage analysis of the damaged box girder (shown in red in Figure 5.21), the same configuration is maintained throughout the loading process until collapse and the contributions of the railing whose properties are not known are not included. By not including the ripping off of the studs and the subsequent transfer of the load to the barrier, the grillage analysis results did not exhibit the softening and subsequent stiffening of the load deflection curve. Yet, the final predicted collapse load obtained by the grillage analysis is only slightly smaller than that observed from the test. The value of the load at collapse reported by Neuman (2009) is 363.3 kips while the collapse load estimated by the grillage analysis is 350.06 kips in addition to the dead loads.

Figure 5.21 also shows that the undamaged box is stiffer than predicted by the grillage analysis. This also may be attributed to the fact that the contributions of the barrier to the response of the bridge are ignored during the grillage analysis. The contributions of the barrier located over the damaged box may not be significant in the

early stages of the loading due to the noncomposite action between the deck and the box in the vicinity of the damaged zone. However, as the box deformed and twisted, the barrier could have acted as a bridge over the damage zone.

5.3 Redundancy Analysis of Steel Box-girder bridge

In this section, the approach proposed in Section 4.2 to model box-girder bridges using the grillage analysis method is applied to do probabilistic redundancy analysis of 120-ft long twin steel box girder bridges shown in Figure 22, which is similar to the bridge shown in Figure 5.6.

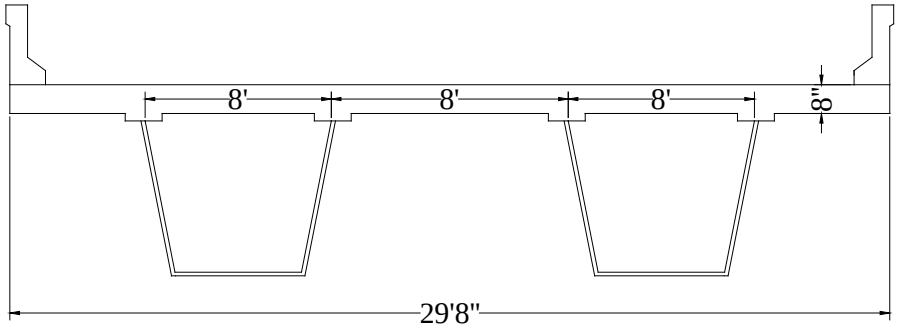

Figure 5.22 Cross section of box-girder bridge

The dead load is entered as a distributed load over the longitudinal beam elements. The weight of the steel box is W1=0.018 kips/in, the weight of the concrete deck is W2=0.071 kips/in and the weight due to the rail W3=0.014 kips/in are applied on each longitudinal beam element.

The intact bridge and fractured bridge are discretized as shown in Figure 5.9 and Figure 5.13, respectively. And the moment-curvature relationship is the same as those shown in Figure 5.18 and Figure 5.19.

5.3.1 Evaluation of Bridge Redundancy

To assess whether this steel box-girder bridge provides a sufficient level of redundancy, The improved subset simulation "RASS" is used to obtain reliability indices β_{member}, $\beta_{functionality}$, $\beta_{ultimate}$, $\beta_{damaged}$, which are respectively for the system's ultimate, functionality and damaged limit states defined in Chapter 2 according to NCHRP Report 406. The distribution of random variable is shown in Table 5.6 (Nowak 1992; Ghosn and Moses 1998).

Table 5.6 Random variable of steel box-girder bridge

Variable	Bias	COV	Distribution type
Main member Resistances	1.12	10%	Lognormal
Dead load	1.05	10%	Normal
Maximum rotation	1.0	20%	Lognormal
75-year Live load	1.89	19%	Lognormal
2-year live load	1.75	19%	Lognormal

And the results of the analysis are checked against the criteria given in Equation (2.9) of Chapter Two.

In this case, β_{member}, $\beta_{functionality}$, $\beta_{ultimate}$, $\beta_{damaged}$ obtained are given in Table 5.7.

Table 5.7 Reliability index for steel box-girder bridge

β_{member}	$\beta_{functionality}$	$\beta_{ultimate}$	$\beta_{damaged}$
5.80	5.47	6.74	1.52

So, $\Delta\beta_u$ =0.94>0.85 O.K.

$\Delta\beta_f$ =-0.33<0.25 N.G.

$\Delta\beta_d$ =-4.28<-2.70 N.G.

This would indicate that the bridge tested at the University of Texas has just met the redundancy criterion for the ultimate limit state with $\Delta\beta_u$ =0.94>0.85. The functionality limit state however has not been met since $\Delta\beta_f$ =-0.33<0.25. Furthermore, the damaged condition limit state criterion is also not met with $\Delta\beta_d$ =-4.28<-2.70. These calculations show that although the bridge tested in Texas is overdesigned with β_{member} =5.80>3.50 which is the target reliability index in AASHTO, it does not provide adequate levels of redundancy.

5.3.2 Sensitivity Analysis of Redundancy Factors

A parametric analysis is performed to study the sensitivity of the results. The sensitivity analysis described in this section looked at the effect of using stiffer and stronger main elements and deck slabs.

The results of the sensitivity analysis are summarized in Table 5.8 for the effect of the capacity of longitudinal main members; Table 5.9 for the effect of the capacity of slab members and Table 5.10 for the effect of the moment of inertia of longitudinal main

members.

To the study the effect of member capacities, the moment versus curvature curve is modified by changing the values of the moments in the curve by ±50%. It is noted that such a 50% increase in the longitudinal member capacities will decrease the R_u by about 8%, R_f by 11% and R_d by 22%. The decreases in R_u, R_f and R_d are 5%, 15% and 32% , respectively for a 50% decrease of the longitudinal member capacities.

Table 5.8 The effect of the capacity of longitudinal main members

Factor*Capacity	Rf	Ru	Rd
1.500	0.823	1.137	0.274
1.400	0.852	1.155	0.287
1.300	0.879	1.161	0.305
1.200	0.892	1.190	0.321
1.100	0.912	1.212	0.334
1.000	0.928	1.239	0.351
0.900	0.958	1.257	0.374
0.800	0.985	1.269	0.390
0.700	1.015	1.287	0.421
0.600	1.046	1.296	0.446
0.500	1.070	1.294	0.465

A 50% increase in the slab's strength increases R_u by 3%. And the increase in R_f and R_d are about 2% and 23%, respectively. If the slab's strength is decreased by 50%, then the decreases in R_u, R_f and R_d are 7%, 5% and 26%, respectively.

Table 5.9 The effect of the capacity of slab members

Factor*Capacity	Rf	Ru	Rd
1.500	0.950	1.275	0.433
1.400	0.949	1.275	0.421
1.300	0.944	1.268	0.402
1.200	0.940	1.255	0.379
1.100	0.937	1.252	0.370
1.000	0.928	1.239	0.351
0.900	0.925	1.226	0.334
0.800	0.912	1.194	0.316
0.700	0.908	1.172	0.292
0.600	0.895	1.171	0.274
0.500	0.886	1.156	0.257

The effect of changes in moment of inertia of the longtudinal members is also investigated. The results of Table 5.13 showed that a 50% increase in moment of inertia leads to the increase of R_f by 4% and R_d by 3% and Ru has negligible effect.. If the moment of inertia is decreased by 50%, then R_u, R_f and R_d have 1%, 4% and 4% decrease, respectively.

Table 5.10 The effect of the moment of inertia of longitudinal main members

Factor*Capacity	Rf	Ru	Rd
1.5	0.968	1.238	0.362
1.4	0.963	1.238	0.360
1.3	0.954	1.238	0.359
1.2	0.946	1.238	0.357
1.1	0.939	1.238	0.353
1.0	0.928	1.239	0.351
0.9	0.924	1.239	0.349
0.8	0.918	1.228	0.346
0.7	0.909	1.227	0.344
0.6	0.899	1.226	0.341
0.5	0.893	1.226	0.338

In summary, the results indicate that the effect of changes in the moments of inertia of the bridge members produces negligible change in the results. However, changes in the strength of the slab and the longitudinal members may produce some change in the final results. The effect of the slab's strength is only significant for the damaged scenario. On the other hand, the effect of changes in the longitudinal members' strength will affect the results of both the intact and damaged bridges.

5.4 Conclusions

This chapter presented an approach to analyze the behavior of damaged steel box girder bridges using a grillage analysis. The results of the analysis are compared to the experimental results performed at Texas University of a fractured box girder bridge. A comparison of the results shows that the grillage analysis can provide a reasonable representation of the behavior of damaged box girder bridges. The results also show that the presence of bracings can help improve the stiffness of damaged bridges and can also help improve their ultimate capacity. The bracings however do not seem to make any significant difference in the response of undamaged bridges. The redundancy analysis shows that this bridge is not adequately redundant even though it may have been so overdesigned as to make capable of carrying a significant amount of live load even after it sustains major damage.

CHAPTER SIX: RELIABILITY-BASED ANALYSIS OF PROGRESSIVE COLLAPSE OF BRIDGES WITH SITE-SPECIFIC TRAFFIC DATA

6.1 Introduction

Structural systems optimized to meet member design criteria as specified in current design codes may not provide sufficient levels of robustness to withstand a possible local failure. In fact, local failure of one structural element may result in the failure of another element creating a chain reaction that might progress throughout the whole structure leading to a catastrophic collapse. Catastrophic events, such as the collapse of the Alfred P. Murrah Federal Building, in Oklahoma City in 1995, the World Trade Center towers in 2001 and the I-35W Mississippi River Bridge in Minnesota, have alerted the structural engineering community to the importance of ensuring structural survivability after an initial local failure.

Existing criteria to reduce the risk of progressive collapse have been developed for buildings using traditional deterministic methods. However, because of the differences in the loads and structural configurations, it is not sure that the criteria developed for buildings are also applicable for bridges. Furthermore, the large uncertainties associated with estimating the capacity of structural systems to resist collapse after the sudden initiation of a local failure require the application of probabilistic analysis methods. Although an outline has been recently proposed by Ellingwood (2006) describing how to account for member and load uncertainties when developing progressive collapse guidelines, as of this date no specific probability-based methods for analyzing the progressive collapse of structural systems have been established for buildings or bridges. The objectives of this chapter are to develop a methodology for proposing progressive collapse criteria for highway bridges accounting for the uncertainties in the applied loads and the load carrying

capacities of the members as well as the system.

The safety evaluation of a bridge structure requires checking if the effects of the loads applied on the structure exceed the capacities of the individual members or the capacity of the whole system. The bridge system must support the permanent loads as well as the live load. Data for the permanent loads have long been established and are available in the literature. According to LRFD design code, the design load HL93 were developed using generic truck data to project a 75-year live load occurrence. Because truck traffic volume and weights vary between regions and states, in this study we use sate-specific load models applicable for New York State. The live load model used in this study is based on site-specific truck weight and traffic data collected using Weigh-In-Motion (WIM) systems. Recent observations made on truck weight data collected from Weigh-In-Motion (WIM) stations at representative New York State sites have shown that truck weights in New York can be significantly heavier than the generic truck weight data used during the calibration of the AASHTO specifications (Sivakumar et al, 2008 & Ghosn et al 2010).

Current methods for the analysis of structural systems are either extremely inefficient or else use many simplifications which sometimes may not lead to accurate estimation of bridge system reliability. This chapter uses a Markov-chain based advanced simulation method proposed in Chapter 3 to perform the reliability analysis of progressive collapse of bridge structures with the final goal of using such results for developing consistent reliability-based progressive collapse criteria that can be used on a regular basis by bridge engineers concerned with the survivability of bridges that may be subject to local failures.

In this chapter, Section 6.2 presents the definitions and describes existing methods for progressive collapse analysis; Section 6.3 describes how to use weigh-In-Motion (WIM) systems to collect vast amounts of truck weight and traffic data that can be used to obtain site-specific and state-specific live load models for bridge safety evaluation; Section 6.4 presents probabilistic progressive collapse methodology; Sections 6.5 and 6.6 provide two examples on the probabilistic progressive collapse analysis of typical bridges; Section 6.7 Probabilistic analysis of bridge system redundancy, robustness and progressive collapse. Sections 6.8 and 6.9 demonstrate how these reliability-based results can be used to calibrate deterministic criteria that can be easily applied in engineering practice using deterministic methods with properly calibrated load factors.

6.2 Reliability-based Progressive Collapse Analysis

Progressive collapse occurs if a local structural damage causes a chain reaction of structural elements failures, disproportionate to the initial damage. According to ASCE 7-05 (ASCE 2005), Progressive Collapse is defined as “the spread of an initial local failure from element to element resulting, eventually, in the collapse of an entire structure or a disproportionately large part of it.” The local damage that triggers progressive collapse is called the initiating damage. Progressive Collapse is a dynamic event, since it involves vibrations of structural elements and creates external and internal dynamic forces, such as inertia and restoring forces, whose energy may or may not be absorbed by the structure. From the analyst’s point of view, progressive collapse occurs when a sudden local change in structural geometry (i.e. loss of load-carrying members) results in dynamic forces exceeding the bearing capacities of surrounding elements, leading to the failure of those elements. This failure, in its turn, transmits additional dynamic forces to the remaining structure until it either stabilizes (absorbs the energy of the vibrations) or collapses. The forces are transmitted rapidly; in general, progressive collapse happens in a matter of seconds.

The Federal Emergency Management Agency provides general guidance for performing progressive collapse analysis (FEMA, 1997). Eurocode 1 gives general comments about designing structures to prevent damage to an extent disproportionate to the original abnormal loading event (Eurocode8,1994). Both the General Services Administration (GSA 2000) and Department of Defense (DoD 2002) have issued guidelines for evaluating the progressive collapse hazard which provides general information about the approach and method of evaluating the progressive collapse analysis. In addition, non-mandatory commentary of the American ASCE 7-98/ANSI A58 standard recommends several general approaches to design against progressive collapse (ASCE 2002).

Progressive Collapse includes two types of loadings (Marjanishvili 2004): The primary load which causes the structural element to fail and secondary loads which are generated due to the structural motions caused by sudden collapse of the element. External abnormal loads, such as blast pressures due to explosive attacks, could cause primary loads, while secondary loads result from internal static and dynamic loads and are caused by sudden changes in the load path through the structure's geometry. Although estimation of primary loads is another interesting topic, this study deals with the effects of the secondary loads.

Analysis methods used to evaluate the possibility of progressive collapse vary widely, ranging from the simple two-dimensional linear elastic procedure to complex three-dimensional nonlinear time history analysis (Kima and Kimb 2009; Marjanishvili 2004; Powell 2009). The simplest analysis methodology is static linear elastic analysis and the most exhaustive procedure is nonlinear dynamic analysis, which yields more accurate results. Powell (2009) and Marjanishvili (2004) have shown that linear static and dynamic analysis cost the least time to run, followed by nonlinear static analysis and nonlinear dynamic analysis which would require and extensive

amount of time.

The analysis of progressive collapse is performed to estimate the capacity of a structural system to survive the sudden failure of a member or component. Well-designed structures should be able to survive such sudden failures and sustain some level of service load until the structure can be rehabilitated. As defined in this thesis, the ability of the damaged structure to continue to carry load after surviving the initial damage is addressed during the analysis of structural redundancy. Progressive collapse is concerned with the ability of the structure to survive the sudden removal of a main structural component.

As mentioned earlier, criteria for the progressive collapse analysis have been established for Federal office buildings. However, no criteria are currently available for important bridge structures. Furthermore, the existing criteria were not established based on reliability principles as has been the norm during the development of recent structural design and safety assessment specifications.

In this Chapter we describe a method to perform probabilistic analyses of progressive collapse and propose a procedure to calibrate adequate reliability-based criteria consistent with the procedures used for calibrating structural design codes. We will use reliability methods for the analysis of typical bridge configurations subjected to a sudden failure of a main component to evaluate the probability of progressive collapse. Through the analysis of several typical bridge configurations, we will calibrate the load factors that can be used to perform deterministic progressive collapse analyses that would produce acceptable levels of reliability. To determine the required load factors, we will design a set of typical bridges that will resist progressive collapse with different load factors and then we will check the probability of failure that these designs will

achieve. If the pre-selected load factors yield the target reliability, then these would be the acceptable load factors.

6.3 Load Modeling

To perform the reliability analysis of bridge systems, it is necessary to have probabilistic models for the dead loads and the lives loads. Section describes the load models used in the probabilistic progressive collapse analysis.

Dead Load

Following Nowak's (1999) approach, the total dead load, DL is divided into the dead load of pre-fabricated members, D_{C1}, the dead load of cast-in-place members, D_{C2}, and the dead load of the wearing surface, D_w, such that the mean total dead load is given by:

$$\overline{DL} = \overline{D_{c1}} + \overline{D_{c2}} + \overline{D_w}\,, \tag{6.1}$$

The standard deviation of the total dead load, σ_{DL}, is expressed as a function of the standard deviations of each dead load component:

$$\sigma_{DL} = \sqrt{\sigma_{DC1}^2 + \sigma_{DC2}^2 + \sigma_{DW}^2} \tag{6.2}$$

The relationship between the standard deviation, σ_{DL}, mean, $\overline{DL}$, and the coefficient of variation (COV) of the dead load, V_{DL}, is obtained as:

$$V_{DL} = \frac{\sigma_{DL}}{\overline{DL}} \tag{6.3}$$

Following Nowak (1999), the dead load effects are assumed to follow Normal probability distributions where the mean values and the COV's of each dead load component are given as:

$$\overline{D_{C1}} = 1.03\ D_{C1} \qquad V_{DC1} = 8\%$$
$$\overline{D_{C2}} = 1.05\ D_{C2} \qquad V_{DC2} = 10\%$$
$$\overline{D_{W}} = 1.0\ D_{W} \qquad V_{DW} = 25\% \tag{6.4}$$

Where Dc1, Dc2 and Dw are, respectively, the nominal values of the dead load of pre-fabricated members, cast-in-place members, and wearing surface.

Live Load

Weigh-In-Motion (WIM) technology was developed over the last three decades to weigh trucks as they travel across highways and roads. Various government and private agencies require information on truck weights for several applications including: highway weight enforcement; traffic data collection; military and industrial operations; and monitoring of economic activity. Particular interest has recently focused on utilizing the data collected from WIM systems for the safety assessment of pavements and bridges. The advantage of WIM over traditional static scale weighing is the efficiency obtained when collecting truck weight information automatically as the trucks travel at normal speeds. WIM operations may be designed to be undetectable to provide unbiased information on overweight trucks. Additionally, most WIM systems are capable of simultaneously providing information on truck traffic patterns including Average Daily Truck Traffic (ADTT), truck headways, platoon formations, as well as collecting information on long term and seasonal changes. Such information is very important for highway engineering purposes including the planning of new highway systems, increasing highway system capacities, designing pavements and bridges, monitoring the behavior and assessing the safety of existing pavements and bridges, as well as forecasting the safe lives of these pavements and bridges. The live load model used in this analysis is based on WIM data collected at representative New York State sites following the methodology developed by Ghosn et al (2012) (ASCE Bridge

Engineering) and Sivakumar, Ghosn and Moses (2011) (NCHRP 12-76).

The live load is evaluated for two-lane traffic condition based on site-specific truck weight and traffic data collected using Weigh-In-Motion (WIM) systems. Using the WIM data for a site, the load effect of each truck loading event is calculated by passing the trucks through the proper influence line. The load effect of each set of trucks that are expected to be on the bridge simultaneously is then normalized by dividing the calculated value by the effect of the HL-93 vehicle. The results are collected into cumulative distribution histograms F(S) for a single lane of trucks or for trucks side by side on multi-lane bridges. For illustration, Figure 6.1 shows in black the moment histogram for a single lane of 100-ft simple span bridge obtained from the data collected at New York WIM site 9121.

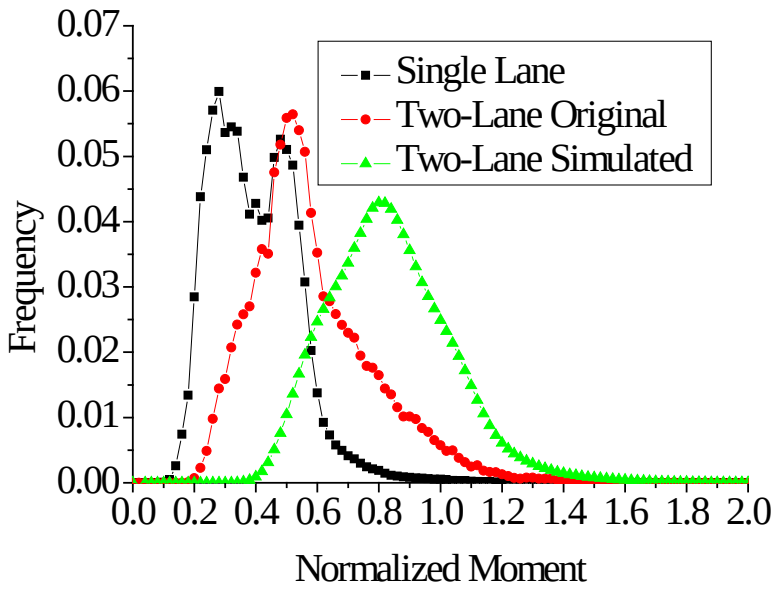

Figure 6.1 - Normalized w/r to HL-93 load of 100-ft moment histogram for trucks of WIM site 9121

When two lanes are loaded, the total load effect is $X_s = X_1 + X_2$ where X1 is the effect of

the trucks in the drive lane and X_2 is the effect those in the passing lane. Assuming independence, the probability density function of the effect of side-by-side trucks $f_s(S)$ can be calculated using the convolution:

$$f_{xs}(X_s) = \int_{-\infty}^{+\infty} f_{x2}(X_s - x_1) f_{x_1}(x_1) dx_1 \tag{6.5}$$

where fxs (…) is the probability distribution of the multi-lane effects, fx1(…) is the probability distribution of the effects of trucks in lane 1, fx2(…) is the probability distribution of the effects of trucks in lane 2. It is assumed that fx2(…)=fx1(…) based on the observation made by Sivakumar et al (2011) that the truck weight statistics in the passing lanes are similar but uncorrelated to those in the drive lane.

Figure 1 shows in green the histogram obtained for the two-lane loading events obtained from Equation (6.5), which is compared to the two-lane loading histogram obtained directly from the WIM data shown in red. The convolution yields more conservative values due to the assumption that trucks in two lanes that are within 60-ft head to head are compressed so that they are placed side-by-side. Also, some additional conservatism is due to the assumption that the percentage of trucks closely following each other is the same in both lanes.

For a bridge member (or structural system) to be safe, the resistance should be large enough to withstand the maximum load effect that could occur within a pre-set service period. The service period for the design of a new bridge is specified to be 75 years as per the AASHTO LRFD code. A 5-year service period has been used for the load rating of existing bridges as specified in the AASHTO LRFR code. It should be clearly stated that it is impossible to obtain exact values for the maximum expected 75-year or 5-year load due to the limitations in the available database. In fact,

to obtain accurate results, one would need several cycles of WIM data collected over 75 years and even for the 5-year period it is not possible at this stage to have sufficient data due to the relative recent adoption of WIM technology in the U.S. even if one assumes that the load spectra are stationary and do not change over time. Therefore, some form of statistical projection should be performed. In this paper, the recommended procedure by Sivakumar et al (2011) and Ghosn et al. (2012) is used to obtain the cumulative distribution of the maximum expected live load effect for a 5-year return period. This approach for obtaining the live load model requires as input the WIM data collected at a site after being "scrubbed" and processed to remove data outliers as described in Sivakumar et al. (2011). Using the WIM data for a site, the load effect of each truck loading event is calculated by passing the trucks through the proper influence line. The load effect of each set of trucks that are expected to be on the bridge simultaneously is then normalized by dividing the calculated value by the effect of the HL-93 vehicle which has been designated in the AASHTO LRFD as the model to use for obtaining the design load on bridges. The results are collected into cumulative distribution histograms F(S) for a single lane of trucks or for trucks side by side on multi-lane bridges. Assuming independence between the various events, the cumulative probability distribution of the maximum load effect in a return period T during which N loading events are expected is then obtained from:

$$F(LL) = F(S)^N \tag{6.6}$$

Where the number of events, N, is obtained from the WIM data based on the Average Daily Truck Traffic (ADTT) and the headways considering the number of multi-lane events and the location of the trucks relative to each other during such events. When N is very large, it is necessary to assume that the tail end of F(S) follows a known probability distribution. In the work

performed by Ghosn et al. (2012), it was determined that the upper 5% of the histogram's tail end approaches that of Normal probability distribution. This will allow for extending the range of the WIM data beyond the upper range limits as described by Ghosn and Sivakumar (2011).

In this study, the live load is from the data collected at NY State WIM site 9121. Figure 2 and Figure 3 show the cumulative probability distribution for the maximum two-lane live load obtained for a 120-ft and a 100-ft simple span for different years, respectively. In Figures 6.2 and 6.3 the live loads for the 120-ft span and 100-ft spans are normalized in terms of equivalent AASHTO 3S2 Legal Load trucks. The Legal truck is used because the nonlinear structural analysis requires the application of loads that resemble actual truck configuration.

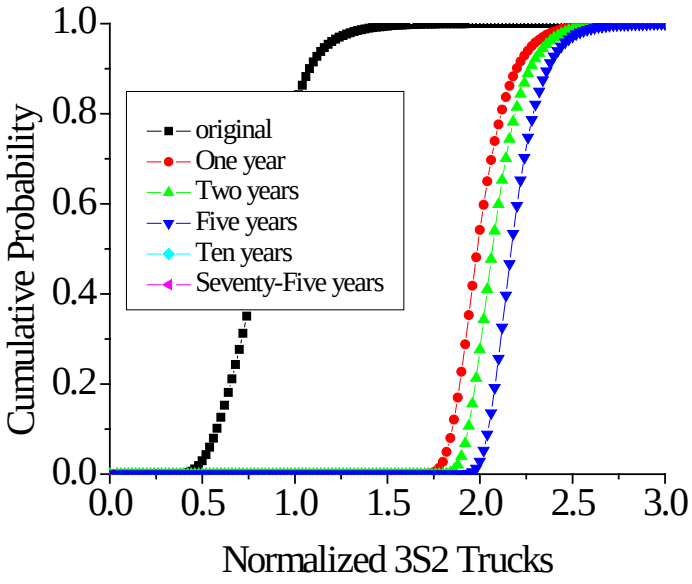

Figure 6.2 - Cumulative probability distribution of live load for 120-ft bridge.

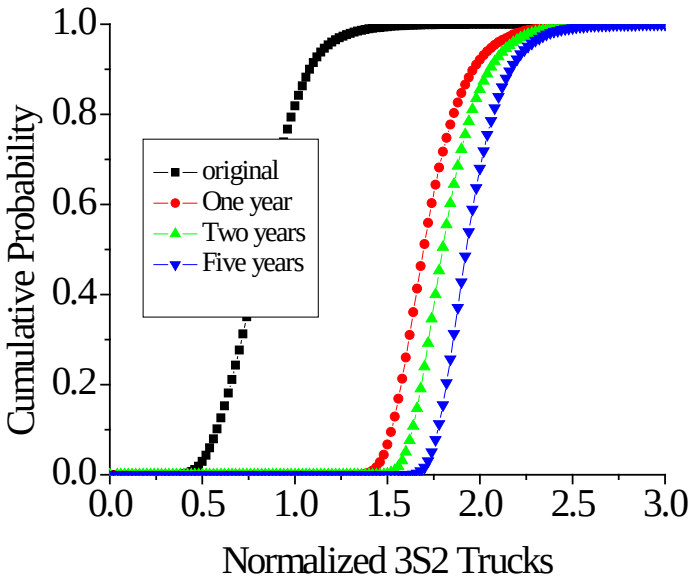

Figure 6.3 - Cumulative probability distribution of live load for 100-ft bridge

6.4 Probabilistic Progressive Collapse Analysis Methodology

Modeling techniques for progressive collapse analysis range from simple two-dimensional linear-elastic static procedures to very complex three-dimensional, nonlinear time history dynamic analysis. In our research, the progressive collapse analysis process is modeled by instantaneously applying reaction loads equal and opposite to those that were originally applied on the damaged element before damage took place. A dynamic load is applied to a damaged structure that is artificially held in its initial, undamaged position. Figure 6.4 shows the instantaneously applied load and structural model for the progressive collapse analysis. Figure 6.5 shows the applied load time history (Buscemi & Marjanishvili 2004).

The progressive collapse analysis using the instantaneously applied load technique follows these steps:

1. Perform static analysis to determine reaction force in the load bearing element to be removed. As an example, in the structure shown in Figure 6.4, the middle column is assumed to be removed;

2. Change structural geometry by removing the load bearing element that is assumed to be damaged as shown in Figure 6.4;

3. Apply a reaction force P dynamically, as shown in Figure 6.5. In this research, tr is taken to be 10 times the first period.

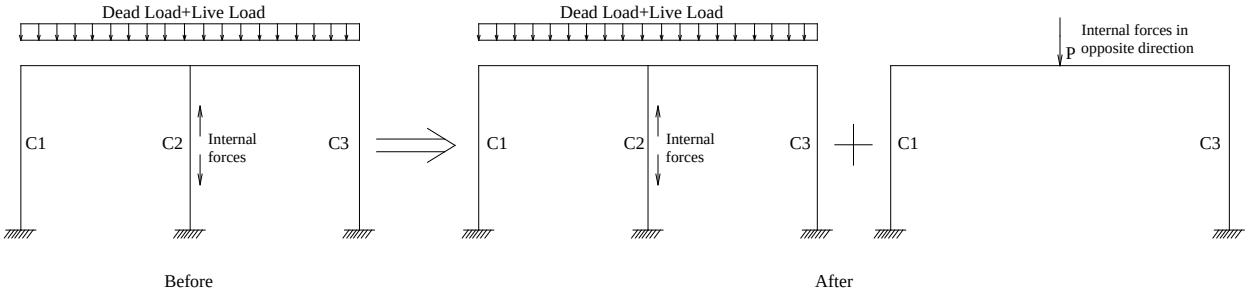

Figure 6.4 Instantaneously applied load model for progressive collapse analysis

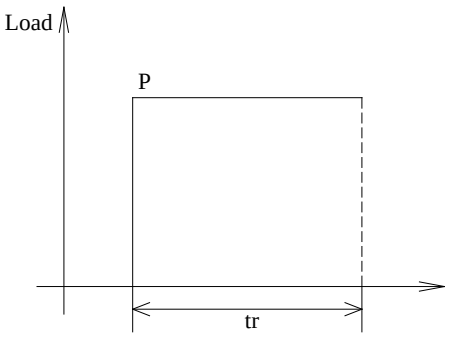

Figure 6.5 Instantly applied load time history view

6.5 Structural Modeling of Box-girder Bridge

According to FHWA and AASHTO criteria, steel two-box girder bridges are considered to be fracture critical, meaning that if a fatigue crack is initiated in one of the two boxes, the system will fail and it will not be able to carry any load. One goal of this study is to develop a methodology to verify whether such bridges are indeed fracture critical. In chapter four we have verified that a two-box bridge will still be able to carry some load after one box is fully fractured at its midspan. In this Chapter, we will verify whether the system will be able to survive the fracture process and the associated release of energy which is affected using a dynamic progressive collapse analysis. To execute the analysis, a structural model is developed as described in this section. The results of the analysis are presented in Section 6.7.

The progressive collapse analysis process is described using the model a 120ft-long steel box-girder bridge, which is shown in Figure 6.6. This bridge is designed following the current AASHTO LRFD code.

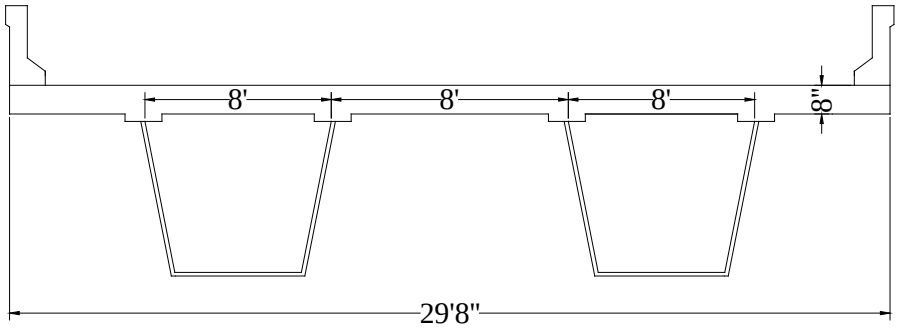

Figure 6.6 Cross section of box-girder bridge

(1) Grillage Model

The dead load is entered as a distributed load over the longitudinal beam elements. The

weight of the steel box is W1=0.018 kips/in, the weight of the concrete deck is W2=0.071 kips/in and the weight due to the guard rail W3=0.014 kips/in are applied on each longitudinal beam element. The fracture occurs in the bottom flange at the mid-span of one girder. This 6-inch fracture cuts all the way through the entire width of the bottom flange.

The intact bridge and fractured bridge are discretized as shown in Figure 6.7 and Figure 6.8, respectively. The moment-curvature relationship for the longitudinal beams representing the composite behavior of each web is shown in Figure 6.9. The moment-curvature relationship for the transverse beams representing the behavior of the slab and its ability to distribute the load transversely is presented in Figure 6.10.

The moments of inertia and torsional constants for each of the beams are listed in Table 1.

Table 6.1 Elastic properties of fractured bridge

	Moment of Inertia I (in4)	Torsional Constant J (in4)
Composite longitudinal beams	82182	17248
Cracked Longitudinal beams	3122	6144
Transverse box beams	261304.	932279
Transverse slab beams	6144	12288

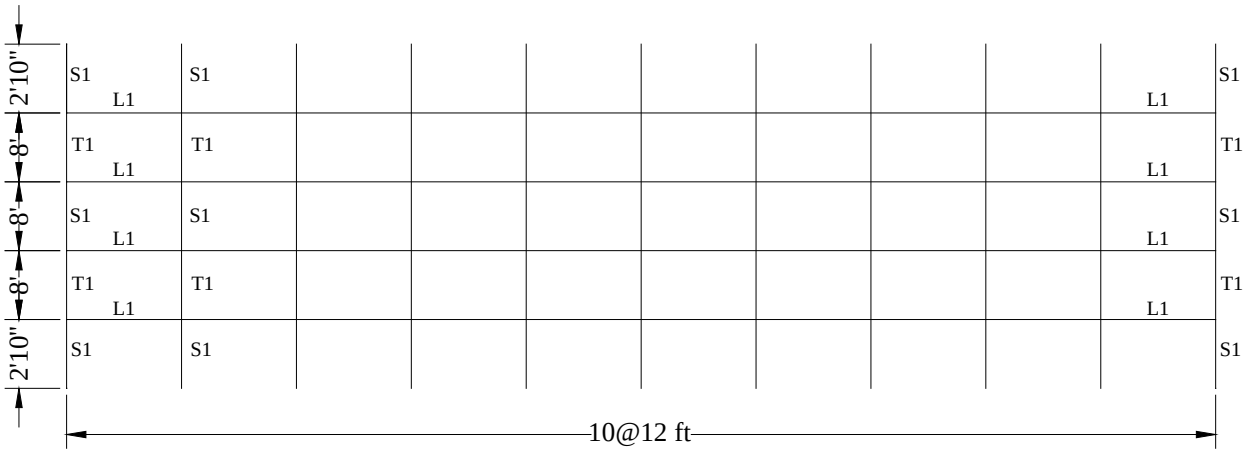

Figure 6.7 Grillage model of intact bridge

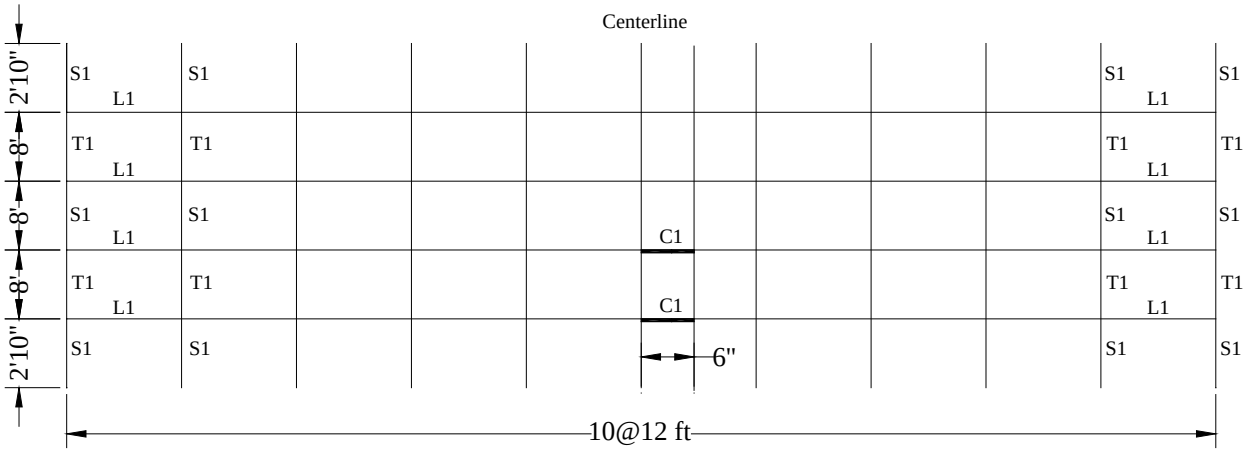

Figure 6.8 Grillage model of fractured bridge

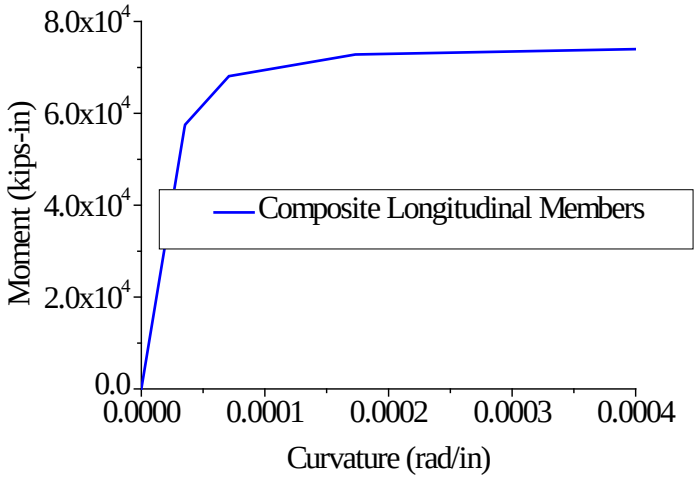

Figure 6.9 Moment-curvature for longitudinal members

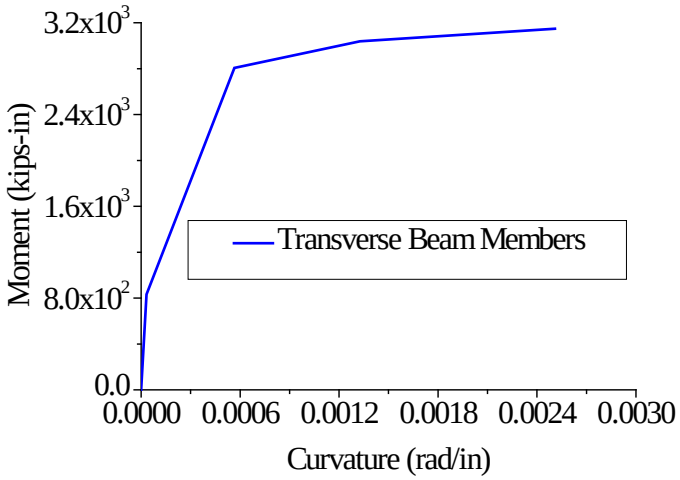

Figure 6.10 - Moment curvature of transverse slab members

Resistance

The nominal resistance values for bridge members are usually on the conservative side. Nowak (1999) assumed that the member resistances can be modeled by lognormal probability distributions where the mean and COV of the moment resistance of bridge girders are related to the nominal values by:

$$\overline{R} = 1.12R_n \quad V_R = 10\% \qquad \text{For composite steel beams}$$

$$\overline{R} = 1.14R_n \quad V_R = 13\% \qquad \text{For reinforced concrete beams} \tag{6.7}$$

6.6 Structural Modeling of Steel Truss Bridge

Following the collapse of the I-35 Bridge in Minnesota, the FHWA is performing a review of similar type structures to avoid similar future failures. One goal of this study is to develop a methodology that engineers can follow to investigate the ability of such structures to investigate their redundancy and their ability to withstand local failures. For that purpose, a truss bridge having the configuration shown in Figure 11 is used as an example to demonstrate how the results of a probabilistic progressive collapse can be used to develop deterministic analyses that can be implemented in engineering g practice.

The through-truss bridge has two parallel trusses similar to the one shown in Figure 11. The two parallel trusses are connected by cross beams and diagonals supporting a concrete deck. The concrete deck is 7-in thick and 408-in wide.

To perform the reliability analysis, statistical models for member strengths and loads are presented in this section. Generally, when modeling structures, most attention is paid to the main structural members. However, a preliminary report by the Federal Highway Administration

(FHWA) (Holt and Hartmann 2008) concluded that the I-35W Minnesota bridge failure initiated at a gusset plate of the bridge. Therefore, in this study, the reliability analysis of truss bridges will model structural members and connections. The connections consist of the bolts and gusset plates. Table 6.2 gives a listing of the truss members along with their cross sectional areas. Tables 6.3a and 6.3b give the dimension of the gusset plate and bolts. The definition of the parameters is provided in the tables are given in Figure 6.12.

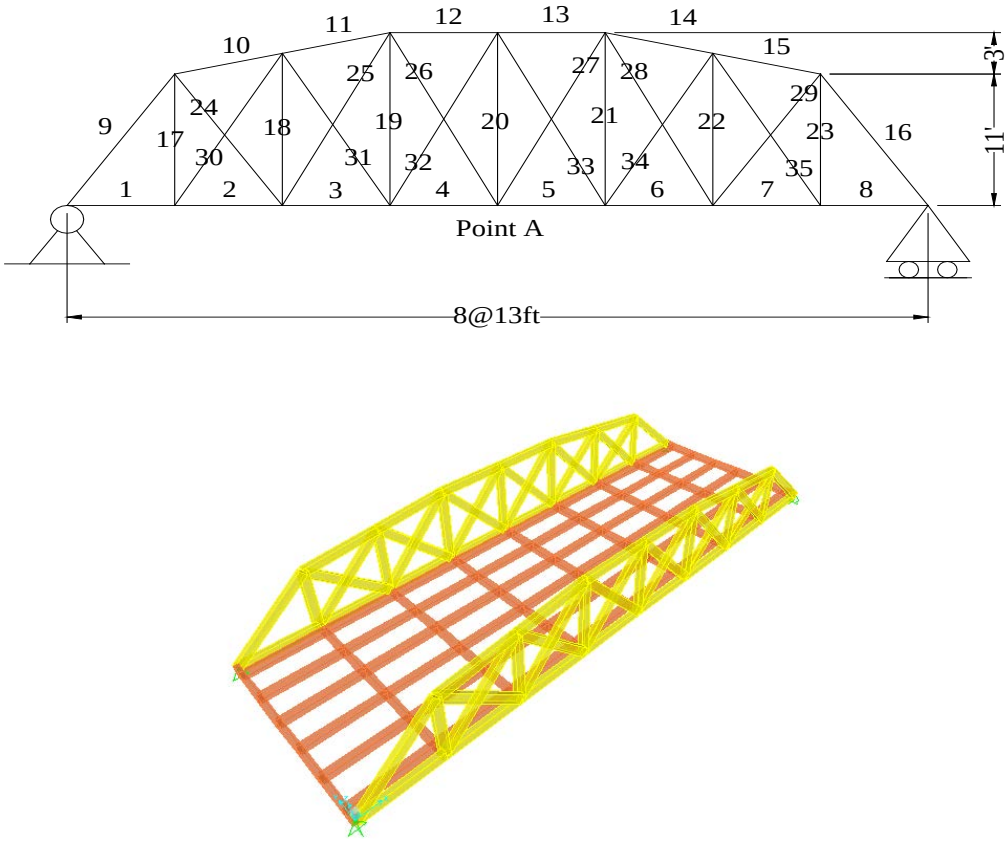

Figure 6.11 Layout of steel truss bridge

Table 6.2 Truss members' cross sectional areas

No.	Area (in2)	No.	Area (in2)	No.	Area (in2)
1	14.00	13	17.59	25	1.84
2	14.93	14	16.24	26	3.68
3	17.22	15	11.21	27	3.68
4	18.85	16	10.69	28	1.84
5	18.85	17	4.08	29	6.38
6	17.22	18	0.87	30	1.98
7	14.93	19	2.46	31	2.65
8	14.00	20	0.19	32	0.55
9	10.69	21	2.46	33	0.55
10	11.21	22	0.87	34	2.65
11	16.24	23	4.08	35	1.98
12	17.59	24	6.38		

Table 6.3a Gusset Plate Design

Gusset Plate Location	Gusset Plate Information								Shear Capacity (ksi)	1 Bottom/top Chord					2 Bottom/top Chord			
			Length			Eccentricity				Diameter (in)	Width (in)	Length (in)	No.of Fasteners		Width (in)	Length (in)	No.of Fasteners	
	Yield Stress (ksi)	Thickness (in)	hA	hB	hC	eA	eB	eC					Nt2	Nl2			Nt2	Nl2
U2	50	0.5	35	40	40	12.25	12	12	25	1	14	12	4	6	14	12	4	6
U3	50	0.5	40	40	40	12.25	12	12	25	1	14	12	4	6	14	12	4	6
U4	50	0.625	40	40	40	12.25	12	12	25	1	14	12	4	6	14	12	4	6
U5	50	0.625	35	40	40	12.25	12	12	25	1	14	12	4	6	14	12	4	6
U6	50	0.625	40	40	40	12.25	12	12	25	1	14	12	4	6	14	12	4	6
U7	50	0.5	40	40	40	12.25	12	12	25	1	14	12	4	6	14	12	4	6
U8	50	0.5	35	40	40	12.25	12	12	25	1	14	12	4	6	14	12	4	6
L21	50	0.5	40	40	40	12.25	12	12	25	1	14	12	4	6				
L30	50	0.5	40	40	40	12.25	12	12	25	1	14	12	4	6	14	12	4	6
L31	50	0.5	40	40	40	12.25	12	12	25	1	14	12	4	6	14	12	4	6
L32	50	0.625	40	40	40	12.25	12	12	25	1	14	12	4	6	14	12	4	6
L33	50	0.625	40	40	40	12.25	12	12	25	1	14	12	4	6	14	12	4	6
L34	50	0.625	40	40	40	12.25	12	12	25	1	14	12	4	6	14	12	4	6
L35	50	0.5	40	40	40	12.25	12	12	25	1	14	12	4	6	14	12	4	6
L36	50	0.5	40	40	40	12.25	12	12	25	1	14	12	4	6	14	12	4	6
L29	50	0.5	40	40	40	12.25	12	12	25	1	14	12	4	6				

Table 6.3b Design of Connections

Gusset Plate Location	3 Left/Right Diagonal					4 Up/Down Vertical					5 Left/Right Diagonal				
	Width (in)	Length (in)	No.of Fasteners		Unsupp. Length (in)	Width (in)	Length (in)	No.of Fasteners		Unsupp. Length (in)	Width (in)	Length (in)	No.of Fasteners		Unsupp. Length (in)
			t2	l2				t2	l2				t2	l2	
U2						8	12	2	5	6	14	12	4	5	5.333
U3	14	12	4	5	5	8	12	2	5	5	14	12	4	5	5.333
U4	14	12	4	5	5	8	12	2	5	5	14	12	4	5	5.333
U5	14	12	4	5	5	8	12	2	5	5	14	12	4	5	5.333
U6	14	12	4	5	5	8	12	2	5	5	14	12	4	5	5.333
U7	14	12	4	5	5	8	12	2	5	5	14	12	4	5	5.333
U8						8	12	2	5	6	14	12	4	5	5.333
L21	14	12	4	5	5										
L30	14	12	4	5	5	8	12	2	5	6					
L31	14	12	4	5	5	8	12	2	5	6	14	12	4	5	5.333
L32	14	12	4	5	5	8	12	2	5	6	14	12	4	5	5.333
L33	14	12	4	5	5	8	12	2	5	6	14	12	4	5	5.333
L34	14	12	4	5	5	8	12	2	5	6	14	12	4	5	5.333
L35	14	12	4	5	5	8	12	2	5	6	14	12	4	5	5.333
L36	14	12	4	5	5	8	12	2	5	6					
L29	14	12	4	5	5										

172

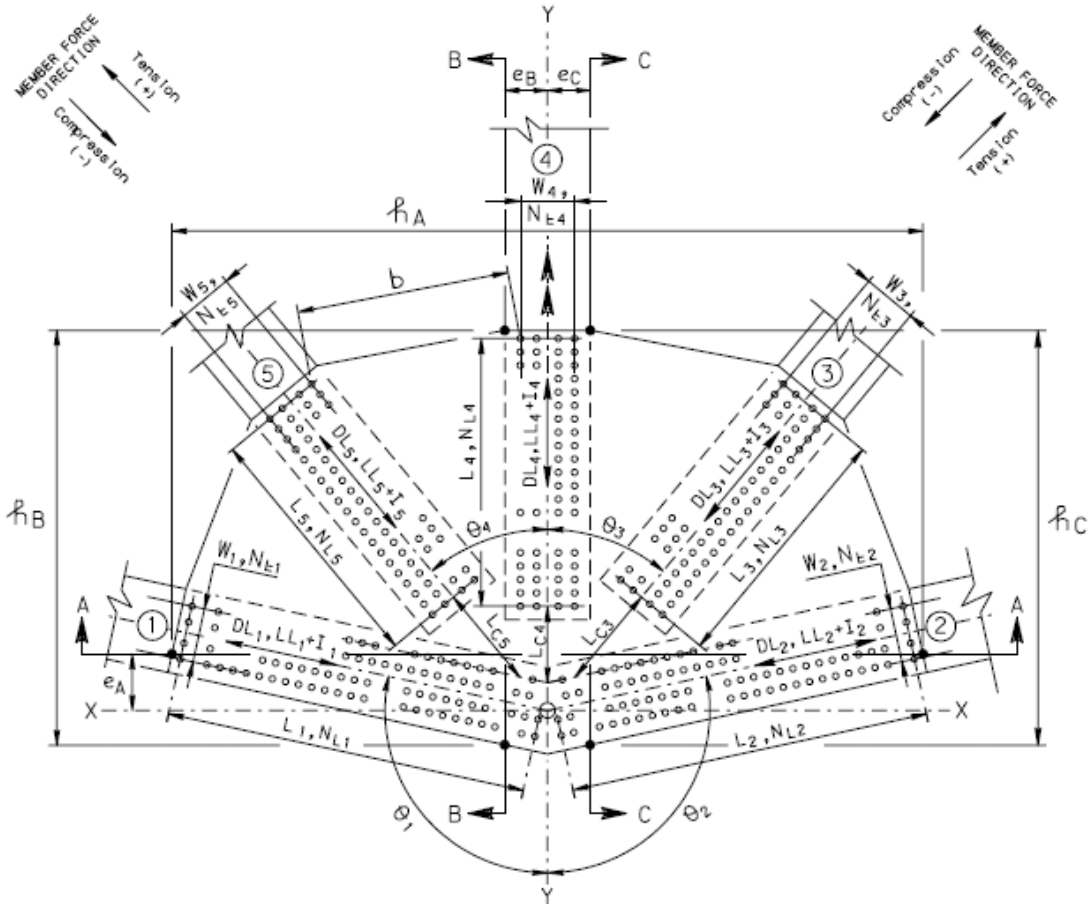

Figure 6.12 - Gusset Plate Geometry

6.6.1 Structural Steel Properties

In this study, the simplified model shown in Figure 6.13 is used for the nonlinear stress-strain behavior of steel members in accordance with several references (Ellingwood et al. 1980; Galambos and Ravindra 1978; Johnson and Opila 1941; Julian 1957; Tall and Alpsten 1969). The stress-strain curve can be divided into have four parts: a) Elastic region, b) plastic region, c) strain-hardening region, and d) descending necking region.

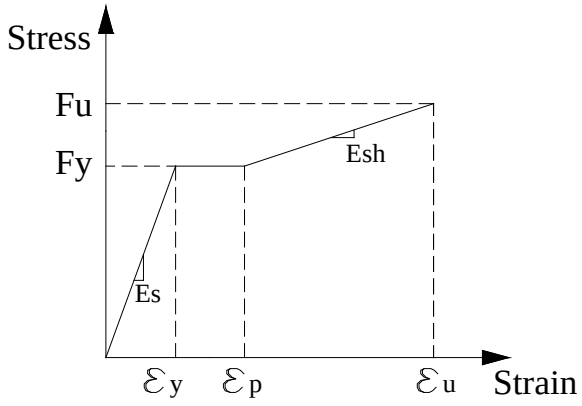

Figure 6.13 Simplified Stress-Strain Relationship Model of Steel

During the calibration of the LRFD Steel Design Manual, Galambos and Ravindra (1978) studied the behavior of steel structural members. The steel properties they investigated included the modulus of elasticity, yield stress, and strain hardening properties. The statistical data for the yield strength and ultimate strength are available in references (Ellingwood et al. 1980; Galambos and Ravindra 1978). Both the yield and ultimate strengths are random variables that are assumed to be log-normally distributed. The bias and coefficient of variation (COV) for the yield strength and ultimate strength are 1.10 and 0.11. Based on data collected by Johnson and Opila 1941; Julian 1957; Tall and Alpsten

1969. the bias and coefficient of variation for the modulus of elasticity which is assumed to be normally distributed are found to be 1.08 and 0.060.

The only directly measured strain-hardening property is the strain-hardening modulus. Doane (1969) made an analysis of strain-hardening modulus data , E_{sh} , for ASTM A7, A36 and A441 steel. He found the mean value to be 600 ksi and the COV to be 0.25. The other property related to the nonlinear behavior of the steel material is the length of the plastic plateau. From tests done at the City College of New York, the plastic strain is found to be consistently 15 times the yield strain. This value is assumed to be deterministic. Table 6.4 summarizes the statistics of random variables.

Table 6.4 Statistics of random variables – steel members

Random Variable	Nominal	Bias	COV	Distribution Type	Reference
F_y	36 ksi	1.10	0.11	Log-normal	(Ellingwood et al. 1980; Galambos and Ravindra 1978)
F_u	58 ksi	1.10	0.11	Log-normal	(Ellingwood et al. 1980; Galambos and Ravindra 1978)
E_s	29000 ksi	1.08	0.06	Normal	(Johnson and Opila 1941; Julian 1957; Tall and Alpsten 1969)
E_{sh}	600 ksi	1.00	0.25	Normal	(Doane 1969; Melchers 1999)

6.6.2 Steel Connections

Generally, the connections of truss members are designed stronger than the members they connect. Accordingly, one should not expect to find fractured connection or gusset plates. However, on Wednesday, August 1, 2007, the bridge carrying Interstate Highway

I-35W over the Mississippi River in Minneapolis, Minnesota, collapsed within a matter of seconds. The collapse of a highway bridge in a major U.S. downtown area was unprecedented. What makes the event peculiar is that the bridge was a very typical structure and that the collapse occurred under what was thought to be normal operating conditions except for minor deck, joint, lighting, and guardrail repairs. The longer spans of the bridge were constructed as a deck-truss bridge. Steel truss bridges such as the I-35W Bridge are a very common form for long-span bridges in the United States and worldwide. Until the event occurred, steel truss bridges had earned the reputation of being economical and reliable. While the low redundancy of the trusses may be of concern, it is believed that mandated maintenance procedures assure that this structural system is as safe and reliable as any other. Forensic evidence from the I-35W Bridge after collapse [Hill et al. 2008; National Transportation Safety Board (NTSB) 2008a, e] suggests that the bridge failure initiated at gusset plates that connected the top chord members to a compression diagonal and tension diagonal. Holt and Hartmann (2008) suggested that the strength of the gusset plates was insufficient to develop the shear forces expected at this panel point.

In summary, the investigation of the collapse of I-35 Minnesota Bridge showed that the collapse of the deck truss portion of the bridge was related to the fractured gusset plates and, in particular, may have originated with the failure of the U10 gusset plates shown in Figure 6.14. In this analysis, we model all the parts of the connections using data collected from the literature as described below.

(a) a view of the west side **(b) Post Collapse**

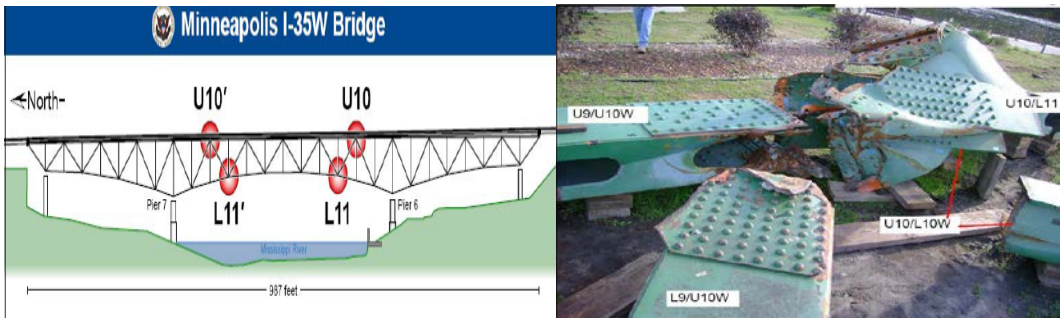

(c) the position of Node U10 **(d) the fracture of Node U10**

Figure 6.14 The collapse of I-35 bridge due to the fractured gusset plates

Bolts shear failure mode

Based on collected data from the literature (Fisher et al. 1978; Fisher and Kulak 1968; Rumpf and Fisher 1963; Wallaert and Fisher 1965), a tri-linear shear stress-deformation model is proposed to model the behavior of bolts as shown in Figure 6.15. The bias for the ultimate shear stress is 1.20 (Fisher et al. 1978). Given a nominal tensile strength for A325 bolts of 120 ksi, the nominal ultimate shear stress is 74.4 ksi, which is 62% of the tensile strength (Kulak et al. 1987). However, in connections transmitting an axial force between members with more than two bolts in the line of the force, non-uniform deformations of the connected material between fasteners causes a non-uniform

distribution of the shear forces in the bolts. Consequently, the strength of the joint decreases (Kulak et al. 1987). Figure 16 indicates how the average strength is affected by the increasing number of fasteners. Rather than provide a decreasing function that reflects this decrease in average strength with joint length, a single reduction factor of 0.80 is applied to the 0.62 multiplier with joint length on the order of 30 in. Based on the data provided in references ((Fisher et al. 1978; Fisher and Kulak 1968; Rumpf and Fisher 1963; Wallaert and Fisher 1965), the statistics of the random variable $\sigma_1, \sigma_2, \sigma_3$ and Δ_1, Δ_2, Δ_3 that describe the behavior of bolts in steel connections are provided in Table 6.5.

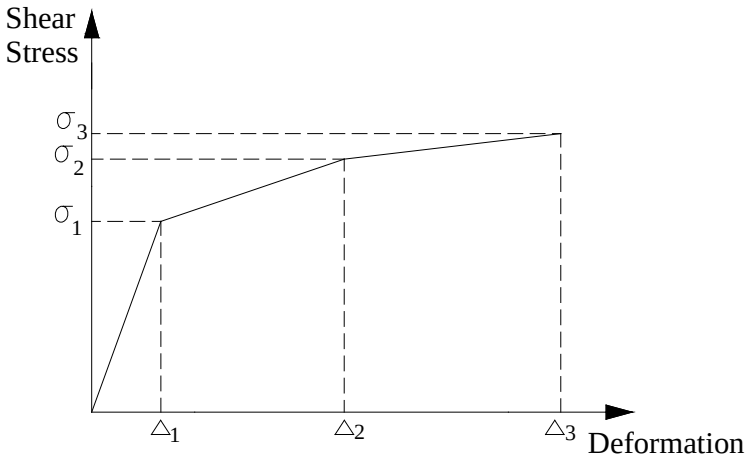

Figure 6.15 Simplified Tri-linear model

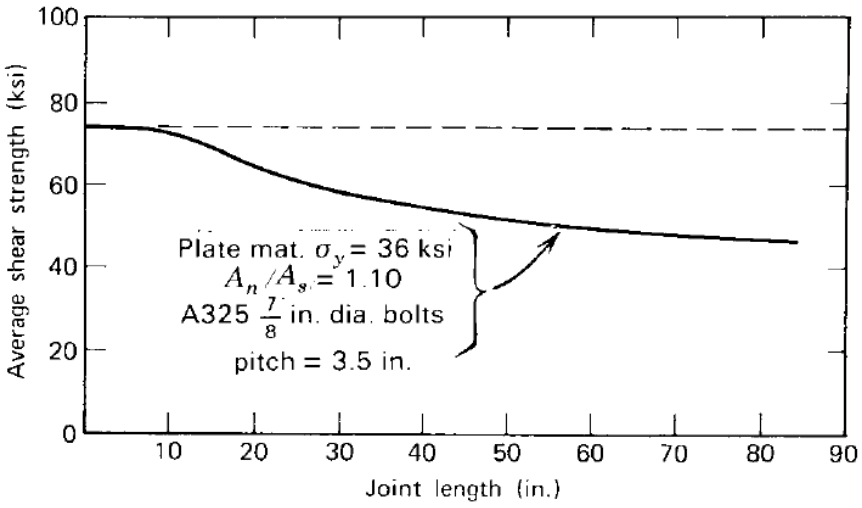

Figure 6.16 Effect of joint length on ultimate shear strength

Table 6.5 Statistics of random variables – steel connections

Random Variable	Mean	COV	Distribution Type	Reference
σ_1	41.30 ksi	0.10	Normal	(Fisher et al. 1978; Fisher and Kulak 1968; Rumpf and Fisher 1963; Wallaert and Fisher 1965)
σ_2	64.54 ksi	0.10	Normal	(Fisher et al. 1978; Fisher and Kulak 1968; Rumpf and Fisher 1963; Wallaert and Fisher 1965)
σ_3	71.42 ksi	0.10	Normal	(Fisher et al. 1978; Fisher and Kulak 1968; Rumpf and Fisher 1963; Wallaert and Fisher 1965)
Δ_1	0.036 in	0.08	Normal	(Fisher et al. 1978; Fisher and Kulak 1968; Rumpf and Fisher 1963; Wallaert and Fisher 1965)
Δ_2	0.12 in	0.08	Normal	(Fisher et al. 1978; Fisher and Kulak 1968; Rumpf and Fisher 1963; Wallaert and Fisher 1965)
Δ_3	0.23 in	0.08	Normal	(Fisher et al. 1978; Fisher and Kulak 1968; Rumpf and Fisher 1963; Wallaert and Fisher 1965)

Bearing Capacity of Gusset Plates

Clinton Rex (2003) and Hyeong J. Kim (1999) performed a large number of experiments to provide data about the strength and load-deformation behavior of a single plate bearing on a single bolt or two bolts. A normalized Load-Deformation relationship for the bearing capacity of connection plates was proposed by Clinton Rex (2003) as given in Equation (6.8).

$$\frac{P}{P_n} = \frac{1.74\,\overline{\Delta}}{\left(1+\overline{\Delta}^{0.5}\right)^2} - 0.009\,\overline{\Delta} \tag{6.8}$$

Where, P=plate load; P_n=nominal plate strength; $\overline{\Delta}$ =normalized deformation= $\Delta\beta K_i / P_n$; Δ =hole elongation; β =steel correction factor=30%/%Elongation (for typical steels taken as one); and K_i=initial stiffness.

Nominal Plate Strength

The most common strength model for predicting the bearing strength F_b of plates was developed by Fisher and Struik (1974):

$$F_b = \frac{P_n}{d_b t_p} = 1.4F_u\left(\frac{L_e}{d_b} - \frac{1}{2}\right) \le 3.0F_u \tag{6.9}$$

Where, d_b=diameter of bolts; t_p=the thickness of plate; L_e= the end distance; F_u=ultimate strength of plate

In addition to Equation (6.9), Fisher and Struik (1974) also recommended a simpler expression that was adopted by the AISC LRFD Specifications (1993):

$$F_b = F_u \frac{L_e}{d_b} \leq 2.4F_u \tag{6.10}$$

More recently, the AISC Specification (AISC 1999) has adopted a modified equation that is based on a physical model similar to that used by Fisher and Struik (1974) and is given as:

$$F_b = 1.2F_u \frac{L_c}{d_b} \leq 2.4F_u \tag{6.11}$$

Where L_c=minimum distance from the edge of the bolt hole to the edge of the plate.

Eurocode 3 (1993) has a slightly different expression for the bearing strength. If it is assumed that the bolt steel tensile strength is greater than the plate steel tensile strength, the expression given in Eurocode 3 (1993) can be written as:

$$F_b = \frac{2.5}{3} F_u \frac{L_c}{d_h} \leq 2.5F_u \tag{6.12}$$

Where d_h=hole diameter

After statistical comparisons of the existing models for evaluating nominal plate strength, Clinton Rex pointed out that the AISC Specification (LRFD 1993) provided the best correlation with experimental results and is therefore used in our analysis.

Based on the data from Rex and Easterling (2003) and Hyeong J. Kim (1999), a bilinear force-displacement model for bearing is developed as shown in Figure 6.17.

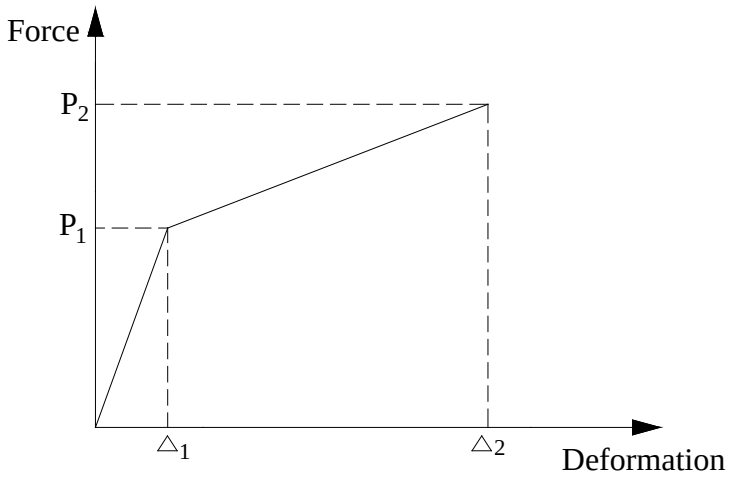

Figure 6.17 A bilinear force-displacement model for bearing plates

Several factors can influence the ultimate deformation Δ_2, such as the distance between the edge of the plate and the bolt L_e, the ultimate strength F_u, and the diameter of the bolts d_b. A regression analysis is performed to give the following relationship between Δ_2 (mm), L_e (mm), F_u (kN/mm) and d_b (mm).

$$\Delta_2 = -7.9462 + 1.1315 * L_e - 0.0129 * F_u + 0.1331 * d_b - 0.0137 * L_e^2 \qquad (6.13)$$

Δ_1 is approximated to be $\frac{1}{6}\Delta_2$ based on the data provided by Clinton Rex (2003).

The initial stiffness is predicted using the model provided by (Rex and Easterling 2003).

$$K_i = \frac{1}{\frac{1}{K_{br}} + \frac{1}{K_b} + \frac{1}{K_v}} \qquad (6.14)$$

Where K_{br} is bearing stiffness=$120 t_p F_y (d_b / 25.4)^{0.8}$;

K_b is bending stiffness= $32Et_p(L_e/d_b - 1/2)^3$;

K_v is shearing stiffness= $6.67Gt_p(L_e/d_b - 1/2)$ where G is shear modulus of elasticity.

Once Δ_1, Δ_2 and K_i are determined, P_1 and P_2 can be obtained from Equation (6.8). The bias giving the ratio of the experimental result for P_2 to the predicted P_2 is defined as γ_p. Assuming that the bias and coefficient of variation for the shear modulus of elasticity G are the same as those for modulus of elasticity E, the random variables that describe the behavior of gusset plates is summarized as shown in Table 6.6.

Table 6.6 Statistics of random variables – plate strength

Random Variable	Nominal	Bias	COV	Distribution Type	Reference
F_y	36ksi	1.10	0.11	Log-normal	(Ellingwood et al. 1980; Galambos and Ravindra 1978)
F_u	58ksi	1.10	0.11	Log-normal	(Ellingwood et al. 1980; Galambos and Ravindra 1978)
E_s	29000ksi	1.08	0.06	Normal	(Ellingwood et al. 1980; Galambos and Ravindra 1978)
G	11153.85ksi	1.08	0.06	Normal	(Rex and Easterling 2003)
γ_p	N.A.	1.05 (mean)	0.05	Normal	(Rex and Easterling 2003)

Buckling of Members in Compression

In this paper, the simplified model shown in Figure 6.18 is used to consider the buckling of bars and gusset plates in compression. The slope is set as a very large number

considering that buckling occurs suddenly.

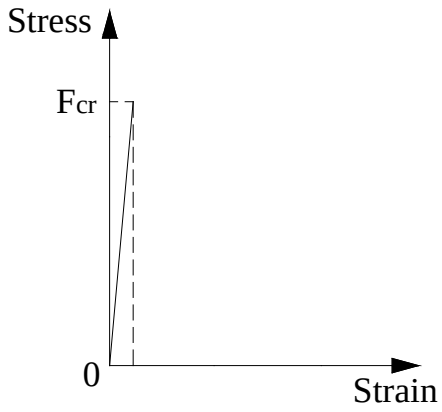

Figure 6.18 - Stress-strain curve

For columns in compression:

$$\text{For } \frac{KL}{r} \le 4.71\sqrt{\frac{E}{QF_y}}, \quad F_{cr} = \left[0.658^{\frac{QF_y}{F_e}}\right]QF_y \tag{6.15}$$

$$\text{For } \frac{KL}{r} > 4.71\sqrt{\frac{E}{QF_y}}, \quad F_{cr} = 0.877F_e \tag{6.16}$$

Where, F_{cr} is the buckling stress; F_y is the yielding stress; K=effective length factor; L=length of member; r=radius of gyration= $\sqrt{I/A_g}$; I=moment of inertia; E=modulus of elasticity; $F_e = \frac{\pi^2 E}{\left(\frac{KL}{r}\right)^2}$; Q=form factor to consider the reduction in efficiency of the cross section in accordance with AISC-E7.

The comparison of experimental data with the AISC equation is shown in Figure

6.19 [Hall 1981]. The bias of AISC Equation (6.15) and Equation (6.16) is 1.13 and its COV is 9% and is assumed to be valid for both plates and bars.

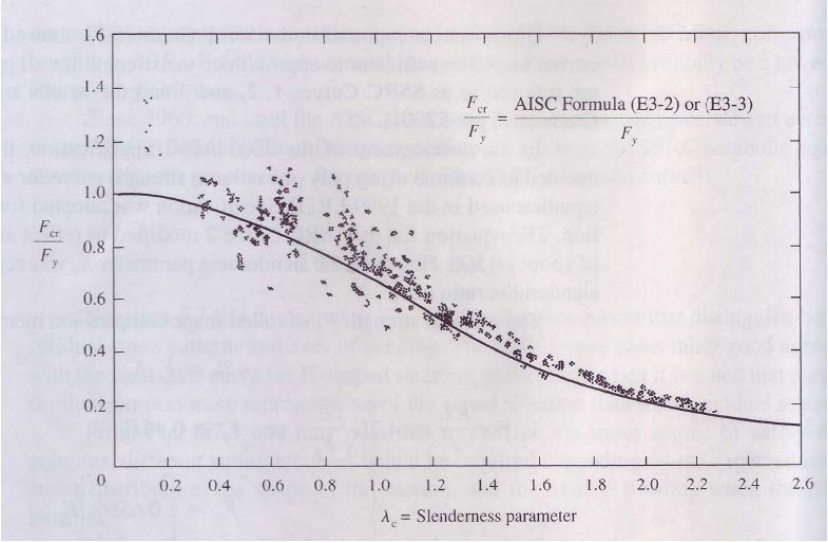

Figure 6.19 Comparison of AISC equations of F_{cr} with data from physical tests

For plates in compression:

$$F_{cr} = k\frac{\pi^2 E}{12\left(1-\mu^2\right)(b/t)^2} \tag{6.17}$$

Where k is a constant depending on type of stress (Gerard&Becker 1957), edge support conditions, and length to width ratio (aspect ratio) of the plate, μ is poisson's ratio, b/t is the width/thickness ratio;

The random variable properties for E, F_y are listed in Table 6.7.

Table 6.7 Statistics of buckling variables - buckling

Random Variable	Nominal	Bias	COV	Distribution Type	Reference
F_y	36 ksi	1.10	0.11	Log-normal	(Ellingwood et al. 1980; Galambos and Ravindra 1978)
E_s	29000 ksi	1.08	0.06	Normal	(Johnson and Opila 1941; Julian 1957; Tall and Alpsten 1969)

6.7 Probabilistic analysis of bridge system redundancy, robustness and progressive collapse.

In this section, we perform the redundancy analysis of the box girder bridge and the truss bridge using the methods described in this Dissertation. In this Dissertation, a damaged truss bridge system which has already lost the load carrying capacity of one member is considered to have collapsed if any of its remaining main members reaches its maximum tension force or buckles or if any of the connections fails. For the damaged box girder bridge, the damage system is assumed to have collapsed if the deck over the fractured section reaches its maximum rotation. The intact truss bridge system is assumed to have collapsed if any two of the members reach their maximum tension forces or buckle or if any of the connections fails. Similarly, the intact box girder bridge system is considered to have collapsed if any of the girder members reaches its maximum rotation.

In a first step, the analysis is performed to find the reliability of the most critical member under the effect of the maximum 75-year load. Subsequently, the reliability of

the intact system is performed for the bridges under the effect of the 75-year maximum load. A reliability analysis of the robustness of the system when one critical member is removed is performed for the maximum 5-year load. This analysis scenario verifies the ability of the damaged system to continue to carry some load if the system survives the damage process. Finally, the dynamic reliability analysis of the damage process is performed assuming that the critical member is dynamically removed when the 5-year maximum load is on the bridge.

For the box-girder bridge, the damage scenario assumes that a fracture occurs in the bottom flange and the two webs of one box at the middle of the span. A 6-inch fracture cuts all the way through the entire steel section but the slab is assumed to continue to carry load.

The differences between the reliability indexes of the intact bridge, the damaged bridges without and with dynamic effect are compared to the reliability index of the members to yield:

$$\Delta\beta_{ultimate} = \beta_{ultimate} - \beta_{member} = 4.69 - 3.5 = 1.19 > 0.85$$

$$\Delta\beta_{static} = \beta_{damaged} - \beta_{member} = 1.39 - 3.5 = -2.11 > -2.70$$

$$\Delta\beta_{dynamic} = \beta_{damaged} - \beta_{member} = 0.81 - 3.5 = -2.69 > -2.70$$

These results indicate that two box-girder bridges designed for member β=3.5 as is the intent of the AASHTO LRD code have sufficient system reliability to allow the bridge to continue to carry load after the fatigue fracture of one box. Additionally, the dynamic reliability analysis shows that the two-box bridge is expected to survive with sufficient reliability the high energy dissipated during a fatigue fracture process.

In the truss bridge example, two damaged scenarios are considered: 1) member 29 removed; 2) member 23 removed. In this case, it is observed that the intact system does have sufficient redundancy but that the bridge is unable to sustain the dynamic removal of the members damaged bridge and even if it survives the damaging event, the bridge will not be able to sustain the 1-month maximum live load.

$$\Delta\beta_{ultimate} = \beta_{ultimate} - \beta_{member} = 4.61 - 3.5 = 1.11 > 0.85$$

$$\Delta\beta_{static} = \beta_{damaged} - \beta_{member} = -0.67 - 3.5 = -4.17 < -2.70$$

$$\Delta\beta_{dynamic} = \beta_{damaged} - \beta_{member} = -2.05 - 3.5 = -5.55 < -2.70$$

6.8 Calibration of Load Factors for Use in Deterministic Analysis

The reliability analysis performed in Section 7 can be used to evaluate the reliability of the bridge system and perform the probabilistic analysis of the redundancy and robustness as well as the probability of progressive collapse should one member be suddenly damaged due to the occurrence of an external hazard. However, such involved reliability analyses are beyond the day-to-day practice of bridge engineers. Therefore, one objective of this Thesis is to develop a methodology that allows a bridge engineer to verify the ability of a bridge system to avoid progressive collapse using traditional deterministic methods. Traditionally, structural engineers checked the progressive collapse of buildings using the nonlinear methodology and criteria provided in the GSA and DOD guidelines. Given the differences in the loads and configurations of bridge systems as compared to those of office buildings, the existing guidelines for buildings may not necessarily be applicable for the evaluation of the progressive collapse of bridges.

Therefore, a new set of criteria must be developed for bridges. Following current practice in the development of structural design codes, criteria for analyzing the progressive collapse of bridges should be calibrated to provide adequate levels of reliability. The process that can be used for developing such reliability-based criteria are described in this Section by illustrating the approach with the truss and steel two-box girder bridges described earlier.

For an engineer to check the ability of a structure to resist progressive collapse using a nonlinear static analysis, he/she needs to know what live loads to apply, and what appropriate load factors can be used. Following the GSA and DOD methods, the simplified analysis procedure must also explicitly consider material nonlinear behavior and implicitly account for the structural dynamic response by applying a dynamic amplification factor that will avoid the need to perform a structural dynamic analysis.

The calibration procedure is summarized in the following:

1. Assume a format where we want to check the safety of a bridge structure to resist progressive collapse after a member is damaged. Following a modified format of the GSA (2000) and DOD (2002) procedures, it was decided to apply the dead load without any safety factor and the 3S-2 AASHTO Legal Truck with one load factor that includes the safety factor and the dynamic amplification factor. In this study, we call this combined factor the dynamic collapse analysis allowance. The Legal truck shown in Figure 6.20 is used in order to model a common type truck configuration rather than a hypothetical load.

2. Initially, the intact structure is designed following the current AASHTO LRFR design code.

3. A nonlinear probabilistic dynamic reliability analysis is performed to study the reliability of the remaining system as one designated member is suddenly removed.

4. A deterministic nonlinear incremental load analysis is performed on the same structure analyzed in Step 3 after removing the same designated member. The analysis is performed by first applying the dead load and incrementing the live load to find the multiple of the live load required to cause collapse. The total load that will be sustained will be designated as $(D_n + \delta_{CA} L_n)$ where D_n is the nominal dead load and δ_{CA} is the dynamic collapse analysis allowance and L_n is the nominal live load due to the 3S-2 Legal Truck.

5. Repeat steps 2 to 4 for different designs.

6. Establish the relationship between the dynamic progressive collapse reliability of each design and the dynamic collapse analysis allowance δ_{CA}.

7. Ideally, the relationship between the reliability and δ_{CA} will be applicable for most typical bridge configurations so that this relationship could be eventually implemented in the appropriate bridge design specifications.

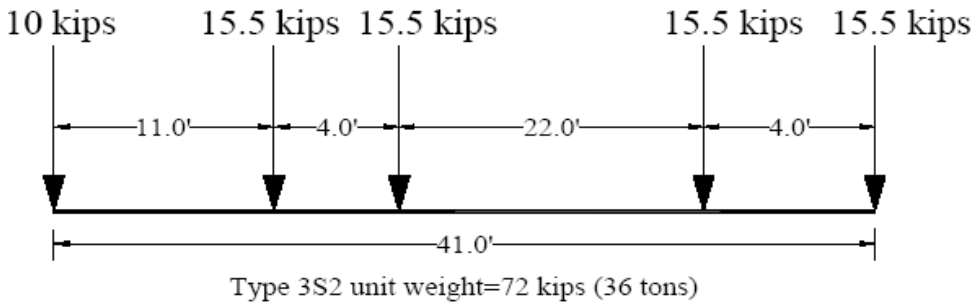

Figure 6.20- AASHTO Type 3s2 truck configuration

Establishing the relationship between the reliability and the dynamic collapse analysis allowance will help engineers evaluate the ability of a system to resist progressive collapse with a certain level of reliability. Specifically, a structural engineer will be able to decide which target δ_{CA} his/her design should satisfy in order to meet a given target reliability. In this manner, an engineer can design a reliable system by simply performing an incremental nonlinear static analysis without the need to perform a dynamic reliability analysis.

The calibration process is applied to the box-girder and truss bridges described in this Chapter as explained below. In this Dissertation, a damaged truss bridge system which has already lost the load carrying capacity of one member is considered to have collapsed if any of its remaining main members reaches its maximum tension force or buckles or if any of the connections fails. For the damaged box girder bridge, the damage system is assumed to have collapsed if the deck over the fractured section reaches its maximum rotation. The intact truss bridge system is assumed to have collapsed if any two of the members reach their maximum tension forces or buckle or if any of the connections fails. Similarly, the intact box girder bridge system is considered to have collapsed if any of the

girder members reaches its maximum rotation.

Box-girder Bridge

With the original design, we perform the dynamic probabilistic analysis assuming that a fracture takes place at the mid-span of one box when the maximum 5-year live load is on the bridge and obtain the reliability index $\beta = 0.813$. With the same design, we perform a deterministic nonlinear static analysis and we find that the dynamic collapse analysis allowance $\delta_{CA} = 1.8$. Subsequently, we increase the capacity of all the longitudinal beams by a factor of 1.5. The corresponding reliability index is $\beta = 1.695$ and the corresponding $\delta_{CA} = 2.1$ is obtained. By repeating the same procedure for different member capacities the results given in Table 6.8 are obtained.

Table 6.8 Live load factors δ_{CA} with different reliability index β for box-girder bridge

δ_{CA}	1.5	1.8	2.1	2.2
β	-1.015	0.813	1.695	2.170

Truss Bridge

The same type of analysis performed for the box-girder bridges is repeated for the truss bridge. Two damage scenarios are considered. The first scenario assumes that member 29 is dynamically removed and the second scenario assumes that member 23 is suddenly removed.

Since the original bridge was not able to survive the sudden removal of the members, we increase the areas for all the bars by a factor 2 and the design of the plates and

connections was adjusted accordingly. For the damage scenario with member 29 removed, we perform the nonlinear dynamic probabilistic analysis and obtain a reliability index $\beta = -1.311$. With the same design, we perform nonlinear static analysis of the system with member 29 removed and obtain $\delta_{CA} = 1.26$. By increasing the original areas for all the bars by a factor equal to 2.5, we obtain $\beta = 0.789$ and the corresponding $\delta_{CA} = 2.00$. By repeating the same procedure with different truss member areas, the results given in Table 6.9a are obtained.

For the damage scenario with member 23 removed and increasing the areas for all the bars by a factor equal to 2, the nonlinear dynamic probabilistic analysis and get reliability index $\beta = 0.088$. With the same design, perform nonlinear static analysis $\delta_{CA} = 1.70$. If we increase the areas for all the bars by a factor equal to 2.5, we obtain $\beta = 1.812$ and the corresponding $\delta_{CA} = 2.29$. By repeating the same procedure, Table 6.9b is obtained.

Figure 6.21 shows a plot for the relationship between dynamic collapse analysis allowance factor and the reliability index for different bridge types and different damage scenarios. It is observed that the relationship is reasonably consistent for the two different bridge configurations and the different damage scenarios. This is an important observation because it demonstrates that the proposed calibration method is solid and can be used to eventually propose a progressive collapse analysis procedure that can be implemented in engineering practice for different types of bridge configurations.

Table 6.9a Live load factors γ_L with different reliability index β for truss bridge

Member 29 removed					
δ_{CA}	1.26	1.70	2.00	2.37	2.66
β	-1.311	0.088	0.789	1.598	2.395

Table 6.9b Live load factors γ_L with different reliability index β for truss bridge

Member 23 removed				
δ_{CA}	1.70	2.07	2.29	2.59
β	0.088	1.311	1.812	2.170

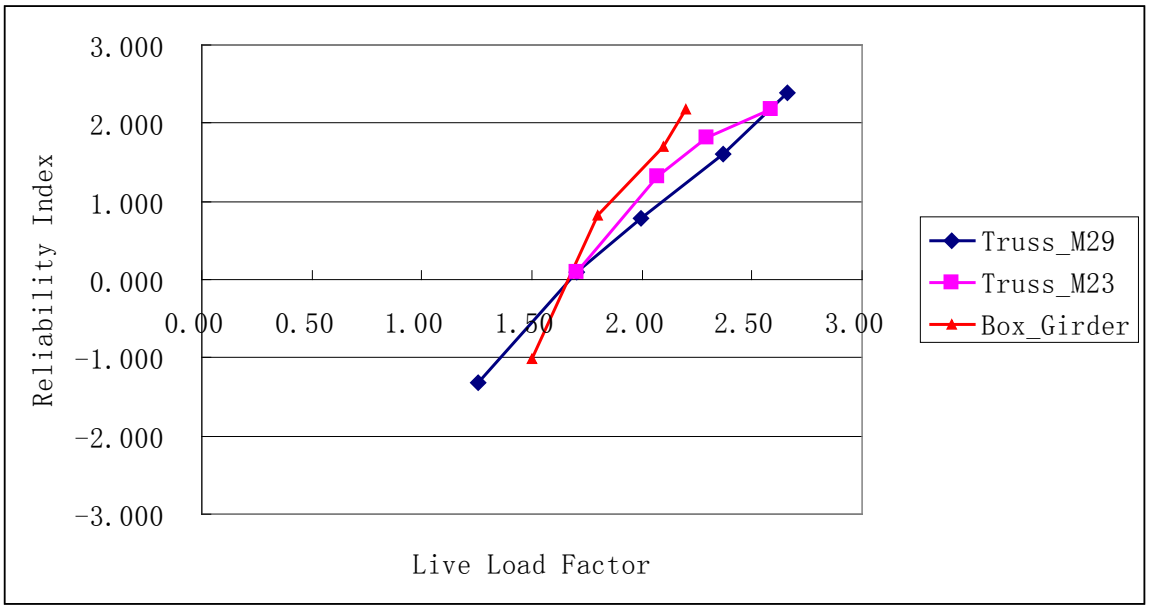

Figure 6.21 Live Load Factor with Reliability index for different bridge types and different damage scenarios

6.9 Implementation

In this section, we illustrate how a practicing engineer can apply the curve provided in Section 6.8 to check the ability of a bridge structure to resist progressive collapse using a deterministic nonlinear analysis and have confidence that the system will survive a local damage with sufficient level of reliability. In this example, we assume that bridge owners require that the system meets a target reliability index β=1.812.

From Figure 6.21, a target reliability β=1.812 corresponds to a dynamic collapse allowance δ_{CA}=2.29 which must be applied during the nonlinear analysis of the structure after removing a member susceptible to external hazard.

In this example we assume that the engineer is evaluating the ability of the bridge system shown in Figure 6.22 to resist progressive collapse. [The same bridge configuration analyzed earlier is used for convenience in this illustrative example]. The bridge is assumed to have the member areas set in Table 6.10. We also assume that an external hazard is likely to damage member 34. To check whether the bridge will survive this damage scenario, the following steps are applied:

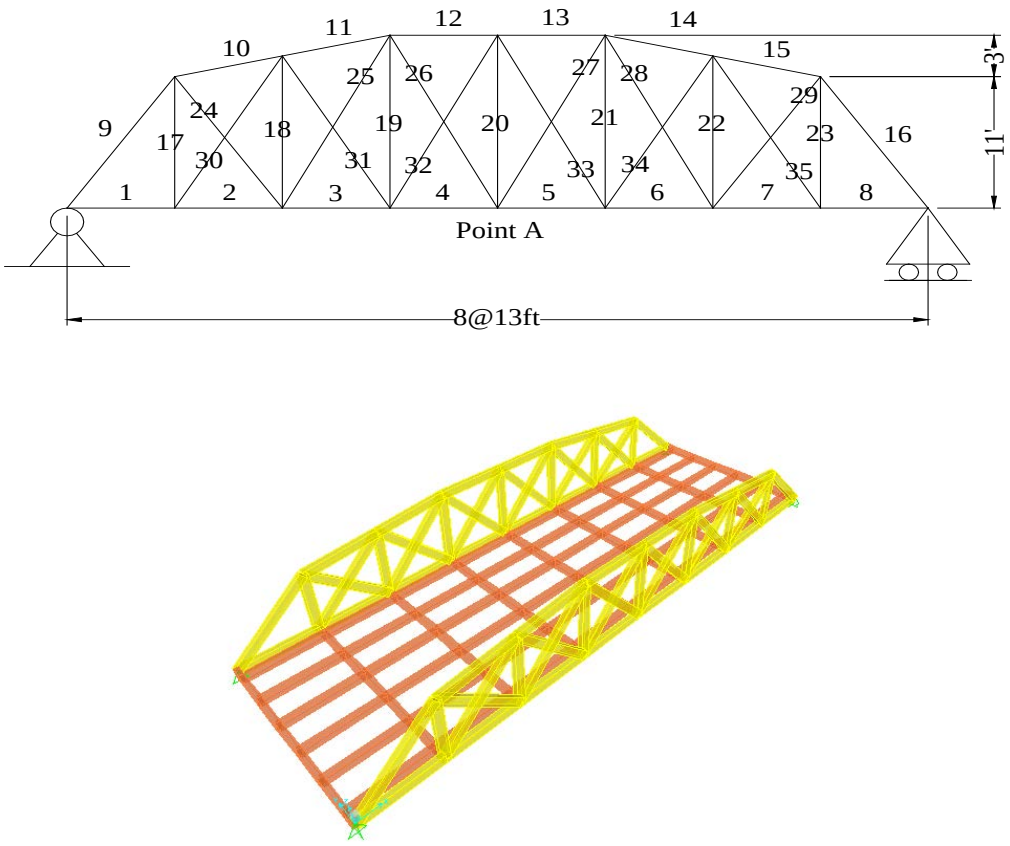

Figure 6.22 Layout of steel truss bridge

Table 6.10 Truss members' cross sectional areas

No.	Area (in2)	No.	Area (in2)	No.	Area (in2)
1	35.00	13	43.98	25	4.60
2	37.33	14	40.60	26	9.20
3	43.05	15	28.03	27	9.20
4	47.13	16	26.73	28	4.60
5	47.13	17	10.20	29	15.95
6	43.05	18	2.18	30	4.95
7	37.33	19	6.15	31	6.63
8	35.00	20	0.48	32	1.38
9	26.73	21	6.15	33	1.38
10	28.03	22	2.18	34	6.63
11	40.60	23	10.20	35	4.95
12	43.98	24	15.95		

1. Develop a structural model of the system including the nonlinear material properties of the bars and the connections.

2. Remove member 34 from the model

3. Apply the dead loads

4. Apply a live load corresponding to the AASHTO 3S2 Legal truck in the most critical position of the bridge.

5. Perform a deterministic nonlinear incremental load analysis using the live load as the control load.

6. Determine the load multiplier that will lead to system collapse. This multiplier will be the actual δ_{CA} for this bridge damage scenario.

7. For this example, δ_{CA} is = 4.0.

8. Compare δ_{CA} =4.0 to the target value 2.29.

9. Since δ_{CA} is higher than 2.29, this bridge will be able to resist progressive collapse after damage to member 34 with sufficient level of reliability.

On the other hand, if member 29 is removed, the dynamic allowance δ_{CA} is calculated to be 2.0 which is less than the target value 2.29. This indicates that the bridge will not meet the reliability criteria for this damage scenario.

In order to further check the consistency of the results, a dynamic reliability analysis is performed for the damaging event, and we found that for the removal of member 29 the reliability index is actually β =0.789 which is lower than the target beta=1.812. Thus, confirming the consistency between the deterministic analysis and the reliability analysis.

Similarly, if the dynamic reliability is performed for the removal of member 34, we obtain a reliability index β=2.93 which is greater than the target 1.812. This observation again serves to confirm the consistency between the outcomes of the reliability and deterministic analyses.

6.10 Conclusions

This Chapter described a probability-based procedure to evaluate the reliability of bridge systems and perform a probabilistic analysis of bridge redundancy and robustness as well as the probability of progressive collapse should one member be suddenly damaged due to the occurrence of an external hazard.

The analysis process is illustrated using two typical bridge configurations: A two-box steel girder bridge and a steel truss bridge. The box girder bridge is assumed to be susceptible to fatigue fracture at the midspan of one box and the truss is assumed to lose the load carrying capacity of a main bar.

The statistical models for the strength of the box girder bridge are assumed to following the models provided during the AASHTO LRFD code calibration effort. The statistical models used to perform the reliability analysis of truss bridge systems were developed in this study to account for bar failures in tension or compression including buckling. Also, probabilistic tri-linear shear stress-deformation and bilinear force-displacement models are developed to represent the behavior of the bolts and gusset plates at the truss connections.

The live load model used in this study is based on site-specific truck weight and traffic data collected using Weigh-In-Motion (WIM) systems. Specifically, the live load model is based on data collected at NY State WIM site 9121.

Since involved reliability analyses are beyond the day-to-day practice of bridge engineers, a methodology is calibrated so that a bridge engineer can verify the ability of a bridge system to avoid progressive collapse using traditional deterministic methods.

The calibration process is illustrated for the two different bridge configurations considered and for different damage scenarios. The results show that the proposed calibration method is robust and leads to consistent results. Such an approach can be used to eventually propose a progressive collapse analysis procedure that is implementable in engineering practice for different types of bridge configurations.

CHAPTER SEVEN: CONCLUSIONS AND FUTURE RESEARCH

7.1 Conclusions

This Dissertation described a probability-based procedure to evaluate the reliability of bridge systems and perform the probabilistic analysis of the redundancy and robustness as well as the probability of progressive collapse should one member be suddenly damaged due to the occurrence of an external hazard.

The main achievements of this study can be summarized as follows:

1. It was observed that most existing work on topics related to structural redundancy and progressive collapse was based on deterministic analysis methods. However, the high levels of uncertainty associated with estimating member strengths and loads, justify the use of probabilistic measures of redundancy, robustness and progressive collapse and the use of reliability-based methods to evaluate bridge system safety. Although NCHRP 12-36 proposed reliability criteria to evaluate the redundancy and robustness of bridge systems, the proposed criteria were based on the simplified analyses models that considered pre-identified single modes of failure. Also, the criteria were developed based on multi-beam bridges only. For other types of bridges, such as truss bridges, additional reliability-based verification of the NCHRP12-36 method need to be performed. For that purpose Chapter two presented a critical evaluation of existing reliability analysis methods for structural systems. The review revealed that a recently developed method known as the subset simulation method showed great potential for application to solve real scale

structural reliability problems in general and to specifically perform reliability analyses of bridge systems susceptible to different modes of failures.

2. We reviewed the existing subset simulation method and proposed an improved version referred to as the Regenerative Adaptive Subset Simulation (RASS). The proposed method is based on advanced Markov Chain Simulation Algorithms and combines the benefits of a Regeneration process, the Delayed Rejection and Adaptive algorithms and the Componentwise Algorithm. Several illustrative examples verified the validity and stability of the proposed simulation method. The advantages of this proposed method include its accuracy, efficiency and its ability to handle structural systems with complex failure regions, large numbers of random variables, and small probabilities of failure.

3. Several examples are used to illustrate how the Regenerative Adaptive Subset Simulation can be used for the reliability analysis of the redundancy, robustness and progressive collapse of bridge structures. To simplify the modeling of a truss bridge that can have different modes of failure and utilize existing probability models for different types of members, a tri-linear shear stress-deformation model and bilinear force-displacement model are developed to model the bolts and gusset plates at truss connections in addition to the traditional multi-linear model of truss bars in tension and the linear model for bar buckling. These models along with models for box-girder bridges were used to illustrate how to apply the proposed simulation method to analyze the redundancy of intact bridges, the robustness of damaged bridges and the ability of a bridge system to resist progressive collapse.

4. A simplified deterministic analysis methodology is developed so that a bridge engineer can verify the ability of a bridge system to avoid progressive collapse using traditional deterministic nonlinear static methods. Appropriate criteria for checking the ability of a bridge to survive a potential damage to one critical member are calibrated to provide consistent reliability levels. By illustrating the process with different bridge configurations and different damage scenarios, the proposed calibration method is found to be stable and can be used to eventually propose a progressive collapse analysis procedure that is implementable in engineering practice for different types of bridge configurations.

7.2 Future Research

In this Dissertation, probabilistic analyses are performed to evaluate the probability of progressive collapse should one member be suddenly damaged due to the occurrence of an external hazard for different types of bridge configurations and different damage scenarios. A methodology has been developed that enables practicing engineers to check the ability of bridge systems to resist progressive collapse by performing a deterministic nonlinear static progressive collapse analysis. More work could be performed in the future to extend the application of these research results and to further improve the presented methodology. Specifically, the following additional tasks could be considered for future work:

Reliability Method: more work can be done to improve the stability and reduce the number of samples of RASS by introducing more advanced Markov-chain based algorithms or combining the Markov chain method with other existing methods.

Progressive Collapse: in this dissertation, one truss bridge and one steel box-girder bridge are used to illustrate the procedure for evaluating the ability of systems to resist progressive collapse due to sudden loss of one member. In the future, the applicability of the Markov-chain simulation method must be tested on complex structural systems such as stayed arch bridges, cable stayed and suspension bridges with very large numbers of components. The applicability of the simplified deterministic analysis methodology for the progressive collapse analysis of these complex systems must be verified and adjusted as necessary.

REFERENCES

AASHTO, (2008) AASHTO MBE-1-M, Manual for Bridge Evaluation, 1st Edition, Washington, DC.

AASHTO. (1993). Load and Resistance Factor Design Specification for Structural Steel Buildings (LRFD), American Institute of Steel Construction, Chicago.

AASHTO. (2002). AASHTO LRFD Bridge Design Specification, Washington, DC.

AISC. (1999). Load and Resistance Factor Design Specification for Structural Steel Buildings (LRFD), American Institute of Steel Construction, Chicago.

Ang, G., Tang, A.-S., and Tang, W. (1992). "Optimal importance sampling density estimator." J Engng Mech, ASCE, 118(6), 1146-1163.

ASCE. (2002). Minimum Design Loads for Buildings and Other Structures (ASCE 7), American Society of Civil Engineers, New York.

ASCE. (2005). "Minimum design loads for buildings and other structures." ASCE/SEI 7-05, American Society of Civil Engineers.

Au, S. K., and Beck, J. L. (1999). "A new adaptive importance sampling scheme." Structural Safety, 21, 135-158.

Au, S. K., and Beck, J. L. (2001). "Estimation of small failure probabilities in high dimensions by subset simulation." Probabilistic Engineering Mechanics, 16, 263-277.

Au, S. K., Papadimitriou, C., and Beck, J. L. (1999). "Reliability of uncertain dynamical systems with multiple design points." Structural Safety, 21, 113-133.

Biondini, F. (2009a). "A measure of lifetime structural robustness." Structural Congress 2009, ASCE.

Biondini, F., Frangopol, D. M., and Restelli, S. "On structural robustness, redundancy and static indeterminacy." Structural Congress 2008, ASCE.

Borri, A., and Speranzini, E. (1997). "Structural reliability analysis using a standard deterministic finite element code." Structural Safety, 19(4), 361-382.

Bucher, C. G. (1988). "Adaptive sampling-an iterative fast Monte Carlo procedure." Structural Safety, 5, 119-126.

Bucher, C. G., and Bourgund, U. (1990). "A fast and efficient resonse surface approach for structural reliability problems." Structural Safety, 7, 57-66.

Chen, K., and Zhang, S. (1996). "Semi-probabilistic Method for Evaluating System Redundancy of Existing Offshore Structures." Ocean Engineering, 23(6), 455-464.

Ching, J., AU, S. K., and Beck, J. L. (2005a). "Reliability estimation for dynamical systems subject to stochastic excitation using subset simulation with splitting." Computer Methods in Applied Mechanics and Engineering, 194, 1557-1579.

Ching, J., Beck, J. L., and AU, S. K. (2005b). "Hybrid Subset Simulation method for reliability estimation of dynamical systems subject to stochastic excitation." Probabilistic

Engineering Mechanics, 20(3), 199-214.

Cowles, M. K., and Rosenthal, J. S. (1996). "A simulation approach to convergence rates for Markov chain Monte Carlo." Technical report, University of Toronto, Department of Statistics.

Der, K. A., and Dakessian, T. (1998). "Multiple design points in first and second-order reliability." Structural Safety, 20, 37-49.

Doane, J. F. (1969). "Inelastic instability of wide-flange steel beams," University of Texas, at Austin, Tex.

DoD. (2002). Unified facilities criteria (UFC), DoD minimum antiterrorism standards for buildings, Department of Defense, UFC 4-010-01, U.S. Army Corps of Engineering, Washington, D.C.

Ellingwood, B. R. (2006). "Mitigating Risk from Abnormal Loads and Progressive Collapse." Journal of Performance of Constructed Facilities, ASCE, November, 315-323.

Ellingwood, B. R. (2009). "Abnormal loads and disproportionate collaspe: risk mitigation strategies." Structural Congress 2009, ASCE.

Ellingwood, B.R., (2011), ICASP conference, Achieving Robustness and mitigating risk of disproportionate collapse in building

Ellingwood, B. R., Galambos, T. V., MacGregor, J. G., and Cornell, C. A. (1980). Development of a probability based load criterion for American national standard A58, NBS Special Publication 577, U.S. Dept of Commerce, Jun.

Engelund, S., and Rachwitz, R. (1993). "A benchmark study on importance sampling techniques in structural reliability." Structural Safety, 12, 255-276.

Engelund, S., and Rackwitz, R. "Experiences with experimental design schemes for failure surface estimation and reliability." ASCE Specialty Conference on Probabilistic Mechanics and Structural and Geotechnical Reliability, New York, USA, 244-247.

Eurocode3. (1993). Part 1.1 Design of Steel Structures, Commission of The European Communities, Brussels.

Eurocode8. (1994). Design Provisions for structures, European Committee for Standardization.

FEMA. (1997). NEHRP guidelines for the seismic rehabilitation of buildings, FEMA-273, Washington, D.C.

Fisher, J. W., Galambos, T. V., Kulak, G. L., and Ravindra, M. K. (1978). "Load and Resistance Factor Design Criteria for Connectors." Journal of the Structural Division, ASCE, 104(9), 1427-1441.

Fisher, J. W., and Kulak, G. L. (1968). "Tests of Bolted Butt Splices." Journal of the Structural Division, ASCE, 94(11).

Fisher, J. W., and Struik, H. A. (1974). Guide to design criteria for bolted and riveted joints, Wiley, New York.

Fishman, G. S. (1996). Monte Carlo: concepts, algorithms, and applications,

Springer, New York.

Florida Load Rating Manual, http://www.dot.state.fl.us/statemaintenanceoffice/LRManual82012.pdf

Frangopol, D., and Nakib, R. (1991). "Effects of Damage and Redundancy on the Safety of Existing Bridges." Third Bridge Engineering Conference, TRR(1290).

Frangopol, D. M., and Curley, J. P. (1987). "Effects of Damage and Redundancy on Structural Reliability." Journal of Structural Engineering, 113(7), 1533-1549.

Galambos, T. V., and Ravindra, M. K. (1978). "Properties of Steel for Use in LRFD." J.Struct. Div, ASCE, 104(9), 1459-1468.

Garrick, B. J., James E. Hallb, Max Kilgerc, J., ohn C. McDonaldd, Tara O'Toolee, Peter S. Probstf, Elizabeth Rindskopf Parkerg, Robert Rosenthalh, Alvin W. Trivelpiecei, Arsdalej, L. A. V., and Zebroskik, E. L. (2004). "Confronting the risks of terrorism: making the right decisions." Reliability Engineering & System Safety, 86, 129-176.

Gelman, A. G., Roberts, G. O., and Gilks, W. R. (1996). Efficient Metropolis jumping rules, Oxford University Press.

Ghosn, M., and Frangopol, D. M. (1999). "Bridge Safety and Reliability." ASCE, 83-112.

Ghosn, M., and Moses, F. (1998). NCHRP Report 406, Redundancy in Highway Bridge Superstructures, Transportation Research Board---National Research Council, National Academy Press, Washington. DC.

Gilks, W. R., Roberts, G. O., and Sahu, S. K. (1998). "Adaptive Markov chain Monte Carlo through regenration." J.Amer.Statist. Assoc., 93, 1045-1054.

Grierson, D. E., Safi, M., Xu, L., and Liu, Y. "Simplified methods for progressive-collapse analysis of buildings." Structural Congress 2005, ASCE.

Grooteman, F. (2008). "Adaptive radial-based importance sampling method for structural reliability." Structural Safety, 30(6), 533-542.

GSA. (2000). Progressive Collapse analysis and design guidelines for new federal office buildings and major modernization projects, Office of Chief Architect, Washington, D.C.

Guan, X. L., and Melchers, R. E. (2001). "Effect of response surface parameter variation on structural reliability estimates." Structural Safety, 23(4), 429-444.

Haario, H., Saksman, E., and Tamminen, J. (2001). "An adaptive Metropolis algorithm." Bernoulli, 7, 223-242.

Haario, H., Saksman, E., and Tamminen, J. (2005). "Componentwise adaptation for high dimensional MCMC." Computational Statistics, 20, 265-273.

Hammersley, J. M., and handscomb, D. C. (1964). Monte-Carlo methods, Methuen, London.

Harbitz, A. "Efficient and accurate probability of failure calculation by th euse of the importance sampling technique." Proc. Fourth Int. Conf. on Applicatoins of Statistics and

Probability in Soil and Structural Engineering, Pitagora Editrice, Bologna, Italy, 825-836.

Hastings, W. K. (1970). "Monte Carlo sampling methods using Markov chains and their applications." Biometrika, 57, 97-109.

Hendawi, S., and Frangopol, D. M. (1994). "System reliability and redundancy in structural design and evaluation." Structural Safety, 16(1-2), 47-71.

Hohenbichler, M., and Rachwitz, R. (1988). "Improvement of second-order reliability estimates by importance sampling." J Engng Mech, ASCE, 114(12), 2195-2198.

Holt, R., and Hartmann, J. (2008). "Adequacy of the U10 & L11 gusset plate design for the Minnesota bridge No. 9340-interim report." Federal Highway Administration Turner-Fairbank Highway Research Center Report.

Iman, R. L., Davenport, J. M., and Zeigler, D. K. (1980). SAND79-1473: Latin hypercube sampling (program user's guide), Risk Assessment and Systems Modeling Department, Sandia National Laboratories, Albuquerque, NM.

Iman, R. L., Helton, J. C., and Campbell, J. E. (1981). "An approach to sensitivity analysis of computer models, part 1. introduction, input variable selection and preliminary variable assessment." Journal of Quality Technology, 13(3), 174-183.

Johnson, B. G., and Opila, F. (1941). "Compression and tension tests of structural alloys." ASTM, Proc., 41, 552-570.

Julian, O. G. (1957). "Synopsis of First Progress Report of Committee on Safety Factors." J. Struct. Div., ASCE, 83(4), 1-22.

Kaewkulchai, G., and Williamson, E. B. (2004). "Beam element formulation and solution procedure for dynamic progressive collapse analysis." Computers and Structures, 82, 639-651.

Karadeniz, H. (2006). "Reliability Calculation of RC Offshore Structures Under Extreme Wave Loading." International Journal of Offshore and Polar Engineering, 16(2), 138-145.

Karamchandani, A., Bjerager, P., and Cornell, C. A. "Adaptive importance sampling." Proceedings of the Fifth ICOSSAR, San Francisco, 855-862.

Katafygiotis, L. S., and Cheung, S. H. "An efficient method for calculation of reliability integrals." Advances in Stochastic Structural Dynamics, Boca Raton, FL,USA, 263-270.

Khandelwal, K., El-Tawila, S., and Sadekb, F. (2009). "Progressive collapse analysis of seismically designed steel braced frames." Journal of Constructional Steel Research, 65(3), 699-708.

Kim, H. J., and Yura, J. A. (1999). "The effect of ultimate-to-yield ratio on the bearing strength of bolted connections." Journal of Constructional Steel Research, 49, 255-269.

Kima, J., and Kimb, T. (2009). "Assessment of progressive collapse-resisting capacity of steel moment frames." Journal of Constructional Steel Research, 65(1), 169-179.

Kiureghian, A. D., Lin, H. Z., and Hwang, S. J. (1987). "Second-order reliability approximations." J Eng Mech DIV, ASCE, 113(8), 1208-1225.

Korkmaz, A., and Johnson, P. A. (2007). "Probabilistic Seismic Structural Assessment." Proceeding of the 2007 ASCE International Workshop on Computing in Civil Engineering.

Koutsourelakis, P. S., Pradlwarter, H. J., and Schueller, G. I. (2004). "Reliability of structures in high dimensions, part I: algorithms and applications." Probabilistic Engineering Mechanics, 19(4), 409-417.

Kulak, G. L., Fisher, J. W., and Struik, H. A. (1987). Guide to design criteria for bolted and riveted joints, 2nd edition, John Wiley & Sons, New York.

Marjanishvili, S., and Agnew, E. (2006). "Comparison of Various Procedures for Progressive Collapse Analysis." Journal of Performance of Constructed Facilities, ASCE, 20(4), 365-374.

Marjanishvili, S. M. (2004). "Progressive Analysis Procedure for Progressive Collapse." Journal of Performance of Constructed Facilities, ASCE, May, 79-85.

McKay, M. D., Beckman, R. J., and Conover, W. J. (1979). "A comparison of three methods for selecting values of input variables in the analysis of output from a computer code." American Statistical Association, 21(2), 239-245.

Melchers, R. E. (1989). "Importance sampling in structural systems." Structural Safety, 6, 3-10.

Melchers, R. E. (1999). Structural Reliability Analysis and Prediction, John Wiley and Sons, New York.

Metropolis, N., Rosenbluth, A. W., Rosenbluth, M. N., and Teller, A. H. (1953). "Equations of State Calculations by Fast Computing Machines." Journal of Chemical Physics, 21, 1087-1092.

Mira, A. (2001). "On Metropolis-Hasting algorithms with delayed rejection." Metron, LIX(3-4), 231-241.

Moarefzadeha, M. R., and Melchers, R. E. (2006). "Nonlinear wave theory in reliability analysis of offshore structures." Probabilistic Engineering Mechanics, 21(2), 99-111.

Mykland, P., Tierney, L., and B.Yu. (1995). "Regeneration in Markov chain samplers." J.Amer.Statist. Assoc., 90, 233-241.

Nowak, A. (1992). Calibration Report for NCHRP Project 12-33, Department of Civil Engineering, University of Michigan, Ann Arbor, MI.

Nowak, A. S. (1999). "Calibration of LRFD Bridge Design Code, NCHRP Report 368." Washington, DC.

Nummelin, E. (1984). general Irreducible Markov Chains and Non-Negative Operators, Cambridge University Press, Cambridge.

Paliou, C., Shinozuka, M., and Chen, Y.-N. (1990). "Reliability and Redundancy of

Offshore Structures." J. Engrg. Mech, 116, 359-378.

Pan, Y. (2006). "Seismic Fragility and risk management of highway bridges in New York State," City University of New York, New York.

Papadimitriou, C., Beck, J. L., and Katafygiotis, L. S. (1997). "Asymptotic expansions for reliabilities and moments of uncertain dynamic systems." J Engng Mech, ASCE, 123(12), 1219-1229.

Powell, G. "Progressive Collapse: Case Studies Using Nonlinear Analysis." Structural Congress 2005, ASCE.

Powell, G. (2009). "Disproportionate Collapse: the Futility of using Nonlinear Analysis." Structural Congress 2009, ASCE.

Rajashekhar, M. R., and Ellingwood, B. R. (1993). "A new look at the response surface approach for reliability analysis." Structural Safety, 12(3), 205--220.

Rex, C. O., and Easterling, W. S. (2003). "Behavior and Modeling of a bolt bearing on a single plate." Journal of Structural Engineering, 129(6), 792-800.

Rosenblatt, M. (1952). "Remarks on a Multivariate Transformation." Ann.Math. Stat., 23, 470-472.

Rubinstein, R. Y. (1981). Simulation and the Monte-Carlo method, Wiley, New York.

Rumpf, J. L., and Fisher, J. W. (1963). "Calibration of A325 bolts." Journal of the Structural Division, ASCE, 89(6).

Schueller, G. I., Pradlwarter, H. J., and Pandey, M. D. "Methods for reliability assessment of nonlinear systems under stochastic dynamic loading-a review." Proceedings of EURODYN'93, Balkema, 751-759.

Schueller, G. I., and Stix, R. (1987). "A critical appraisal of methods to determine failure probabilities." Structural Safety, 4, 293-309.

Shinozuka, M. (1983). "Basic analysis of structural safety." J. Struct. Engng., ASCE, 109, 721-740.

Starossek, U., and Haberland, M. (2009). "Evaluating Measures of Structural Robustness." Structural Congress 2009, ASCE.

Stewart, M. G., and Netherton, M. D. (2006). "Security risks and probabilistic risk assessment of glazing subject to explosive blast loading." Reliability Engineering & System Safety, 93(4), 627-638.

Tall, L., and Alpsten, G. A. "On the scatter of yield strength and residual stresses in steel members." Symp. on concepts of safety of structures and methods of design, IABSE, London, 151-163.

Tierney, L. (1994). "Markov chains for exploring posterior distributions." Annals of Statistics, 22, 1701-1762.

Wallaert, J. J., and Fisher, J. W. (1965). "Shear strength of high-strength bolts." Journal of the Structural Division, ASCE, 91(3).

Wirsching, P. H. (1984). "Fatigue Reliability for Offshore Structures." J. Struct. Engrg, 110, 2340-2356.

Wyss, G. D., and Jorgensen, K. H. (1998). A user's guide to LHS: Sandia's Latin Hypercube Sampling Software, Risk Assessment and Systems Modeling Department, Sandia National Laboratories, Albuquerque, NM.

Yan, D., and Chang, C.C., (2009). "Vulnerability Assessment of Cable-Stayed Bridges in Probabilistic Domain." Journal of Bridge Engineering, ASCE, !4(4), 270-278.